SSC-334

INFLUENCE OF WELD POROSITY ON THE INTEGRITY OF MARINE STRUCTURES

SHIP STRUCTURE COMMITTEE

1990

SHIP STRUCTURE COMMITTEE

THE SHIP STRUCTURE COMMITTEE is constituted to prosecute a research program to improve the hull structure of ships and other marine structures by an extension of knowledge pertaining to design, materials and methods of construction.

RADM J. D. Sipes, USCG, (Chairman)
Chief, Office of Marine Safety,
Security and Environmental Protection
U. S. Coast Guard

Mr. Alexander Malakhoff
Director, Structural Integrity
Subgroup (SEA 55Y)
Naval Sea Systems Command

Dr. Donald Liu
Senior Vice President
American Bureau of Shipping

Mr. H. T. Haller
Associate Administrator for Ship-
building and Ship Operations
Maritime Administration

Mr. Thomas W. Allen
Engineering Officer (N7)
Military Sealift Command

CDR Michael K. Parmelee, USCG,
Secretary, Ship Structure Committee
U. S. Coast Guard

CONTRACTING OFFICER TECHNICAL REPRESENTATIVES

Mr. William J. Siekierka
SEA 55Y3
Naval Sea Systems Command

Mr. Greg D. Woods
SEA 55Y3
Naval Sea Systems Command

SHIP STRUCTURE SUBCOMMITTEE

THE SHIP STRUCTURE SUBCOMMITTEE acts for the Ship Structure Committee on technical matters by providing technical coordinating for the determination of goals and objectives of the program, and by evaluating and interpreting the results in terms of structural design, construction and operation.

U. S. COAST GUARD

Dr. John S. Spencer (Chairman)
CAPT T. E. Thompson
Mr. David L. Motherway
CDR Mark E. Noll

NAVAL SEA SYSTEMS COMMAND

Mr. Robert A. Sielski
Mr. Charles L. Null
Mr. W. Thomas Packard
Mr. Allen H. Engle

MARITIME ADMINISTRATION

Mr. Frederick Seibold
Mr. Norman O. Hammer
Mr. Chao H. Lin
Dr. Walter M. Maclean

MILITARY SEALIFT COMMAND

Mr. Glenn M. Ashe
Mr. Michael W. Touma
Mr. Albert J. Attermeyer
Mr. Jeffery E. Beach

AMERICAN BUREAU OF SHIPPING

Mr. John F. Conlon
Mr. Stephen G. Arntson
Mr. William M. Hanzalek
Mr. Philip G. Rynn

SHIP STRUCTURE SUBCOMMITTEE LIAISON MEMBERS

U. S. COAST GUARD ACADEMY

LT Bruce Mustain

U. S. MERCHANT MARINE ACADEMY

Dr. C. B. Kim

U. S. NAVAL ACADEMY

Dr. Ramswar Bhattacharyya

STATE UNIVERSITY OF NEW YORK
MARITIME COLLEGE

Dr. W. R. Porter

WELDING RESEARCH COUNCIL

Dr. Glen W. Oyler

NATIONAL ACADEMY OF SCIENCES
MARINE BOARD

Mr. Alexander B. Stavovy

NATIONAL ACADEMY OF SCIENCES
COMMITTEE ON MARINE STRUCTURES

Mr. Stanley G. Stiansen

SOCIETY OF NAVAL ARCHITECTS AND
MARINE ENGINEERS-
HYDRODYNAMICS COMMITTEE

Dr. William Sandberg

AMERICAN IRON AND STEEL INSTITUTE

Mr. Alexander D. Wilson

Member Agencies:

United States Coast Guard
Naval Sea Systems Command
Maritime Administration
American Bureau of Shipping
Military Sealift Command

Ship Structure Committee

An Interagency Advisory Committee
Dedicated to the Improvement of Marine Structures

Address Correspondence to:

Secretary, Ship Structure Committee
U.S. Coast Guard (G-MTH)
2100 Second Street S.W.
Washington, D.C. 20593-0001
PH: (202) 267-0003
FAX: (202) 267-0025

August 2, 1990

SSC-334
SR-1305

INFLUENCE OF WELD POROSITY ON THE
INTEGRITY OF MARINE STRUCTURES

In the marine industry, we are concerned with the quality of weldments and the effect of weld defects on the strength and integrity of marine structures. This report is intended to provide a better understanding of the influence of weld metal porosity on the integrity of marine structures by examining the effects of porosity on fatigue resistance of ship steel weldments.

J. D. SIPES
Rear Admiral, U. S. Coast Guard
Chairman, Ship Structure Committee

Technical Report Documentation Page

1. Report No.	2. Government Accession No.	3. Recipient's Catalog No.
SSC-334		

4. Title and Subtitle	5. Report Date
STUDY TO DETERMINE THE INFLUENCE OF WELD POROSITY ON THE INTEGRITY OF MARINE STRUCTURES	February, 1989
	6. Performing Organization Code SHIP STRUCTURE COMMITTEE
7. Author(s) William J. Walsh, Brian N. Leis, and J. Y. Yung	8. Performing Organization Report No. SR-1305
9. Performing Organization Name and Address Battelle 505 King Avenue Columbus, Ohio 43201-2693	10. Work Unit No. (TRAIS)
	11. Contract or Grant No. DTCG23-85-C-20077
12. Sponsoring Agency Name and Address Ship Structure Committee U.S. Coast Guard Washington, D.C. 20593	13. Type of Report and Period Covered Final
	14. Sponsoring Agency Code G-M

15. Supplementary Notes

16. Abstract

This study examined the influence of porosity on the fatigue resistance of ship steel weldments. A literature review was conducted to determine parameters which have been found to control the fatigue life of welds containing porosity. A predictive model was developed incorporating those parameters to account for both crack initiation and propagation. Four types of porosity; single pore, uniform porosity, co-linear porosity, and cluster porosity, were examined using the model. The models sensitivity to the parameters (plate thickness, stress ratio, residual stress, pore size and porosity type) was studied and discussed.

A variable amplitude loading history was developed from SL-7 loading history data, and used to predict actual service lives.

The main conclusion of the study was that porosity is of little concern in welds if the weld reinforcement is left intact. If the reinforcement is removed, the type and size of porosity will control fatigue life. When subjected to the service history the welds were not predicted to fail during any normal design life. Finally, the results are related to the American Bureau of Shipping's Rules for Non-destructive Inspection of Hull Welds. The code was found to be conservative from a fatigue standpoint.

17. Key Words	18. Distribution Statement
Welds Porosity, Fatigue, Variable Amplitude Loading, Low Cycle Fatigue, Linear Elastic Fracture Mechanics	DOCUMENT IS AVAILABLE TO THE PUBLIC THROUGH THE NATIONAL TECHNICAL INFORMATION SERVICE, SPRINGFIELD VIRGINIA 22161

19. Security Classif. (of this report)	20. Security Classif. (of this page)	21. No. of Pages	22. Price
UNCLASSIFIED	UNCLASSIFIED	105	–

Form DOT F1700.7 (8-72) Reproduction of completed page authorized

METRIC CONVERSION FACTORS

Approximate Conversions to Metric Measures

Symbol	When You Know	Multiply by	To Find	Symbol
	LENGTH			
in	inches	*2.5	centimeters	cm
ft	feet	30	centimeters	cm
yd	yards	0.9	meters	m
mi	miles	1.6	kilometers	km
	AREA			
in^2	square inches	6.5	square centimeters	cm^2
ft^2	square feet	0.09	square meters	m^2
yd^2	square yards	0.8	square meters	m^2
mi^2	square miles	2.6	square kilometers	km^2
	acres	0.4	hectares	ha
	MASS (weight)			
oz	ounces	28	grams	g
lb	pounds	0.45	kilograms	kg
	short tons (2000 lb)	0.9	tonnes	t
	VOLUME			
tsp	teaspoons	5	milliliters	ml
Tbsp	tablespoons	15	milliliters	ml
fl oz	fluid ounces	30	milliliters	ml
c	cups	0.24	liters	l
pt	pints	0.47	liters	l
qt	quarts	0.95	liters	l
gal	gallons	3.8	liters	l
ft^3	cubic feet	0.03	cubic meters	m^3
yd^3	cubic yards	0.76	cubic meters	m^3
	TEMPERATURE (exact)			
°F	Fahrenheit temperature	5/9 (after subtracting 32)	Celsius temperature	°C

*1 in = 2.54 (exactly). For other exact conversions and more detailed tables, see NBS Misc. Publ. 286, Units of Weights and Measures, Price $2.25, SD Catalog No. C13.10:286.

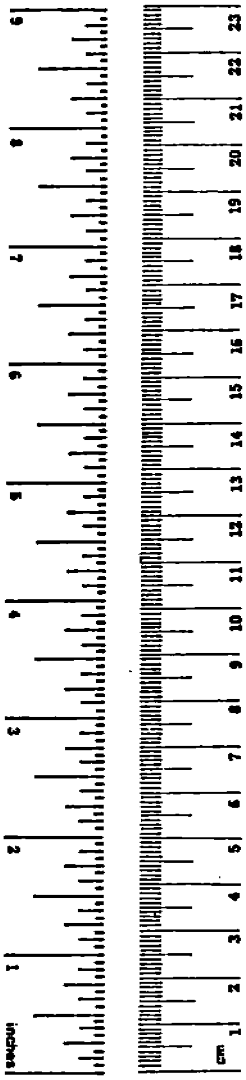

Approximate Conversions from Metri

Symbol	When You Know	Multiply by
	LENGTH	
mm	millimeters	0.04
cm	centimeters	0.4
m	meters	3.3
m	meters	1.1
km	kilometers	0.6
	AREA	
cm^2	square centimeters	0.16
m^2	square meters	1.2
km^2	square kilometers	0.4
ha	hectares (10,000 m^2)	2.5
	MASS (weight)	
g	grams	0.035
kg	kilograms	2.2
t	tonnes (1000 kg)	1.1
	VOLUME	
ml	milliliters	0.03
l	liters	2.1
l	liters	1.06
l	liters	0.26
m^3	cubic meters	35
m^3	cubic meters	1.3
	TEMPERATURE (exact	
°C	Celsius temperature	9/5 (then add 32)

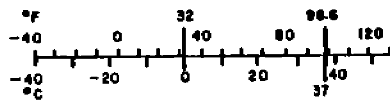

TABLE OF CONTENTS

TABLE OF CONTENTS
(Continued)

LIST OF TABLES

LIST OF TABLES
(Continued)

LIST OF FIGURES

LIST OF FIGURES (CONTINUED)

LIST OF FIGURES (CONTINUED)

LIST OF FIGURES (CONTINUED)

STUDY TO DETERMINE THE INFLUENCE
OF WELD POROSITY ON THE INTEGRITY
OF MARINE STRUCTURES

by

William J. Walsh, Brian N. Leis and J. Y. Yung

1. INTRODUCTION

The objective of this study is to obtain a better understanding of the influence of weld porosity on the integrity of marine structures. Understanding the effects of porosity on the mechanical properties of weldments is important for the safe design of welded marine structures. Information on the porosity effects for a weldment would be useful in specifying welding processes and procedures. The expected service conditions of a weld could dictate the amount of porosity allowed. A welding process which would be expected to result in porosity levels corresponding to that allowable amount could be rationally determined and specified. The inspection and maintenance of welded structures would also benefit from a refined understanding of the detrimental effects of various sizes, shapes, and patterns of porosity.

Previous investigations on the effects of weld porosity on integrity of structures indicate that there is very little influence of porosity upon brittle fracture properties[1]. However, porosity has been shown to influence the fatigue properties of welds[1-7]. The motivation for the present study comes from the potential of modern fatigue technology and fracture mechanics principles to analytically predict the fatigue performance of weldments. The literature provides sufficient information on the dependence of fatigue performance on parameters such as size of pores, number of pores, pore shape and pattern. These parameters will be incorporated into a fatigue life estimation model based upon fatigue and fracture concepts.

2. DISCUSSION OF THE PROBLEM

2.1 Limits of Concern

The results of most of the studies examining the effects of porosity conclude that porosity does not effect the mechanical properties of a weldment unless the amount of porosity is extremely large[1-5]. Regarding fatigue, the most critical location for a weld is generally the weld toe. This abrupt change in geometry from the weld metal reinforcement to the base metal results in a stress concentration and acts as a fatigue crack initiation site. Pores are, by comparison, much less severe stress concentrations.

The severity of the weld-toe stress concentration decreases with decreasing weld reinforcement size. That is, the smaller the weld reinforcement, the less effect the weld toe will have in initiating a fatigue crack. This fact suggests that if the weld reinforcement is shallow enough, the stress concentration due to the weld toe will be less than that resulting from a pore. The pore would then be the critical location for fatigue.

Consider the following example. The stress concentration factor, K_t, for a pore in an infinite body subjected to an axial stress is 2.05 (for Poisson's ratio of 0.3). The stress concentration factor for the toe of a butt weld subjected to axial tension[8] is 3.06 for a 0.5 inch thick plate, having a reinforcement width of 0.29 inch (60 degree bevel) and height of 0.17 inch, and a weld toe radius of 0.02 inch. This means that if a pore (K_t = 2.05) were present in the weld, the more highly stressed location would still be the weld toe (K_t = 3.06). The reinforcement height at which the stress concentrations would be equal for both the weld toe and the pore is 0.11 inch. At this reinforcement height, there would be an equal chance of a fatigue crack initiating at the toe or at the pore. At heights below this value, the fatigue crack would be expected to initiate at the pore.

This example is an over simplification of a rather complex stress analysis problem. Factors such as bending stress, almost always present in actual service, and difficulty in accurately measuring the weld toe radius have not been considered. Both of these effects would increase the weld-toe stress concentration. The example does illustrate, however, that unless the weld reinforcement is shallow, fatigue cracks would not be expected to initiate from a pore.

2.2 Factors of Concern

Having discussed the fact that weld porosity is generally only a problem when the weld reinforcement is shallow or removed, or when porosity is excessive, the factors that must be addressed in analyzing this specific problem will be outlined.

2.2.1 Fracture Mechanics

Porosity can be characterized as a blunt defect having no sharp asperities which can be analyzed as cracks. Since cracks do initiate from pores, at some point in the cracks growth, the assumptions of fracture mechanics should be valid for describing the problem. Assuming that the blunt defect is a sharp crack will give conservative answers, but they may not be realistic. Some accounting must be made of the life spent initiating and growing a crack from the pore to a fracture mechanics size flaw. This initial period of growing a crack can be a significant part of the total life, especially for high cycle fatigue.

The general finding in the literature is that porosity does not behave like planar weld defects, such as lack of fusion, which are more clearly crack-like. (See, for example, References 2 and 8.)

2.2.2 Pore Geometry and Interaction

Porosity, though generally spherical in shape, can assume many shapes and configurations. These include elongated pores, rows of single pores or collinear pores, and pore clusters. Determining the effects of various sizes and shapes of pores is an important factor affecting the structural integrity of weldments. Unfortunately, almost no work reported in the literature has dealt directly with the mechanisms of crack growth from potentially interacting voids. Instead, researchers have concentrated on correlating total fatigue lives with parameters describing the weld porosity. Examples are percent of porosity, reduction in area, and maximum pore size. From these indirect measurements one may be able to extract some of the rules governing the interaction of pores.

2.2.3 Residual Stresses

Residual stresses have been shown to significantly decrease the fatigue life of welds[8-10]. Compared to welds not containing residual stresses, tensile residual stresses can decrease the life, while compressive residual stresses can increase the life. Measurements in HY-80 butt welds have revealed longitudinal and transverse residual stresses locally as high as the yield strength[8]. Similar results have been found for mild steel butt welds[11]. Residual stress magnitudes and distributions can vary greatly[8,10]. Generally, tensile stresses are seen at the surfaces and compressive stresses at mid-thicknesses. Because of this variation, the initiation and propagation of a fatigue crack may depend on its position in the weld--i.e., on its position in the residual stress field.

2.2.4 Threshold Crack Growth Behavior

Below some arbitrary crack growth rate, from an engineering viewpoint, a crack is not of concern because it does not threaten the integrity of the structure in a reasonable amount of time. Although there is some debate concerning the determination of threshold stress intensities, the concept is an important one for the present study.

It has been noted that under variable amplitude loading, threshold behavior may not be as significant as under constant amplitude loading[12]. This is because there will probably be some large loads which cause the small crack to grow; and as it does, more and more of the load spectrum will produce stress intensities above the threshold values.

2.2.5 Crack Retardation

Under variable amplitude loading similar to actual service conditions, linear elastic fracture mechanics methods have been shown to give overly conservative crack growth predictions under actual ship load histories when load interactions are not accounted for[12]. Large loads, such as bottom slamming, superimposed on smaller loads, such as low frequency wave induced stresses, result in crack growth retardation, which slow crack growth below rates that would be expected by additive linear cumulative damage.

3. SCOPE

The objective of this study was to research and define the parameters which affect the fatigue performance of marine weldments containing porosity. A model which accounts for the defined parameters was developed and exercised to study the sensitivity of fatigue life upon these factors. The model uses both low cycle fatigue concepts and fracture mechanics techniques to predict fatigue crack initiation and subsequent growth. It is important to emphasize that all of the predictions performed during this study were for weldments with the reinforcement removed. Weldments with reinforcement left intact will generally fail at the weld toe which proves to be a much more severe defect than internal porosity[1-5].

The developed model was used to predict fatigue lives of tests performed on a limited number of weld specimens containing internal porosity as a calibration exercise. The predicted lives were generally within a factor of two of the actual lives.

Four types of porosity were examined using the predictive model: uniform porosity, a single pore, co-linear porosity and cluster porosity. Fatigue life predictions are made for each of the porosity types using different plate thicknesses, residual stresses, pore sizes, and loading. For constant amplitude loading, three stress ratios are used. A variable amplitude history based upon SL-7 stress data was developed and applied in the model for all four types of porosity. The material used for all the predictions is EH36. Because the fatigue and crack growth properties of a wide class of steels do not differ significantly from this material, the trends developed are probably applicable to many ship steels.

4. LITERATURE SURVEY

The work in the literature review was directed at definition of the problem, identification of factors controlling fatigue life and identification of available life prediction concepts and approaches to deal with porosity. Areas of emphasis were: stress analysis and stress-intensity solutions for volumetric stress raisers; weld induced residual stress fields; nondestructive inspection sensitivity and threshold in the laboratory and in field applications; materials, da/dN, and K_{Ic} for marine materials, particularly those with porosity problems; and analysis methods used to assess porosity effects on integrity.

4.1. Stress Analysis and Stress-Intensity Solutions for Volumetric Stress Raisers

4.1.1. Stress Analysis of Cavities

Sternberg[13] and Savin[14] have made literature surveys on theoretical stress concentration factors for cavities and holes. These references list the papers related to three-dimensional stress concentrations around spherical, spheroidal and ellipsoidal cavities in an infinite or finite elastic medium. The mutual effect of two or more spherical cavities in an infinite body and the interference between a spherical cavity and external boundary are also included in these references. Tsuchida and Nakahara[15] studied a three dimensional stress concentration around a spherical cavity in a semi-infinite elastic body. Mokarov[16] experimentally determined the stress distribution around a chain consisting of three spherical pores and a chain consisting of two different pores.

Lundin[17] described the primary types of porosity that may be of concern in welding as follows: (1) uniformly scattered (distributed) porosity; (2) cluster (localized) porosity; (3) linear (aligned) porosity; (4) wormhole (elongated) porosity. (Porosity in weld metals is generally spherical or wormshaped. Elongated spherical porosity is rarely found in the weld metal.) Masubuchi[18] has shown that stress concentration factors around porosity (under uniaxial loading) are generally below K_t = 4.0. Stress concentration factors around porosity are generally low. A qualitative discussion of stress fields near cavities is presented in Section 6 titled "Ellipsoidal Cavities".

4.1.2. Stress Intensity Factor for Volumetric Stress Raiser

Using a superposition method, Krstic[19] obtained a stress intensity factor solution for an annular flaw emanating from the surface of a spherical cavity. Stress intensity factor handbooks[20,21] contain three-dimensional solutions for circular and elliptical cracks in a solid.

4.2. Weld-Induced Residual Stress Fields

In Chapter 6 of Reference 22, Masubuchi has a comprehensive discussion of the magnitude and distribution of residual stresses in steel, aluminum alloys, and titanium alloys weldments. Local residual stresses at the surface of pores are not reported in the literature.

The fatigue severity of porosity relative to other weld discontinuities such as weld toe or ripple depends on both the stress concentration factors and residual stresses. Porosity which is located in zones of high tensile residual stresses might be the critical sites for fatigue failure. Babev[23] has found that the dimensions and distributions of porosity had little influence on the fatigue resistance of welds if it is located in a high residual tensile stress field.

4.3. Nondestructive Inspection Sensitivity and Threshold in the Laboratory and in Field Applications

Barsom[24] has found that the probability of detecting small discontinuities is remote. Porosity might obscure other defects. For example, planar defects may be embedded in cluster porosity and can not be detected using nondestructive methods.

4.4. Fatigue Crack Growth Data, Fracture Toughness, and Strain-Controlled Fatigue Behavior for Marine Materials (Particularly Those With Porosity Problems)

Masubuchi[22,25] has extensively reviewed the materials used for marine engineering. Marine welded structures are primarily made of steels, aluminum alloys, and titanium alloys. The steels include carbon steels, high strength low alloy steels, quenched-and-tempered steels, and maraging steels. Aluminum alloys in the 5xxx series and the 7xxx series are used extensively in marine applications. Among the titanium alloys, pure titanium and the Ti-6Al-4V alloy have been most commonly used. Although there are many causes of porosity in fusion welds, aluminum alloys and titanium alloys are more active than steels and thus prone to weld porosity.

4.4.1 Fatigue Crack Growth Data

Hudson and Seward[26,27] have compiled a list of sources of fracture toughness and fatigue crack growth data for alloys. This list covers many marine metallic materials. Most of the fatigue crack growth data is for the base metal. There is very little data available for weld metals and heat affected-zone (HAZs). Maddox[28] has conducted tests on a variety of structural C-Mn steels base-metals, weld-metals, and HAZs. The test results show that the rates of fatigue crack growth in weld metals and HAZs are equal or less than that in the base metal. Therefore, the upper scatter band of fatigue crack growth rates for base metals can be used to obtain conservative engineering estimates of the fatigue crack growth rates in base metals, weld metals, and HAZs. Barsom[29] has suggested upper scatter band equations for martensitic steels, ferritic-pearlitic steels, and austenitic steels.

4.4.2. Fracture Toughness

In general, there are four types of fracture toughness tests used for marine welded structures[30]: (1) the Charpy impact tests; (2) the Drop Weight tests (DWT), or the closely related Dynamic Tear Test; (3) fracture mechanics tests to measure critical stress intensity factors (K_c or K_{Ic}) or critical values of the J-integral (J_c or J_{Ic}); (4) the Crack-Tip-Opening Displacement (CTOD or COD) test. Masubuchi, et al.[31] have done a literature survey on the notch toughness of weld metals and the HAZs, evaluated primarily by the Charpy V-notch impact test. Ship Structure Committee Reports 248[32] and 276[33] present fracture toughness characterization of ship steels and weldments using Charpy impact test, DWT test, and explosion structural tests. References[26,27] list fracture toughness for many of the marine metallic materials. Lawrence, et al.[34] studied the effects of porosity on the fracture toughness of three aluminum alloy weldments using DWT energy and J integral.

4.4.3. Strain-Controlled Fatigue Behavior

Very few strain-controlled fatigue properties are available for marine materials. References[35,36] provide several cyclic fatigue properties for the base metals, weld metals, and HAZs of various steels and aluminum alloys.

4.5. Analysis Methods Used to Assess the Effects of Porosity on Structure Integrity

British Standards institute Document PD6493:1980[37] provides guidance on some methods for the derivation of acceptance levels (fitness for service) for defects in fusion welded joints. In the section below, the analysis methods used to assess the effect of porosity on the fatigue performance of weldments will be discussed.

4.5.1 Previously Used Methods

4.5.1.1. Harrison's "Quality Bands" Method

Harrison[1] presented a fitness-for-service evaluation of porosity as shown in Figure 1. The levels shown for quality bands denoted as V, W, X, Y, Z and corresponding to 0, 3, 8, 20 and 20+ percent porosity were drawn based on the available data. Figure 1 also shows the comparison of quality band method with fatigue test results. This method generally gives conservative and lower-bound fatigue resistance estimates for weldments with porosity.

4.5.1.2. Hirt and Fisher's LEFM Analysis

Hirt and Fisher[38] have studied the influence of porosity on the fatigue behavior of longitudinal web-to-flange welds by assuming the pores to be circular penny-shaped cracks. Linear elastic fracture mechanics was used to calculate the fatigue crack propagation life. This approach may be very conservative because the pores are generally rounded.

4.5.2. An Analysis Based on Total Fatigue Life - A Proposal

The most serious deficiency of the method of Hirt and Fisher is the neglect of the period of life devoted to fatigue crack initiation and early growth. A more accurate assessment of the effects of porosity on the fatigue life of marine structures could be obtained by adding estimates of fatigue crack initiation life to the fatigue propagation life using methods such as those of Lawrence, et al.[39] and Reemsnyder[40]. Both of these methods provide estimates of the fatigue crack initiation life and consider the important effects of mean and residual stresses. While LEFM provides good estimates of long crack growth, methods developed by Leis[41] could be used to improve the accuracy of fatigue crack propagation life estimates for the portion of the fatigue crack propagation life in which the dominant crack is located within the inelastic stress field of the notch (pore).

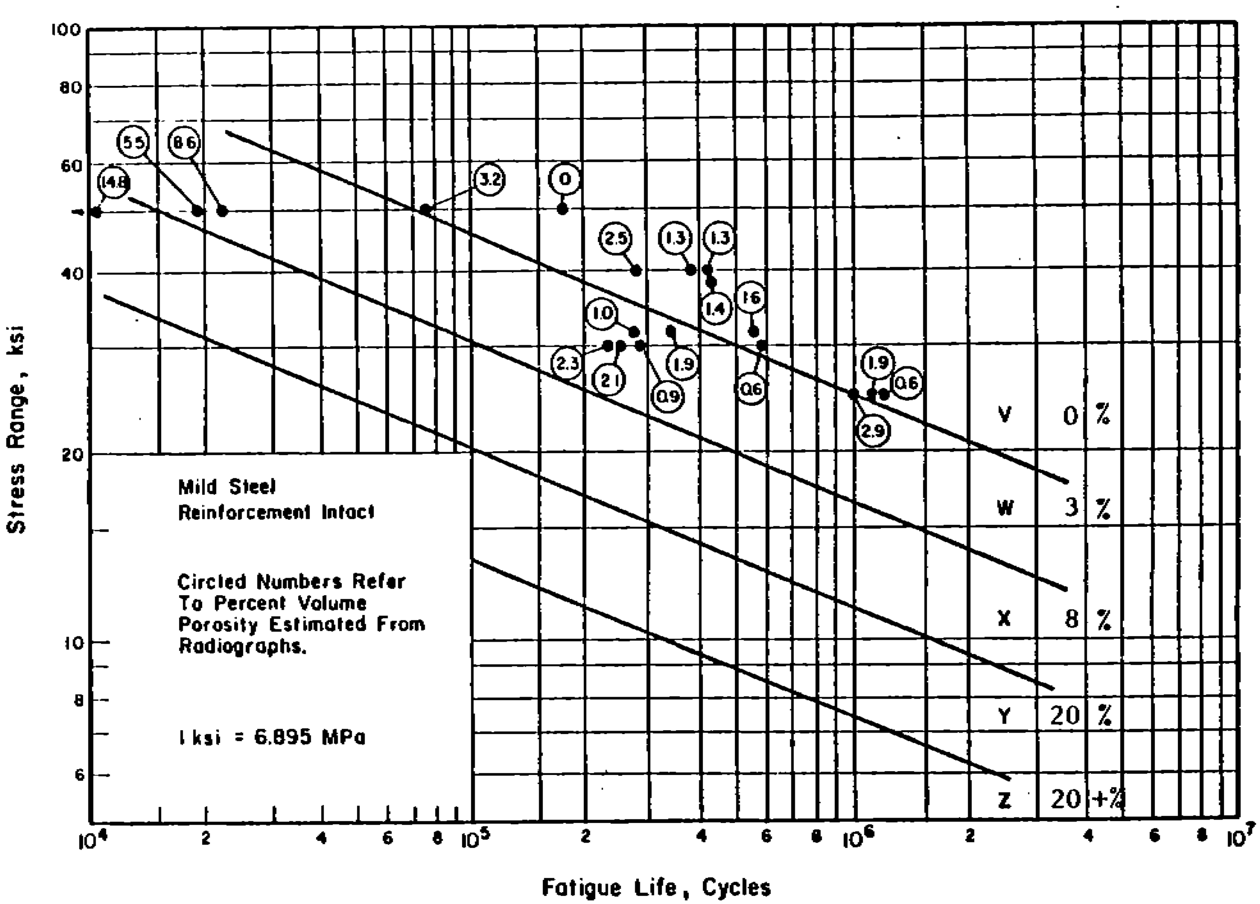

FIGURE 1. COMPARISON OF FATIGUE TEST RESULT WITH QUALITY BAND APPROACH FOR POROSITY

5. ANALYTICAL MODELING BACKGROUND

The model used to predict the fatigue lives of weldments used during this study consists of two parts; the crack initiation life, N_i, in cycles, and the crack propagation life, N_p, in cycles. The sum of these two components is the total life, N_t,

$$N_i + N_p = N_t \quad . \tag{1}$$

The crack initiation life is estimated using low cycle fatigue concepts and the crack propagation life is estimated using linear elastic fracture mechanics concepts. The intent of this section is to provide the low cycle fatigue and fracture mechanics background used in the development of the predictive model. In Section 7, titled Analytical Program, these concepts will be applied to single pores, co-linear porosity, uniform porosity, and pore clusters.

5.1 Initiation Life Model

Fatigue cracks generally initiate at a geometrical discontinuity such as a notch or pore. These act as stress concentrations, raising the stress in the region of the notch to levels above the nominal stresses. The material at the notch root may deform plastically while the rest of the component remains essentially elastic. Subjecting the region to cyclic loading resulting in plastic deformation will eventually result in a fatigue crack.

5.1.1 Notch Analysis

Determining the stresses and strains in the notch region after the onset of local plasticity requires a notch analysis technique. In the elastic range, the notch stress can be calculated using the elastic stress concentration factor, K_t. The K_t value is simply a conversion factor between the maximum principal notch stress, σ, and remote stress, S,

$$\sigma = K_t \; S \quad , \tag{2}$$

and is determined using elasticity theory or by finite element analysis. After the notch region material deforms plastically, however, the elastic stress concentration factor no longer applies as a direct conversion factor. The stress will rise at a lesser rate and the strain at a greater rate than during elastic deformation where both stress and strain rates were equal. Neuber's rule[42] is used to estimate the local stresses and strains in this situation. Nueber's rule states that the elastic stress concentration, K_t, will remain equal to the geometric mean of the instantaneous stress and strain concentration factors, K_σ and K_ϵ, respectively,

$$K_t = \left(K_\sigma \; K_\epsilon\right)^{1/2} \quad . \tag{3}$$

Rewriting this relation in terms of stress and strain ranges as

$$K_t = \left(\frac{\Delta\sigma \; \Delta\epsilon}{\Delta S \; \Delta e}\right)^{1/2}$$

where ΔS is the nominal stress range, and Δe is the nominal strain range, and recalling that

$$\Delta e = \Delta S \; / \; E \tag{4}$$

where E is the elastic modulus, Neuber's rule may be written for nominally elastic response as

$$\frac{\Delta S^2 \; K_t^2}{E} = \Delta\sigma \; \Delta\epsilon \quad .$$

This expression relates the local stress-strain response at the notch root to the nominal stress and elastic stress concentration factor. Furthermore, representing the stress-strain response of the material with power law hardening constants,

$$\Delta\epsilon = \frac{\Delta\sigma}{E} + \left(\frac{\Delta\sigma}{K}\right)^{1/n} \tag{5}$$

where K is the strength coefficient, and n is the strain hardening exponent, the relation can be written with $\Delta\sigma$ as the only unknown,

$$\frac{\Delta S^2}{E} \quad K_t^2 = \Delta\sigma \left(\frac{\Delta\sigma}{E} + \left(\frac{\Delta\sigma}{K}\right)^{1/n} \right) \quad .$$

Solving for $\Delta\sigma$ is accomplished using an iterative technique such as Newton's method.

5.1.2 Fatigue Notch Factor

In fatigue testing, it is generally observed that the actual lives of notched components are somewhat longer than would be expected for the notch root stress calculated using the elastic stress concentration factor, K_t. That is, notches have a less detrimental effect on fatigue life than would be predicted. This effect is dependent upon both defect size and material. To account for this difference, a fatigue notch factor, K_f, is often used in place of K_t for fatigue life predictions. The fatigue notch factor is defined as

$$K_f = \frac{\sigma_{\text{unnotched at a finite life (e.g. } 10^7)}}{\sigma_{\text{notched}}} \quad . \tag{6}$$

The value of K_f for a given notch geometry and material can be determined experimentally or by the use of analytical relations. A commonly used fatigue notch factor relation is Peterson's equation[43],

$$K_f = 1 + \left(\frac{K_t - 1}{1 + a/r} \right) , \tag{7}$$

where a is a material constant dependent on strength and ductility and r is the notch tip radius. The material constant a can be approximated for ferrous-based wrought metals by an equation fitted to Peterson's data,

$$a = \left(\frac{300}{S_u} \right)^{1.8} \times 10^{-3} \text{ in.} \tag{8}$$

where S_u is the ultimate strength in ksi units. Peterson's equation indicates that small notches are least sensitive in fatigue, and that ductile materials are less sensitive to notches in fatigue than strong materials.

5.1.3 Notch Strains and Low Cycle Fatigue

Using Nueber's rule for notch root stress-strain behavior along with Peterson's equation for the fatigue notch factor, it is possible to estimate the stress-strain response of the notch root material subjected to fatigue loading. It still remains to relate these local stresses and strains to actual fatigue life data. Because the plastically deformed notch root material is constrained by the surrounding elastic material, the notch root is nearly in a strain-control condition. The notch root material is essentially cycled between strain limits analogous to strain-control, low cycle fatigue testing. The assumption, therefore, is that strain-life fatigue data obtained using unnotched, low cycle fatigue specimens can be used to predict the cycles to crack initiation, N_i, at a notch root. Low cycle fatigue strain-life data is often represented by the Coffin-Manson equation with Morrow's mean stress correction,

$$\frac{\Delta\epsilon}{2} = \epsilon_f'(2N_f)^c + \left(\frac{\sigma_f' - \sigma_m}{E}\right)(2N_f)^b \tag{9}$$

where $\Delta\epsilon/2$ is the strain amplitude, ϵ_f' is the fatigue ductility coefficient, σ_f' is of the fatigue strength coefficient, σ_m is the mean stress, $2N_f$ is the reversals to failure, N_f is the cycles to failure, c is the fatigue ductility exponent, and b is the fatigue strength exponent. By relating the strain calculated at the notch root to the strain-life data, the number of cycles to initiate a fatigue crack at the notch can be estimated. This is the basis of the initiation life predictions. The strain-life data parameters, ϵ_f', σ_f', c, and b, are obtained either by low cycle fatigue testing or by using estimates.[44]

5.2. Propagation Life Model

5.2.1. Fatigue Crack Growth Rate

Paris and Erdogan[45] have shown that fatigue crack growth rates are dependent upon the stress intensity associated with the fatigue crack tip. The power-law relationship is of the form

$$\frac{da}{dN} = A\,\Delta K^m \quad . \tag{10}$$

where da/dN is the fatigue crack growth rate, ΔK is the stress intensity factor range, and A and m are material constants dependent upon environment, stress ratio, temperature, and frequency. This relationship is considered valid above an experimentally determined threshold stress intensity value. Below the threshold value, fatigue cracks grow so slowly as to be of no practical consequence. The growth rate expression used throughout this study has a correction factor to account for mean stress effects,

$$\frac{da}{dN} = \frac{A\ \Delta K^m}{1-R} \quad ,$$

where R is the stress ratio,

$$R = S_{min}/S_{max} \quad . \tag{11}$$

<u>5.2.2. Stress Intensity Factor</u>

The general relationship for the stress intensity factor range is written as

$$\Delta K = Y\ \Delta S\ (\pi\ a)^{1/2} \quad , \tag{12}$$

where Y is a geometry dependent factor, ΔS is the stress range, and a is the crack length. The geometry factor Y is actually composed of a number of separate multplicative geometry factors which account for the shape of the crack, the thickness of the component or specimen, and the position of the crack within the body. The value Y is written as

$$Y = \frac{M_s\ M_t\ M_k}{\Phi_0} \tag{13}$$

where M_s accounts for the free front surface, M_t accounts for the finite plate thickness, M_k accounts for the nonuniform stress gradient due to the stress concentration of the geometric discontinuity, and Φ_0 accounts for the crack shape.

The M_s factor, which accounts for the front free surface, is expressed by the relation[46]

$$M_s = 1.0 - 0.12(1 - a/2c)^2 \tag{14}$$

where a/c is the ratio of the minor and major ellipse axes. The majority of cracks examined in this study, however, are embedded in the material, so the free surface correction is equal to unity.

The M_t factor, which accounts for the finite plate thickness, is found in stress intensity handbooks such as[20,21]. The M_k factor requires a brief explanation. The need for such a factor arises because the stress, σ, near a discontinuity is greater than the remotely applied stress, S, used to calculate ΔK. A crack tip growing through the stress gradient is therefore subjected to higher stresses which result in a greater stress intensity factor range, ΔK. Not accounting for this increase in stress intensity would lead to unconservative predicted growth rates near the discontinuity. The discrepancy in total life would be greatest for large notches because the stress gradient is sustained in proportion to the absolute notch size. The subject of stress intensity factors in stress gradients is examined by Albrecht and Yamada[47]. The method presented in Reference 47 is used to calculate M_k in the present study.

The crack shape correction factor, Φ_0, is expressed by the integral

$$\Phi_0 = \int_0^{\pi/2} [1-(1-a^2/c^2) \sin^2\Phi]^{1/2} \quad d\Phi \tag{15}$$

where a is the length of minor axis of ellipse and c is the length of the major axis.

6. STRESS FIELDS NEAR INTERNAL CAVITIES

Porosity is defined as cavity type discontinuities (voids) formed by gas entrapment during solidification. The shape of the void is dependent on the relative rates of solidification of the weld metal and the nucleation of the entrapped gas. The resultant stress field surrounding the pore depends upon the pore shape and the loading.

6.1. Ellipsoidal Cavities

The shape of porosity can be generalized for analytical purposes as an ellipsoid. The coordinate system defining the cavity is shown in Figure 2. Pore shapes can range from an oblate ellipsoid (a=b=1) to a sphere (a=b=c=1) to a prolate ellipsoid (b=c=1) or any shape in between, as shown in Figure 3. The elastic solution for the stress field around a triaxial ellipsoidal cavity in an infinite medium has been found by Sadowsky and Sternberg[48]. The stress in the plots in Figure 3, σ_z, is the local stress resulting from an applied uniaxial stress, S_z, of unity.

Some general characteristics of the stress fields are worth noting. Subject to a uniaxially applied stress of S_z, the maximum stress concentration will always occur at the minor axis of the x-y plane ellipse, point B. The stress σ_z, therefore, is plotted relative to point B along the y axis. In the limiting cases, when a=b=1 and c approaches 0, the stress σ_z tends toward infinity, representing the case of an embedded penny-shaped crack. As c approaches infinity, σ_z tends toward the remote stress, S_z. When b=c=1, and a also equals 1, the solution is that for a sphere. As a approaches infinity, the solution coincides with that of a hole in a plate with a stress concentration of 3.

These solutions are for cavities in an infinite medium. In application to weld porosity, they are valid if the size of the cavity is small in relation to the dimensions of the weldment.

6.2. Spherical Cavities in a Semi-Infinite Medium

The elastic solution for the stress field near a spherical cavity in a semi-infinite medium has been found by Tsuchida and Nakahara[15]. Figure 4 shows the effect of increasing stress concentration as the distance between the surface and the pore decrease. The plot also shows that the presence of the surface has little effect on the stress field

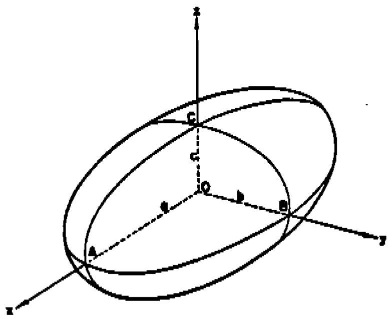

FIGURE 2. ELLIPSOIDAL CAVITY AND CARTESIAN CO-ORDINATE SYSTEM

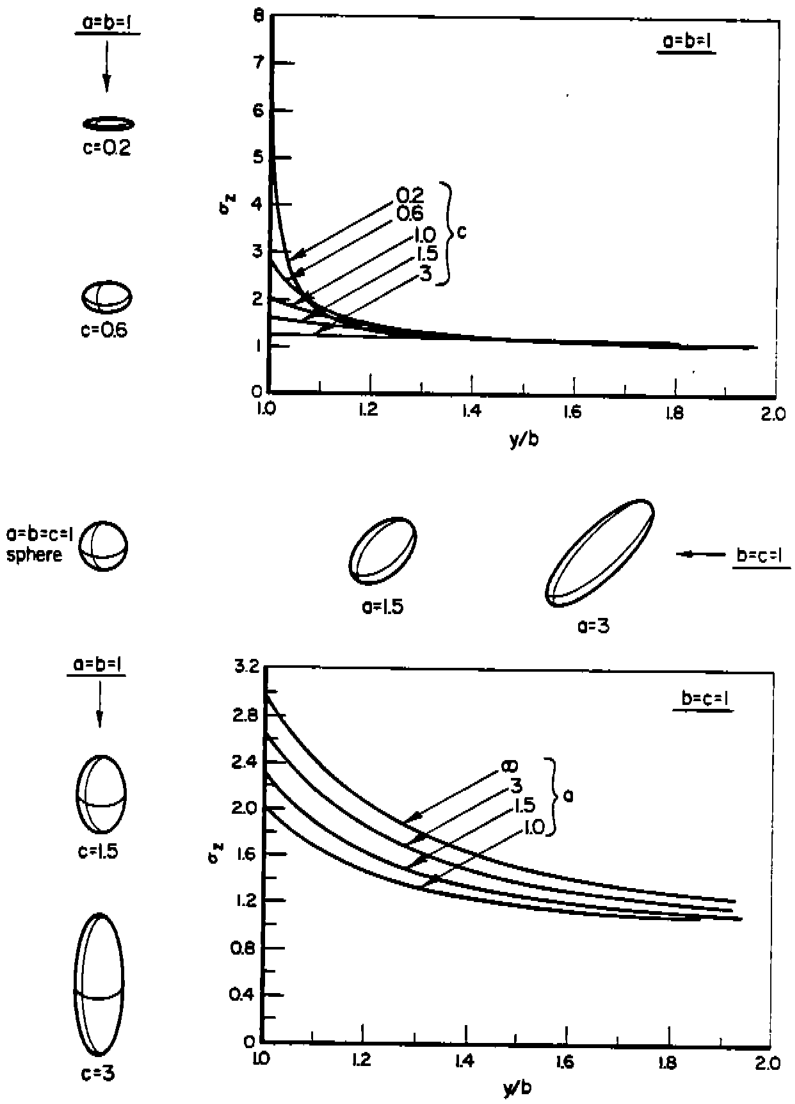

FIGURE 3. LOCAL STRESS, σ_Z, ALONG Y AXIS, FOR VARIOUS ELLIPSOIDAL CAVITIES SUBJECTED TO NOMINAL STRESS, S_Z, OF UNITY

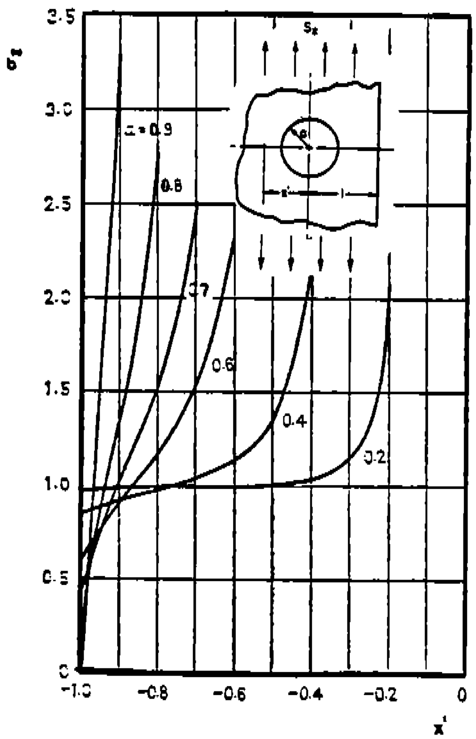

FIGURE 4. LOCAL STRESS, σ_Z, ALONG X' AXIS, FOR SPHERICAL CAVITY NEAR A SURFACE, SUBJECTED TO NOMINAL STRESS, S_Z, OF UNITY

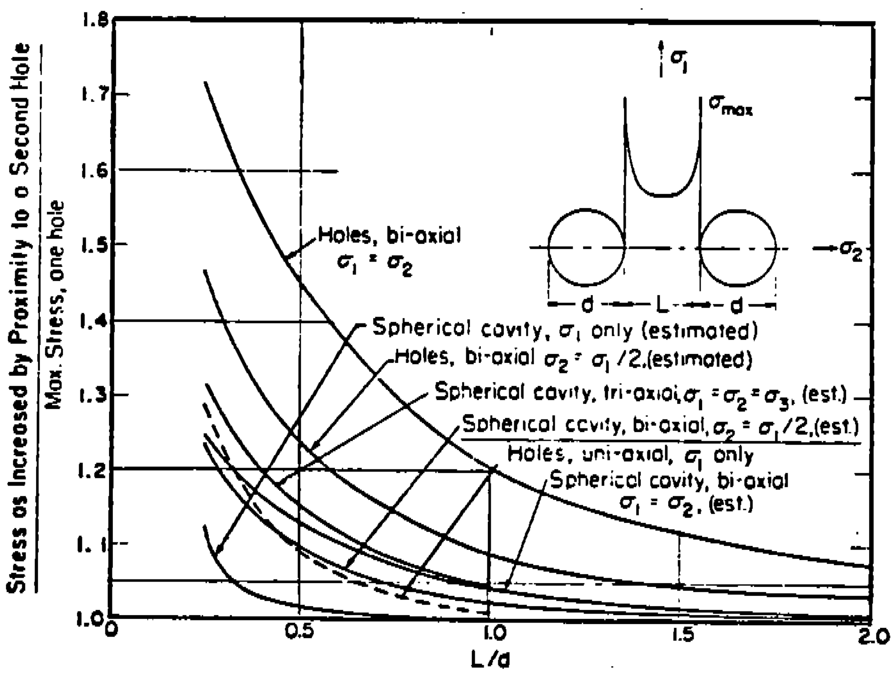

FIGURE 5. INTERACTION EFFECT OF TWO HOLES OR CAVITIES IN AN INFINITE PLATE OR BODY

when the ratio of the pore radius to the distance between pore center and surface is less than 0.4.

6.3. Cavity Interaction

The problem of cavity interaction is complex and correspondingly there is little information available on the topic. Sadowsky and Sternberg[48] examined the problem and solved two specific cavity spacings for triaxial loading. Peterson[49] took these results and made approximations for the uniaxial case. The results are presented in Figure 5 along with solutions for holes. During the present study, cavity interaction was assumed only for the case of cluster porosity where pores are expected to be in close proximity to each other. All other pores were assumed to be non-interacting. Markarov[16] has demonstrated through photoelastic techniques that cavities separated by two pore diameters do not effect the stress distribution of the other.

7. ANALYTICAL PROGRAM

7.1. Application of Initiation-Propagation Model to Porosity

7.1.1 Initiation Life

Volumetric discontinuities such as pores act as relatively mild stress concentrations because of their rounded asperities. A spherical cavity, for instance, has a stress concentration factor of only 2.05 (with Poisson's ratio of 0.3). The low stress concentration suggests that a fatigue crack would take a large number of stress cycles to initiate. For smaller pores more cycles would be needed because of the fatigue notch size effect, K_f. Larger pores would be expected to initiate cracks sooner.

7.1.2 Propagation Life

When a crack does form, it initially has a high stress intensity factor range, ΔK, while growing through the pore stress gradient. The stress gradient, however, decays rapidly as is characteristic of volumetric defects. The larger the pore size, the longer the distance that the crack is subjected to the higher stress because the gradient is sustained in proportion to the absolute pore size. The crack shape is assumed to remain circular while it propagates. A circular crack shape is the most energetically stable planar flaw configuration for Mode I crack growth. Considering Equation 13, Φ_0 for a circular crack is 1.57 whereas Φ_0 for an elliptical crack with a small a/c aspect ratio is nearly 1.0. This means that a circular crack will have only 0.6 times the stress intensity factor range, ΔK, than an elliptical crack with a small aspect ratio and an equal crack front (a) dimension.

A plasticity crack length correction factor was not used in the crack growth calculations. The generally low stresses (nominally elastic) used in this study results in a small plastic zone size at the crack tip. The confined yield zone assumption means that LEFM is valid for most of the propagation calculation.

7.1.3 Initial Crack Size

The initial crack size used in the propagation estimates was taken as 0.05 times the pore diameter. This assumption starts the crack at the same distance relative to the stress gradient in all cases. The initial crack length is considered to be beyond the region were anomalous crack growth behavior when analyzed in terms of LEFM occurs. Smith and Miller[50] found that the transition length between anomalous behavior and that governed by LEFM to be 0.065 times the diameter for a circular hole. This distance would be expected to be somewhat less for a three-dimensional flow such as a pore.

7.1.4 Failure Criteria

The failure criteria for all cases is through thickness cracking.

7.2. Viability of the Fatigue Life Model

The literature was searched for fatigue tests on weldments containing porosity with sufficient documentation to apply the predictive model. The most useful type of documentation was fractographs of the surfaces which clearly showed the sizes, shapes, and positional relationships of the porosity. Only two test programs[6,51] were found which included such fractographs. A total of eight fatigue tests were found to which the model could be applied. Neither of these test programs, however, included material property data for the weld metal. Both test series used E70 weld metal in a gas-metal-arc welding process. The method for introducing porosity into the weld metal was interruption of the shielding gas flow in both studies.

Because no fatigue material property data was available for E70 weld metal, E60 S-3 (2 pass) weld metal[36] properties were used as the baseline data. The mechanical properties of E60 S-3 (2 pass) weld metal is shown in Table 1 and Figures 6 and 7.

Leis, et al.[6] performed axial fatigue tests on pipe wall segments with girth welds in A106B steel. The weld reinforcement was left intact, but the weld toe was ground to a large radius to cause fatigue crack initiation from the internal flaws. Three tests contained sufficient porosity that allowed application of the model. The fractographs of these specimens are shown in Figure 8(a-c). The porosity clusters are ellipsoidal in shape and include individual pores of approximately 0.02 inches in diameter. Within the cluster area, the percent porosity is approximately forty percent by area.

Ekstrom and Munse[51] performed fatigue tests on a double V butt weld geometry. In this test program, the reinforcement was completely removed to cause internal crack initiation. Five tests included welds with severe porosity. The fracture surfaces for these test pieces are shown in Figure 8(d-h).

TABLE 1. MECHANICAL PROPERTIES OF E60 S-3(2P) WELD METAL

Monotonic Properties			
Young's Modulus,	E	27400 ksi	188923 MPa
Yield Strength (0.2%)	S_y	59 ksi	408 MPa
Tensile Strength	S_u	84 ksi	579 MPa
Reduction in Area	% RA	60.7	60.7
True Fracture Strength	σ_f	126 ksi	869 MPa
True Fracture Ductility	ϵ_f	0.933	0.933
Cyclic Properties			
Cyclic Yield Strength	σ'_y	53 ksi	373 MPa
Cyclic Strength Coefficient	K'	179 ksi	1234 MPa
Cyclic Strain Hardening Exponent	n'	0.197	0.197
Fatigue Strength Coefficient	σ'_f	149 ksi	1027 MPa
Fatigue Strength Exponent	b	-0.09	-0.09
Fatigue Ductility Coefficient	ϵ'_f	0.602	0.602
Fatigue Ductility Exponent	c	-0.567	-0.567
Propagation Properties			
Crack Growth Coefficient	A	2.69×10^{-12}	3.95×10^{-14}
Crack Growth Exponent	m	5.8	5.8

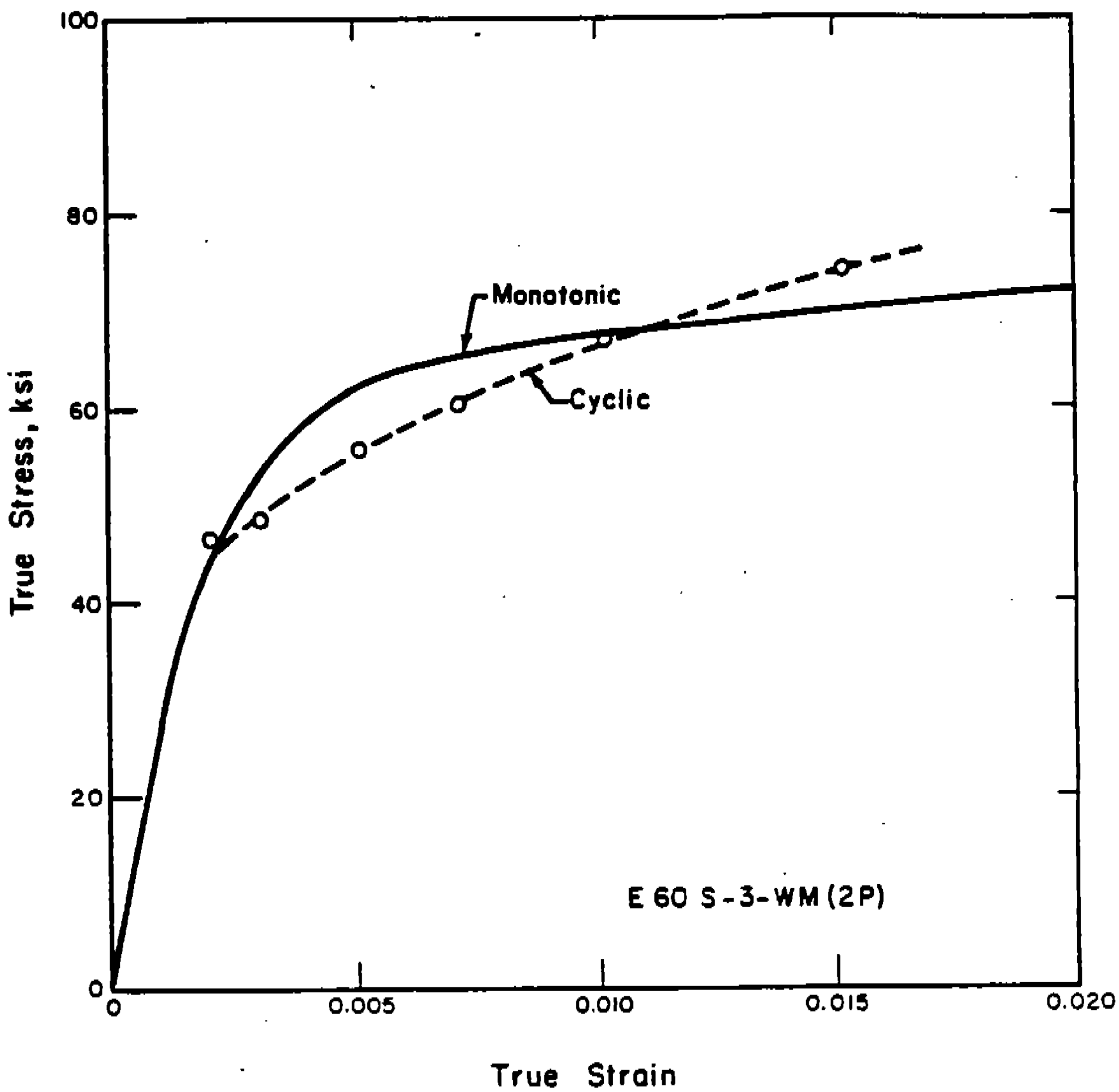

FIGURE 6. MONOTONIC AND CYCLIC STRESS-STRAIN RESPONSE FOR E60 S-3 WELD METAL (2 PASS)

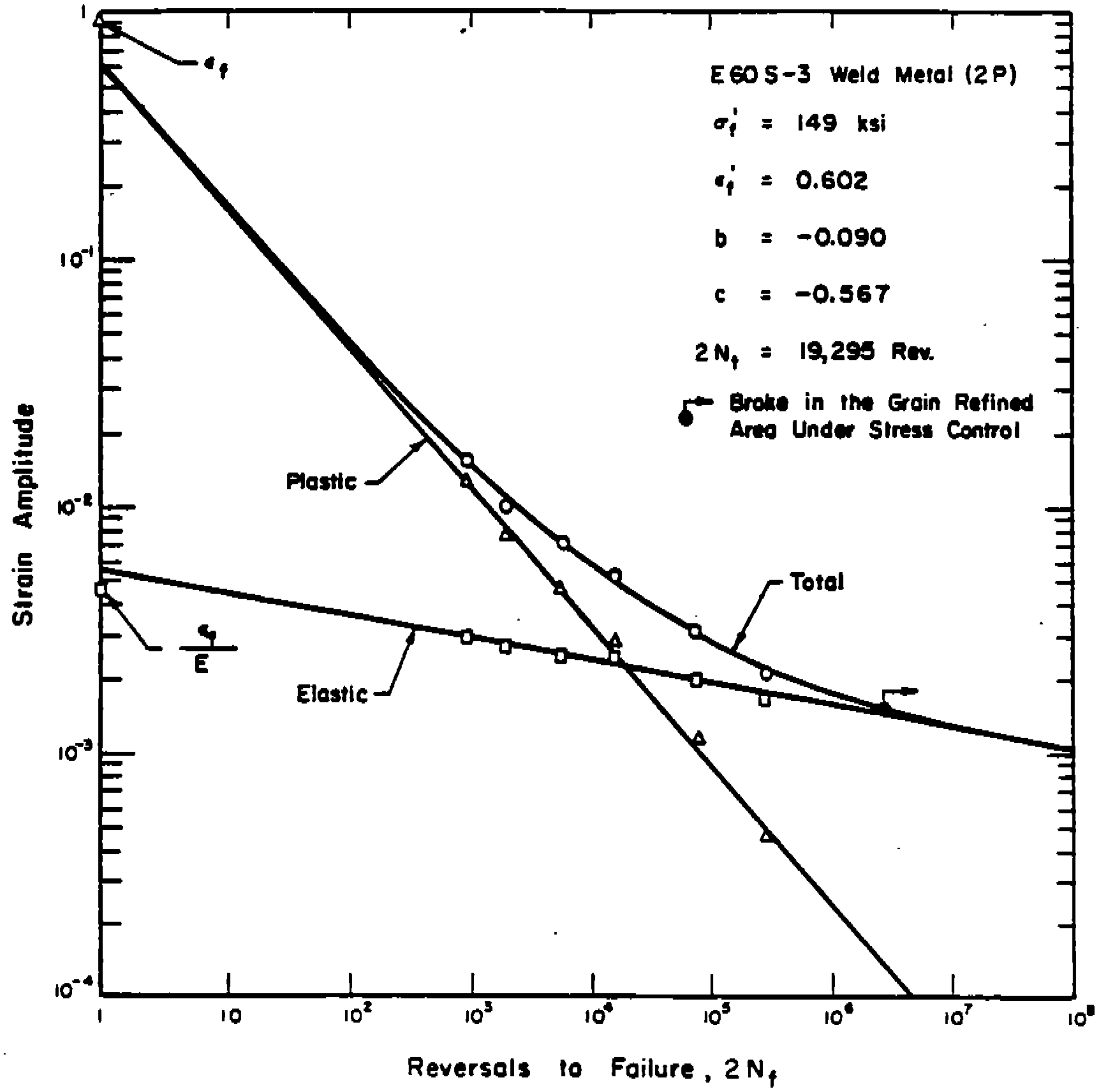

FIGURE 7. STRAIN-LIFE DATA FOR E60 S-3 WELD METAL

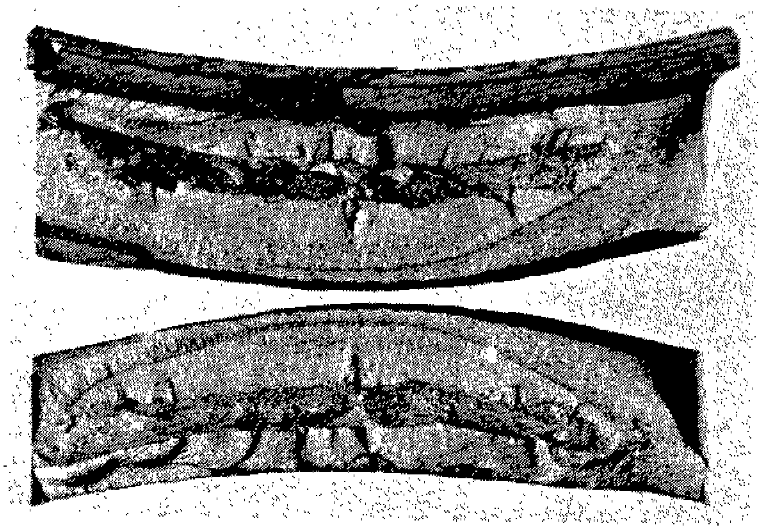

(a) CPN-2 Stress Range 27.5 ksi, Life - 2,115,600

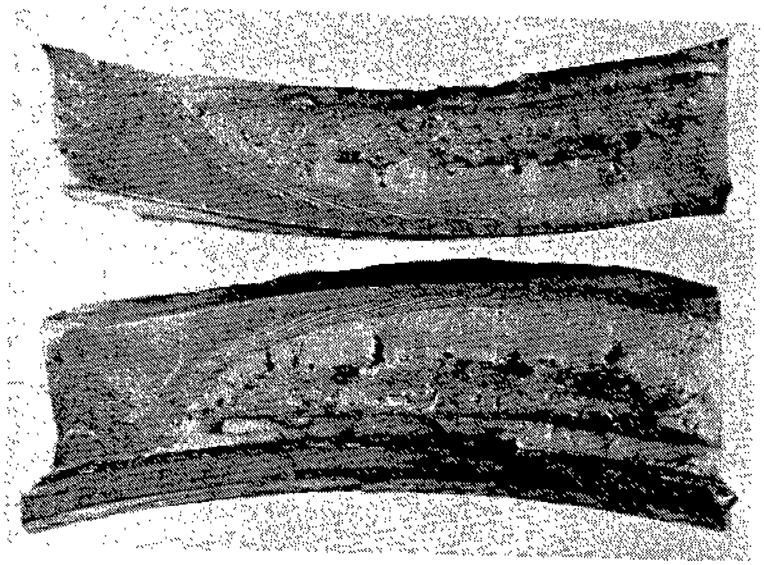

(b) CPN-4 Stress Range 33 ksi, Life - 54,600

(c) CPN-5 Stress Range 27.5 ksi, Life - 334,100

FIGURE 8. FRACTURE SURFACES OF WELDS WITH CLUSTERS OF POROSITY

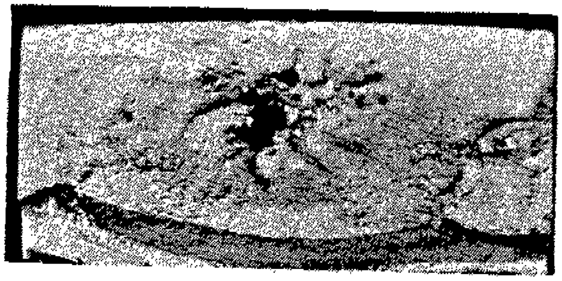

(d) PS 5-1
Stress Range 34 ksi
Life - 713,300

(e) PS 5-2
Stress Range 34 ksi
Life - 325,500

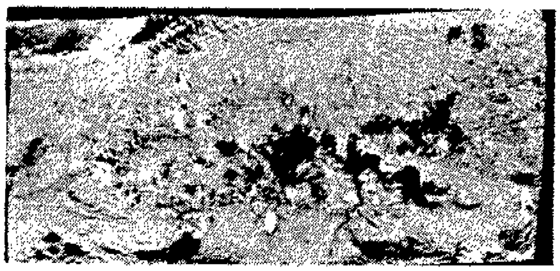

(f) PS 5-3
Stress Range 44 ksi
Life - 80,300

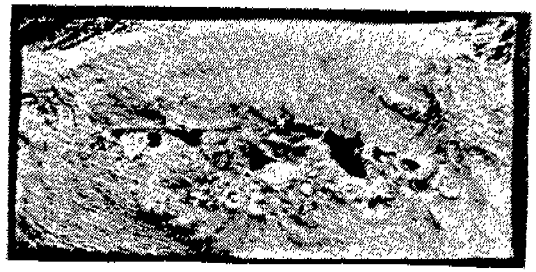

(g) PS 5-4
Stress Range 29 ksi
Life - 633,000

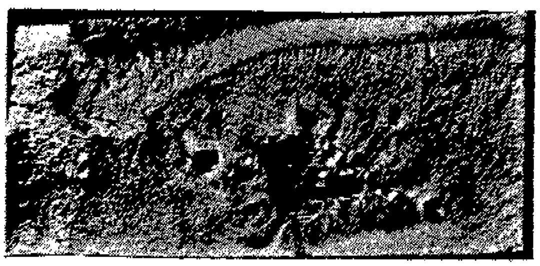

(h) PS 5-5
Stress Range 27 ksi
Life - 1,024,900

FIGURE 8. FRACTURE SURFACES OF WELDS WITH CLUSTERS OF POROSITY
(Continued)

Fatigue life predictions were made for all eight tests using the model described in Section 7.3.6. All the individual pores were assumed to be spherical so an elastic stress concentration factor, K_t, of 2.05 was applied. In those cases were interaction was assumed an additional factor of 1.12 was applied. Table 2 lists the experimental test results and the fatigue predictions for each test. For each test, the following predictions are presented: predicted fatigue life at the specified test stress range; predicted stress range for the specified fatigue life; predicted fatigue life for specified test stress range treating the porosity cluster as a gross ellipsoidal cavity with dimensions a, b, and c; and fatigue life predictions using only the reduced cross sectional area without assuming a stress concentration. The results show that treating the pore cluster as a gross ellipsoidal cavity is somewhat conservative while considering the flaw as merely a reduction in cross sectional area is very unconservative. Applying the model for cluster porosity resulted in good estimate for fatigue life and, when viewed in terms of stress, even better estimates. The absolute magnitude of the predictions are not as important as the trends because of the uncertainty in material properties. Figure 9(a) shows the comparison between experimental and predicted fatigue lives and Figure 9(b) shows the comparison between the experimental and predicted stress ranges for the test life.

The predicted lives are dominated by the crack initiation period. This is due mainly to the size of the defects with respect to the cross sectional area of the specimen. The initiation life is considered to be the number of cycles until the crack begins growing radially away from the defect cluster. This includes the period of crack coalescence between the pores. After the cracks between the pores coalesce, the material at the outer portion of the periphery pores are assumed to initiate a crack and grow toward the surface. At this point the net cross sectional area is greatly decreased and the resultant higher stresses propagate the crack rapidly until failure.

These predictions are based on a limited sample of weldments and therefore can not be considered conclusive evidence that the predictive model is viable or not. It should be noted, however, that assuming an

TABLE 2. FATIGUE TEST RESULTS AND PREDICTIONS OF WELDS CONTAINING PORO

Specimen Number	Nominal Stress Range, ksi	Stress Ratio	Area Percent Porosity	Gross Flaw Dim.	Actual Fatigue Life, cycles		Predicted Fatigue Life, cycles Ni	Np	Nt
CPN-4	32.7	0.1	6.3	a=0.67	54,600	Cluster Method:	135,083	68	135,151
				b=0.075		Gross Flaw:	1,271	68	1,339
				c=0.038		Percent Area:			3.0e6
CPN-2	27.2	0.1	6.3	a=0.80	2,115,600	Cluster Method:	771,973	319	772,292
				b=0.063		Gross Flaw:	3,106	319	3,425
				c=0.032		Percent Area:			2.3e9
CPN-5	27.2	0.1	11.8	a=0.75	334,100	Cluster Method:	463,788	17	463,805
				b=0.12		Gross Flaw:	145	17	162
				c=0.032		Percent Area:			6.7e9
PS5-3	44.0	0.222	8.4	a=0.34	80,300	Cluster Method:	21,540	12	21,552
				b=0.13		Gross Flaw:	1,174	12	1,186
				c=0.078		Percent Area:			1.7e7
PS5-2	34.0	-0.056	4.6	a=0.29	325,500	Cluster Method:	570,142	29	570,171
				b=0.14		Gross Flaw:	1,534	29	1,563
				c=0.062		Percent Area:			2.9e7
PS5-1	34.0	-0.056	2.2	a=0.27	713,300	Cluster Method:	717,814	394	718,208
				b=0.12		Gross Flaw:	30,865	394	31,259
				c=0.12		Percent Area:			3.7e7
PS5-4	29.0	0.195	3.1	a=0.43	633,000	Cluster Method:	444,026	119	444,145
				b=0.12		Gross Flaw:	6,776	119	6,895
				c=0.093		Percent Area:			7.7e7
PS5-5	27.0	0.250	4.5	a=0.39	1,024,900	Cluster Method:	2,177,281	142	2,177,423
				b=0.12		Gross Flaw:	2,119	142	2,261
				c=0.062		Percent Area:			1.8e9

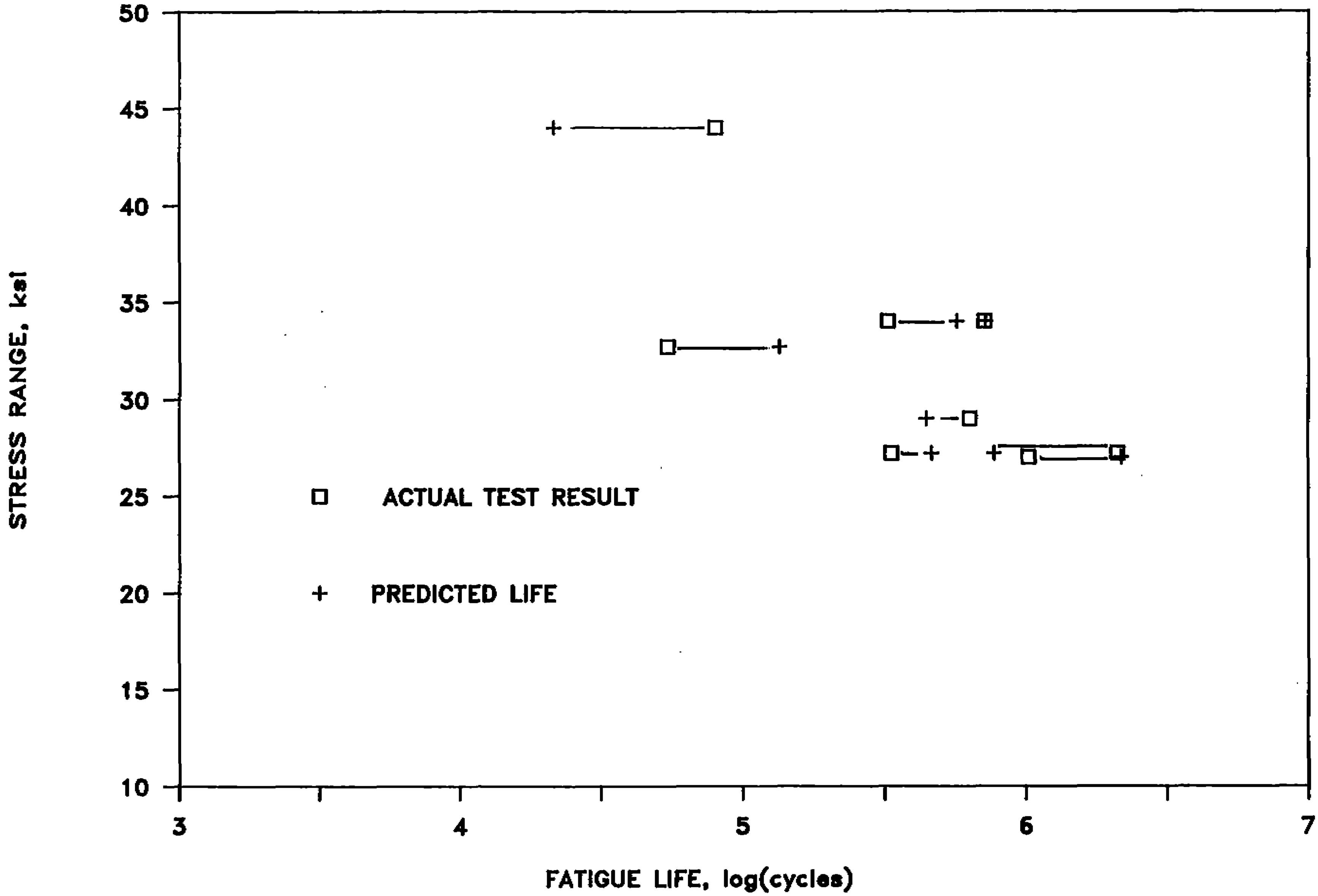

FIGURE 9(a). STRESS-LIFE PLOT SHOWING ACTUAL FATIGUE LIVES VERSUS PREDICTED FATIGUE LIVES OF WELDS CONTAINING POROSITY

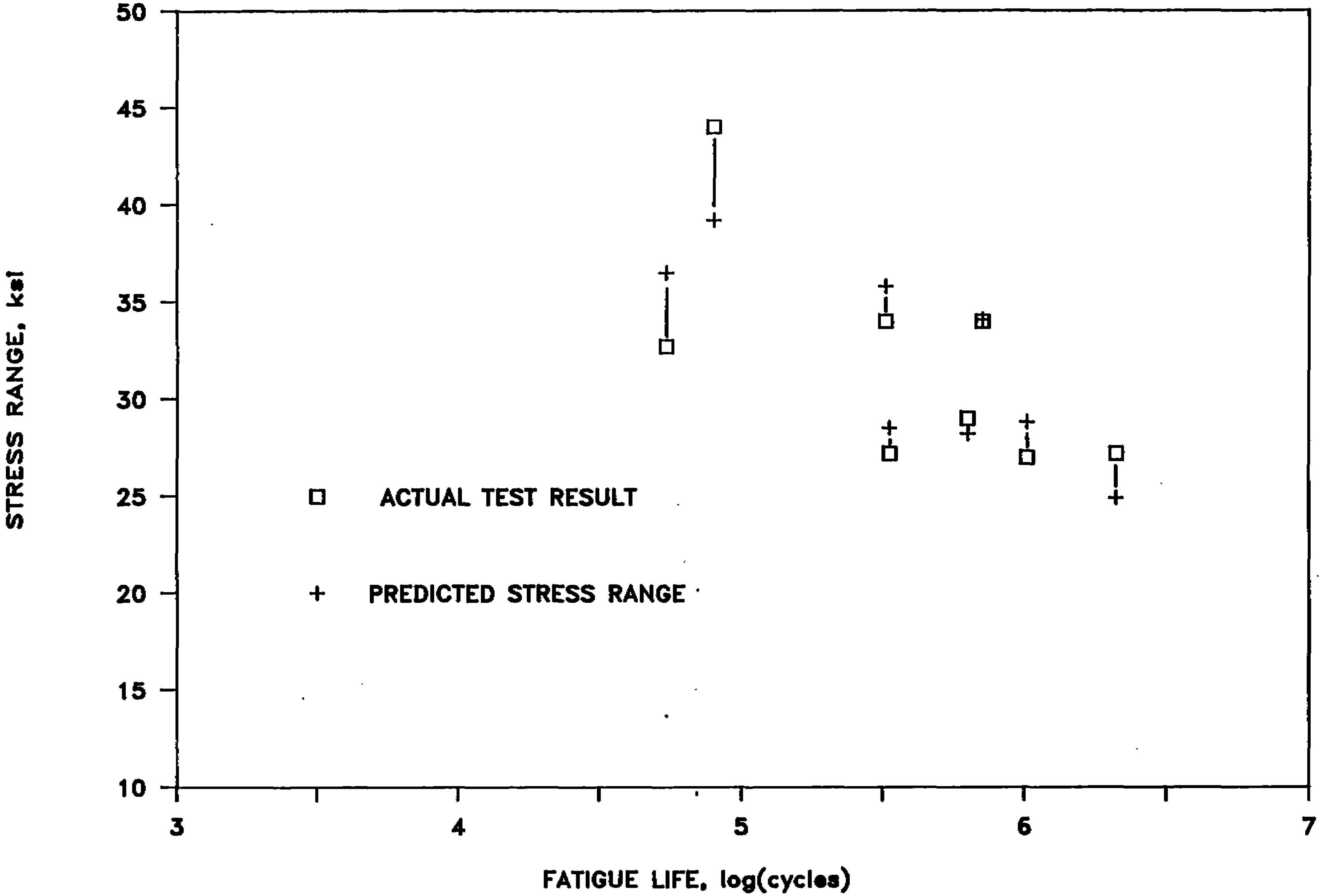

FIGURE 9(b). STRESS-LIFE PLOT SHOWING ACTUAL STRAIN RANGE VERSUS PREDICTED STRESS RANGE OF WELDS CONTAINING POROSITY existing crack-like defect equal to the size of the cluster would lead to grossly conservative life estimates (equal to the propagation lives). The model seems to reflect the correct trends for the fatigue lives of the specimens tested. The results are even more encouraging when considering percent error in stress range predicted to yield the fatigue life of the sample. A number of uncertainties such as using approximate mechanical properties data and estimating the percent area porosity and pore sizes from photographs will certainly contribute to the scatter in the predictions. The small sample size also compounds the problem. The results are encouraging, but further testing is warranted to validate its accuracy.

7.3. Parametric Study

From the literature review, the parameters which have been found to influence the fatigue lives of weldments containing porosity are: weld type, material, thickness, residual stress, loading, porosity type, and pore size. In order to explore the effects of these parameters, four distinct analytical procedures are presented; one each for the four types of porosity being considered. Because of the limited amount of actual test data, the procedures rely in large part on assumptions which are considered to be consistent with the mechanisms of crack initiation and growth. The assumptions for each procedure are presented in the appropriate sections.

7.3.1. Matrix of Fatigue Life Predictions

The matrix of fatigue life predictions is shown in Table 3. For the constant amplitude loading, there are 144 separate cases to be examined. Each case requires loading at four stress ranges to generate

TABLE 3. MATRIX OF FATIGUE PREDICTIONS

Parameters	Options
Weld type	Transverse butt weld
Steel	EH36
Thickness	0.5 in., 1.0 in.
Residual stress	+Sy, 0
Loading:	
Constant amplitude	R = -1, 0, 0.5
Variable amplitude	SL-7 history, 0 and 6.5 ksi mean stress bias

Porosity Type	Porosity Size, inch					
	0.5-inch weld			1-inch weld		
Uniform porosity	0.015	0.030	0.045	0.015	0.045	0.075
Single pore	0.125	0.1875	0.25	0.1875	0.25	0.30
Co-linear porosity	0.125	0.1875	0.25	0.1875	0.25	0.30
Cluster porosity	0.125	0.1875	0.30	0.1875	0.25	0.40

stress ranges; 80, 60, 40, and 20 percent of the yield strength were used to construct S-N curves.

The geometry and coordinate system used in this study is shown in Figure 10. Note that no width dimension is included on the plate. The calculations for all life estimates in the parametric analysis are based on the assumption of infinite width. This means that the size of the pore and subsequent crack will not change the nominal applied stress, S. The results can be applied to a finite geometry correcting for a decrease in net cross sectional area.

All life predictions are made for a butt weld with the reinforcement removed to model crack initiation from internal porosity. The size and number of the porosity was chosen according to Section 2.6.4: Radiographic Inspection for Porosity in the Rules for Nondestructive Inspection of Hull Welds[54]. Figures 11 and 12 show the porosity acceptance charts from this code for the thicknesses examined in this study. The code states that the maximum area percent porosity allowable in any size weld is 1.5 percent. Three porosity sizes were used. One was equal to the maximum allowable porosity size as defined in the code. The other two sizes are chosen larger than the first one.

The S-N curves presented were constructed using a smooth fit to the total lives. Cases where lives were greater than 10^8 are not shown on the plots. The curves terminate at the greatest predicted life less than 10^8. Those predictions greater than 10^8 are indicated in the tables.

7.3.2. Material Properties

The material properties for ABS EH36 used in this study are presented in Table 4 and in Figures 13 and 14. The material is assumed to be homogeneous and isotropic. In reality, weld metal is seldom homogeneous, due to non-equilibrium cooling rates, thermal gradients, and the introduction of impurities. Also, the pressure of porosity suggests

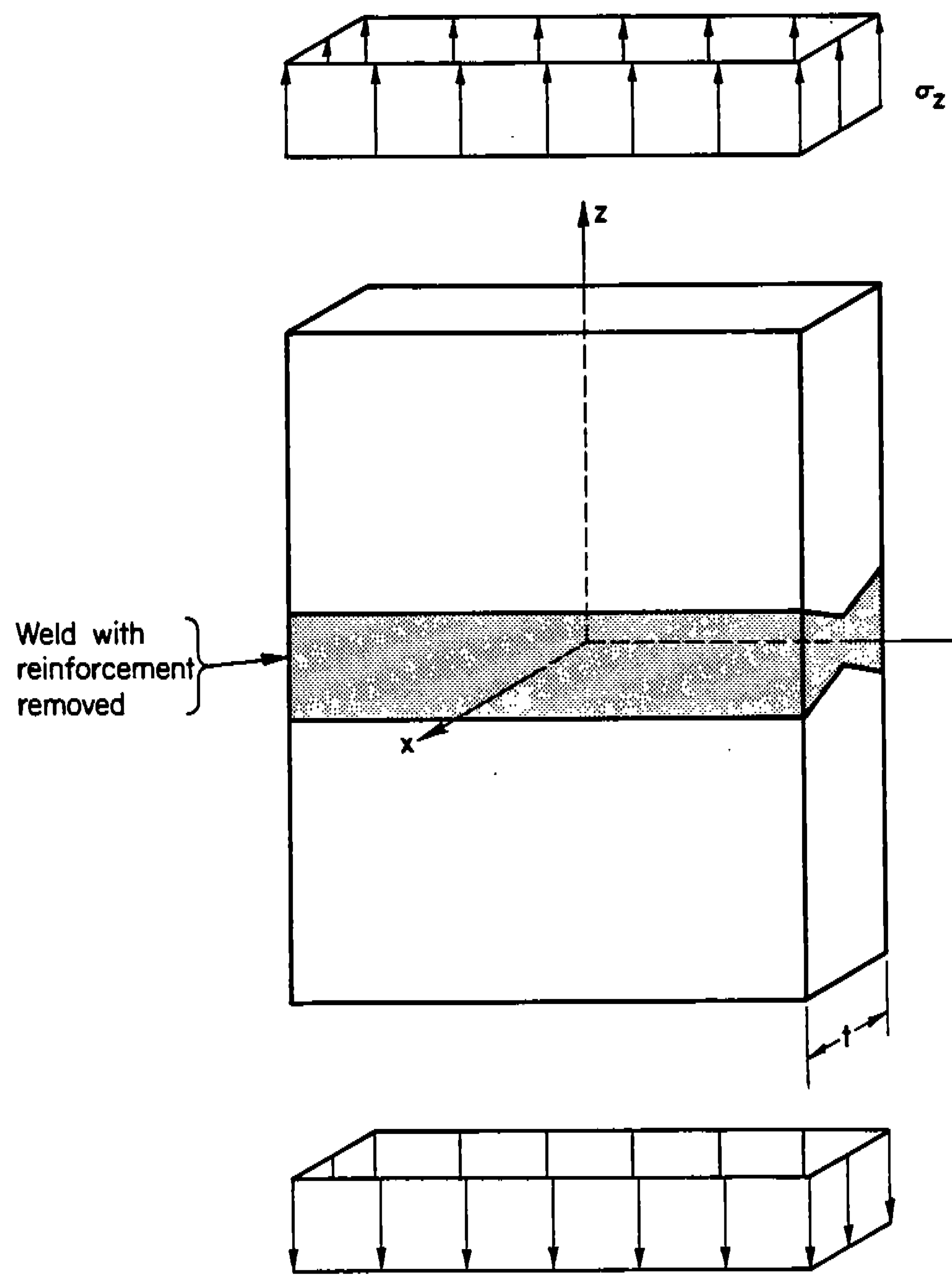

FIGURE 10. GEOMETRY AND CO-ORDINATE SYSTEM OF BUTT WELD FOR FATIGUE LIFE PREDICTIONS. THE WELD REINFORCEMENT IS REMOVED. THE WIDTH OF THE PLATE IS ASSUMED MANY TIMES THE THICKNESS OF THE WELD

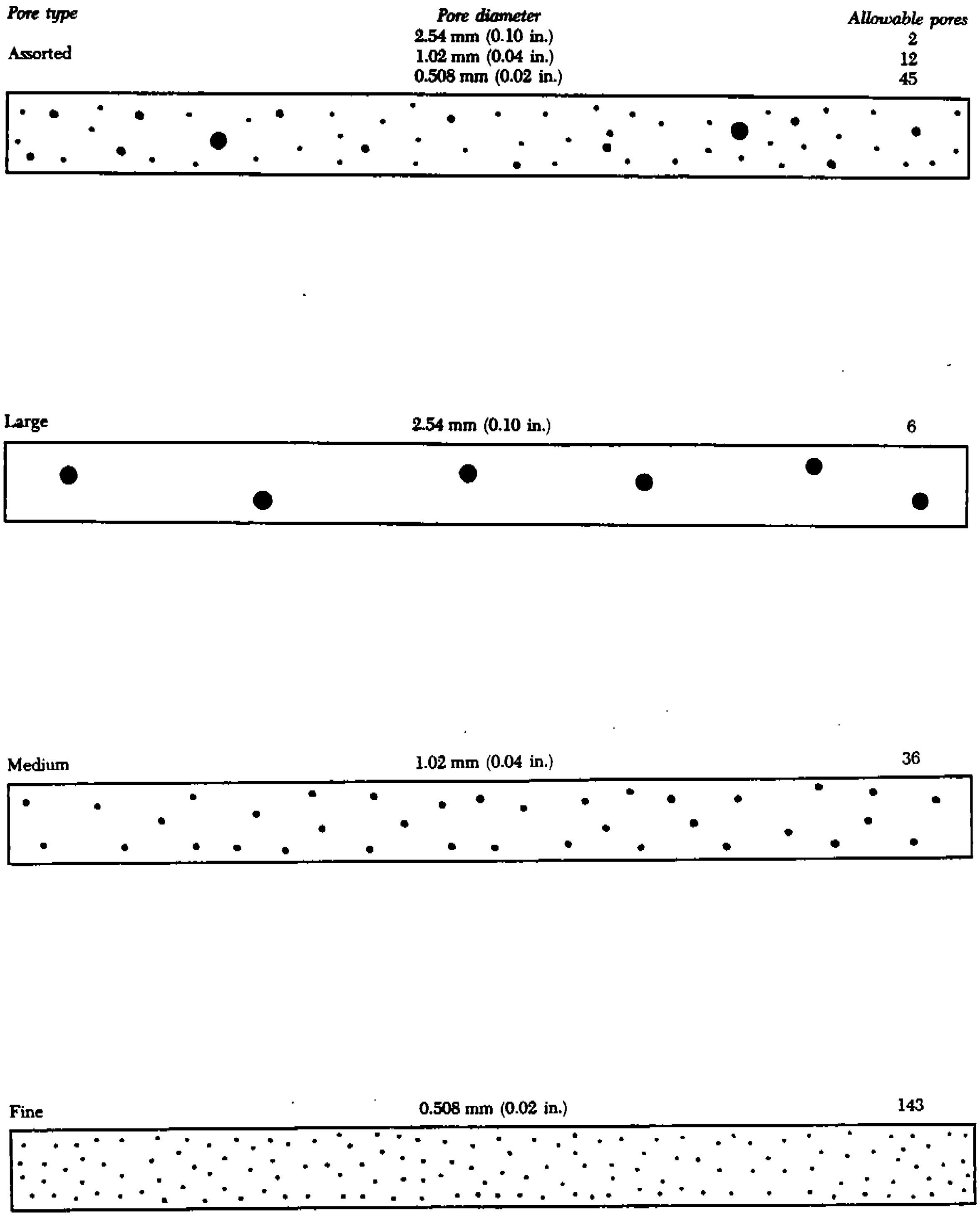

FIGURE 11. CLASS A AND CLASS B POROSITY CHART FOR 0.5 INCH (12.5 MM) THICK MATERIAL

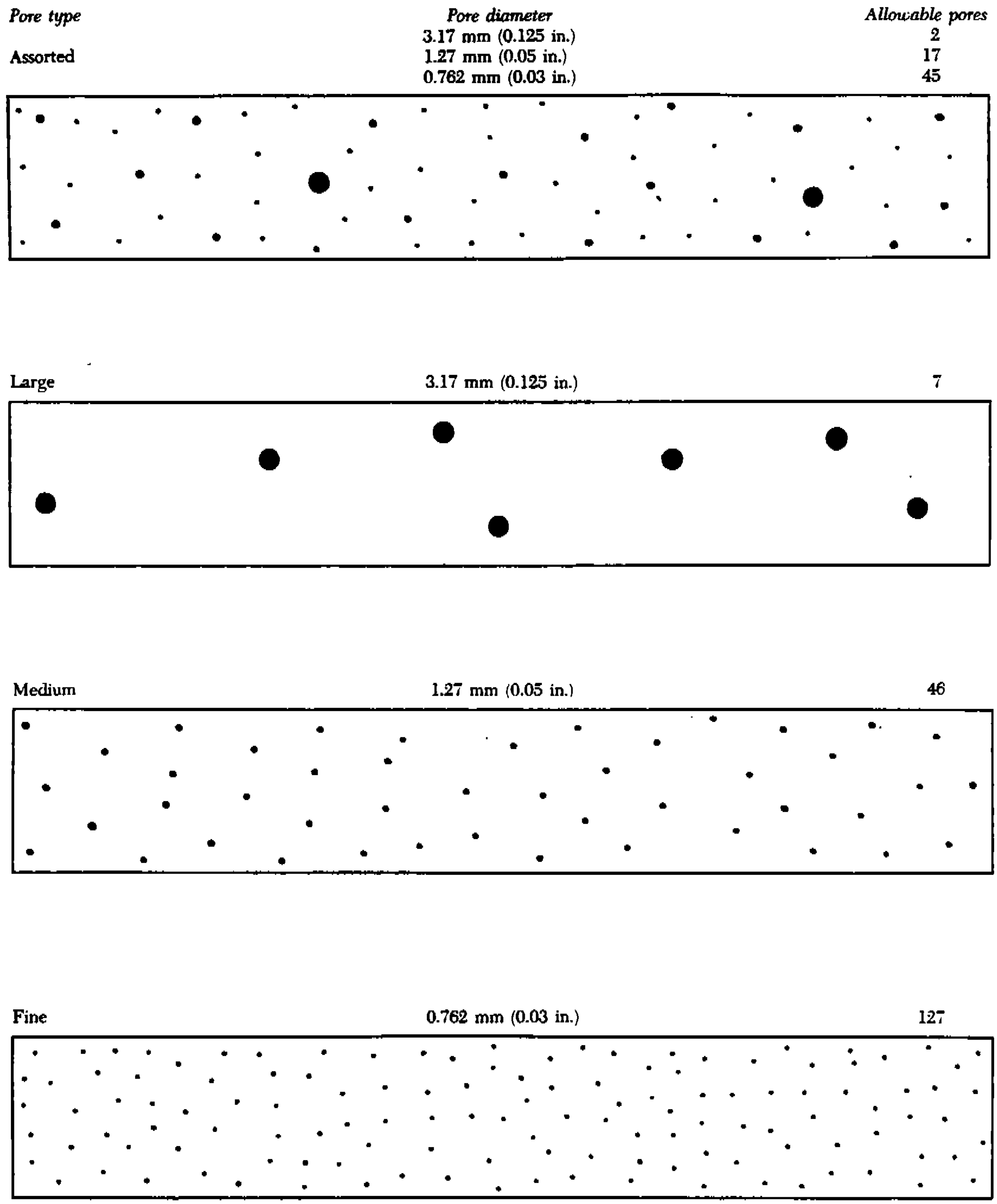

FIGURE 12. CLASS A AND CLASS B POROSITY CHART FOR 1.0 INCH (25.3 MM) THICK MATERIAL

TABLE 4. MECHANICAL PROPERTIES OF ABS EH36 STEEL

Monotonic Properties			
Young's Modulus,	E	30,700 ksi	211,677 MPa
Yield Strength (0.2%)	S_y	61 ksi	421 MPa
Tensile Strength	S_u	75 ksi	518 MPa
Reduction in Area	% RA	77.4	77.4
True Fracture Strength	σ_f	186.3 ksi	1285 MPa
True Fracture Ductility	ϵ_f	1.49	1.49
Cyclic Properties			
Cyclic Yield Strength	σ'_y	49 ksi	338 MPa
Cyclic Strength Coefficient	K'	132 ksi	912 MPa
Cyclic Strain Hardening Exponent	n'	0.162	0.162
Fatigue Strength Coefficient	σ'_f	103 ksi	713 MPa
Fatigue Strength Exponent	b	-0.075	-0.075
Fatigue Ductility Coefficient	ϵ'_f	0.227	0.227
Fatigue Ductility Exponent	c	-0.462	-0.462
Propagation Properties			
Crack Growth Coefficient	A	1.76×10^{-12}	2.92×10^{-14}
Crack Growth Exponent	m	4.5	4.5

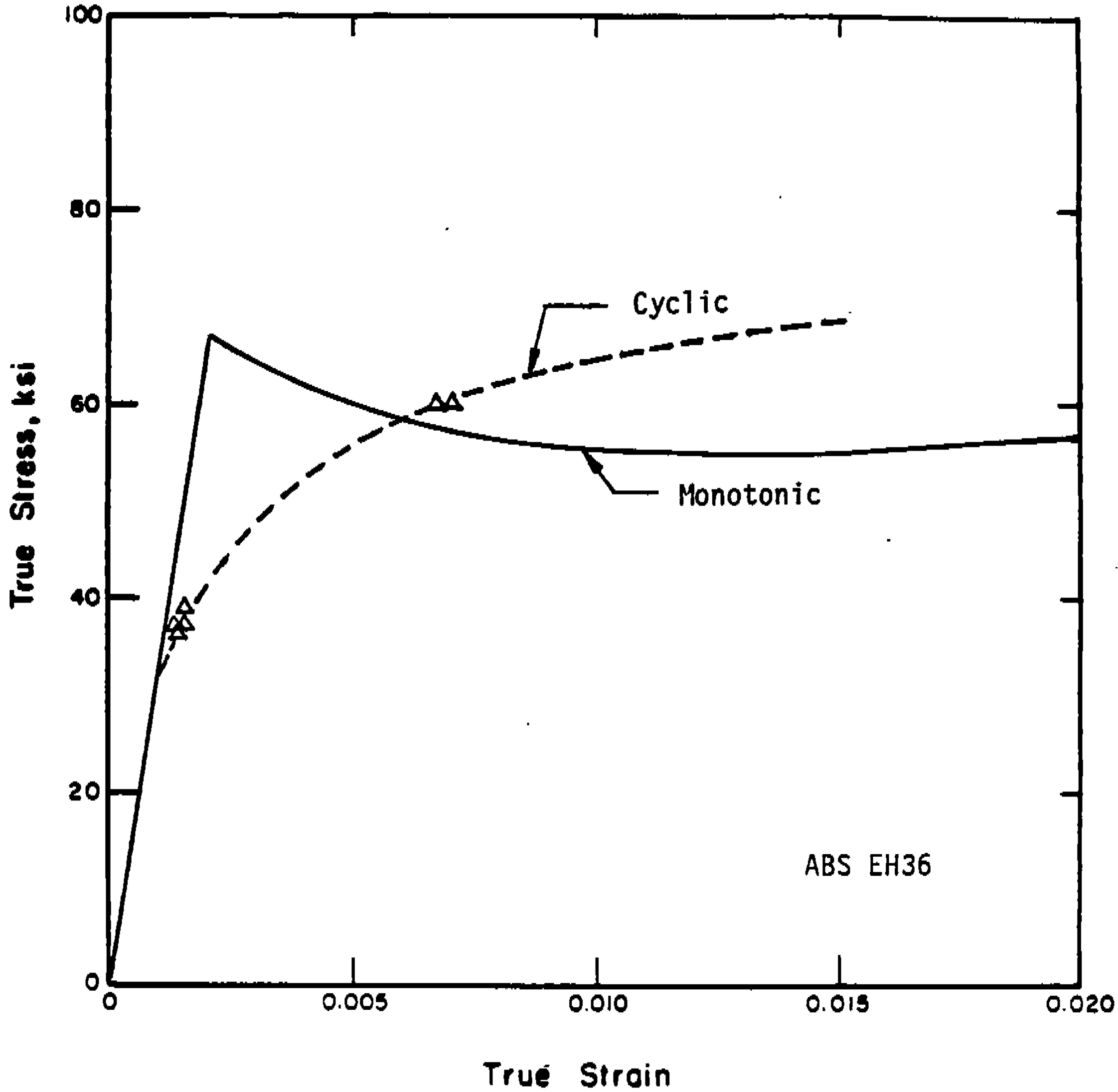

FIGURE 13. MONOTONIC AND CYCLIC STRESS-STRAIN RESPONSE FOR ABS EH36

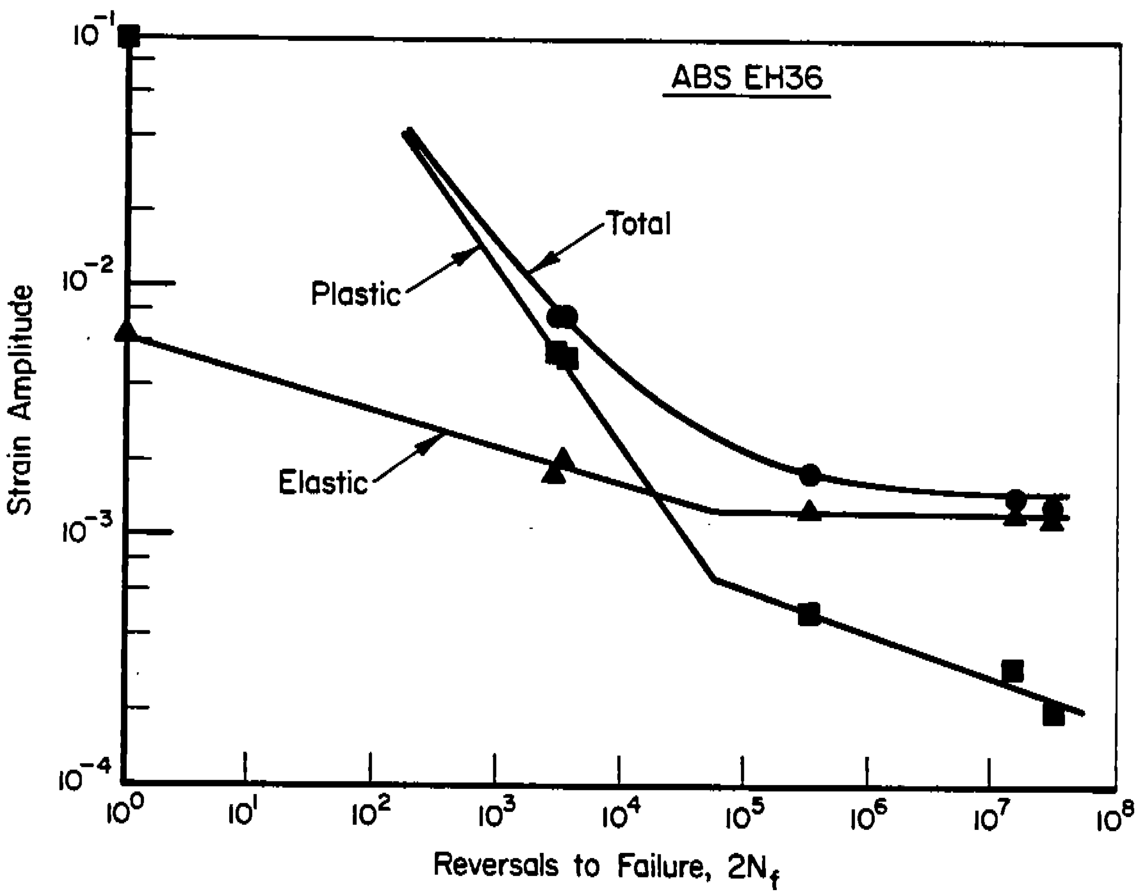

FIGURE 14. STRAIN-LIFE DATA FOR ABS EH36

7.3.3. Single Pore

The single pore geometry and assumed crack growth pattern are shown in Figure 15. The maximum pore size allowed for an isolated pore in the Rules for Nondestructive Inspection of Hull Welds[54] is given as 0.25t or 0.1875 inch, whichever is less. The pore sizes chosen represent the largest allowable pore size and two larger sizes. The pore is assumed spherical and positioned at the centroid of the cross section. The crack growth pattern is assumed to remain circular throughout the crack propagation stage. The finite thickness correction factor, M_t, for a circular crack is approximated by the polynomial expression

$$M_t = 1.46 - 1.85(a/(t/2)) + 1.79(a/(t/2))^2 \quad . \qquad (16)$$

This expression is the result of a regression of solutions of different crack depths found on pages 294-295 in Rooke and Cartwright[21] for elliptical cracks in a semi-infinite medium. The stress intensity solutions are presented in Figure 16. Note that the initial stress intensity factor is quite high. As the crack becomes larger and grows out of the region of influence of the stress gradient, the stress intensity value decreases.

The results of the fatigue life predictions are presented in Tables 5 and 6 and plotted as S-N curves in Figures 17-20.

7.3.4. Uniform Porosity

The uniform porosity geometry and assumed crack growth pattern are shown in Figure 21. The porosity is assumed to be uniformly distributed throughout the weld. The Rules for Nondestructive Inspection of Welds[54] states that no more than 1.5 percent area porosity is allowed. It also states that pores smaller than 0.015 inch may be disregarded. The smallest pore size chosen is therefore 0.015 inch. Two other larger pores are also considered for both thicknesses. The analysis assumes that the maximum allowable area percent porosity is always present throughout the weld. This reduction in net cross sectional area has the

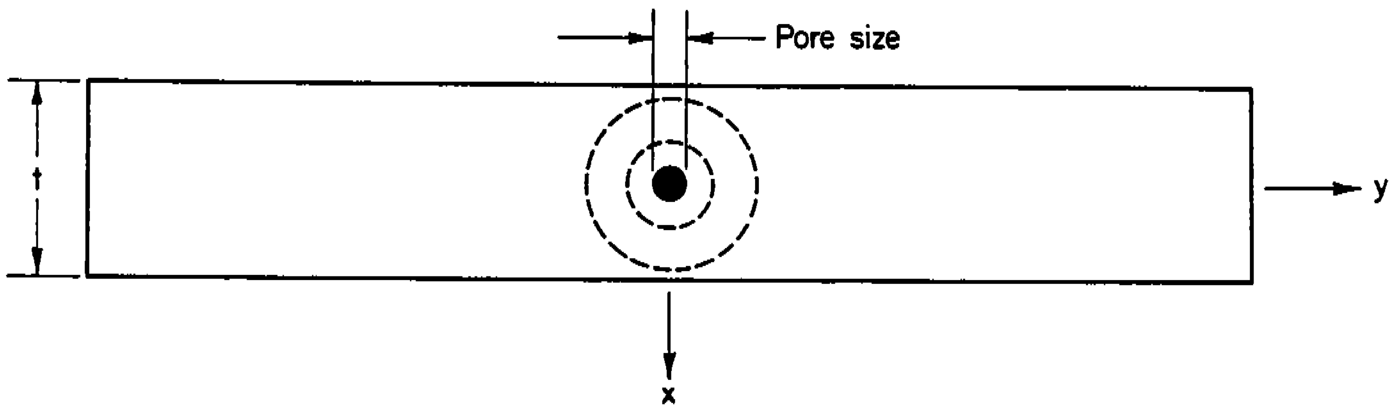

FIGURE 15. GEOMETRY AND ASSUMED CRACK GROWTH PATTERN (DASHED LINE) FOR SINGLE PORE

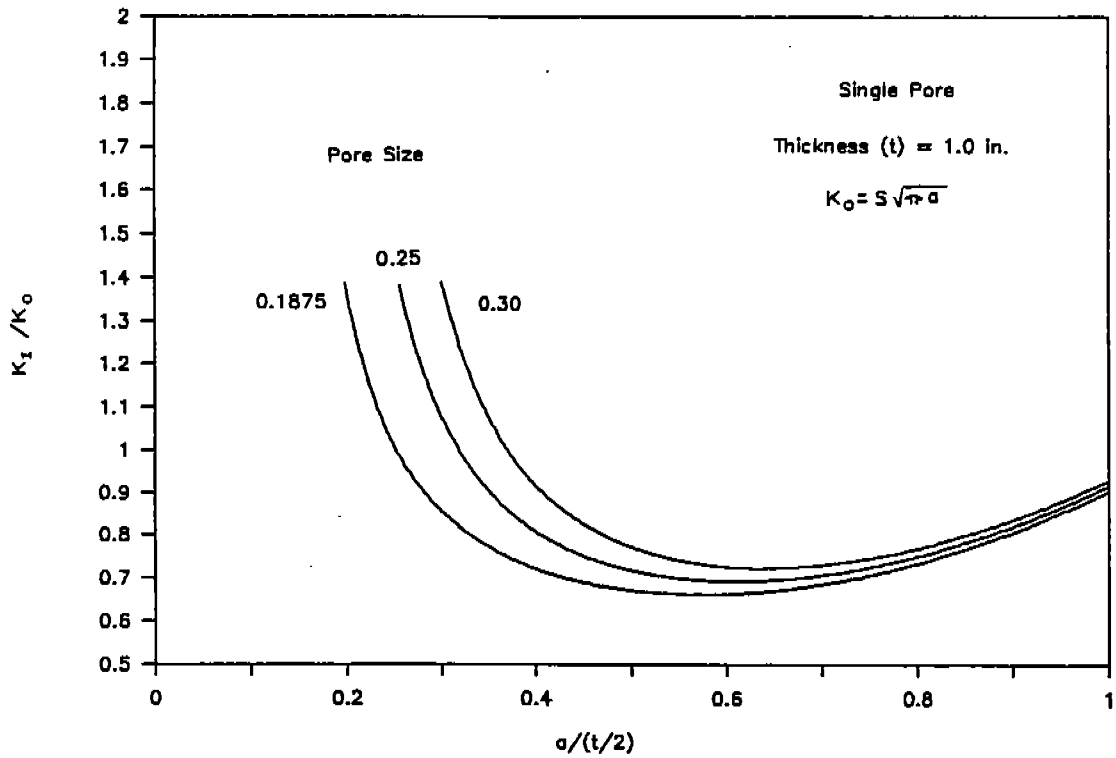

FIGURE 16. STRESS INTENSITY SOLUTION FOR SINGLE PORES IN A 1-INCH THICK PLATE

TABLE 5. SINGLE PORE CONSTANT AMPLITUDE FATIGUE LIFE PREDICTIONS
THICKNESS = 0.5 INCH
ABS EH36

Stress Ratio=-1 Residual Stress=51 ksi		Pore=0.125 inch			Pore=0.1875 inch			Pore=0.250 inch		
	Stress Range (ksi)	N-Init	N-Prop	N-TOTAL	N-Init	N-Prop	N-TOTAL	N-Init	N-Prop	N-TOTAL
	81.60	2590	10709	13299	2362	3983	6345	2251	1362	3613
	61.20	8835	39081	47916	7971	14538	22509	7554	4968	12522
	40.80	79753	242320	322073	68868	90120	158988	63821	30800	94621
	20.40	32537876	5482800	38020676	25656872	2039600	27696472	22652879	696900	23349779

Stress Ratio=0 Residual Stress=51 ksi		Pore=0.125 inch			Pore=0.1875 inch			Pore=0.250 inch		
	Stress Range (ksi)	N-Init	N-Prop	N-TOTAL	N-Init	N-Prop	N-TOTAL	N-Init	N-Prop	N-TOTAL
	40.80	25725	121167	146892	22024	45066	67090	20317	15405	35722
	30.60	245351	442150	687501	201521	164480	366001	181869	56200	238069
	20.40	13532427	2741500	16273927	10576766	1019800	11596566	9285158	348500	9633658
	10.20			>100000000			>100000000			>100000000

Stress Ratio=0.5 Residual Stress=51 ksi		Pore=0.125 inch			Pore=0.1875 inch			Pore=0.250 inch		
	Stress Range (ksi)	N-Init	N-Prop	N-TOTAL	N-Init	N-Prop	N-TOTAL	N-Init	N-Prop	N-TOTAL
	20.40	3346237	1370860	4717097	2585648	509860	3095508	2258772	174280	2433052
	15.30			>100000000	78718952	1860800	80579752	67927084	635800	68562884
	10.20			>100000000			>100000000			>100000000
	5.10			>100000000			>100000000			>100000000

Stress Ratio=-1 Residual Stress=0 ksi		Pore=0.125 inch			Pore=0.1875 inch			Pore=0.250 inch		
	Stress Range (ksi)	N-Init	N-Prop	N-TOTAL	N-Init	N-Prop	N-TOTAL	N-Init	N-Prop	N-TOTAL
	81.60	9766	10709	20475	8691	3983	12674	8175	1362	9537
	61.20	48345	39081	87426	42170	14538	56708	39270	4968	44238
	40.80	942751	242320	1185071	772719	90120	862839	696953	30800	727753
	20.40			>100000000			>100000000			>100000000

Stress Ratio=0 Residual Stress=0 ksi		Pore=0.125 inch			Pore=0.1875 inch			Pore=0.250 inch		
	Stress Range (ksi)	N-Init	N-Prop	N-TOTAL	N-Init	N-Prop	N-TOTAL	N-Init	N-Prop	N-TOTAL
	40.80	122443	121167	243610	101635	45066	146701	92270	15405	107675
	30.60	1867610	442150	2309760	1469932	164480	1634412	1297597	56200	1353797
	20.40			>100000000			>100000000			>100000000
	10.20			>100000000			>100000000			>100000000

Stress Ratio=0.5 Residual Stress=0 ksi		Pore=0.125 inch			Pore=0.1875 inch			Pore=0.250 inch		
	Stress Range (ksi)	N-Init	N-Prop	N-TOTAL	N-Init	N-Prop	N-TOTAL	N-Init	N-Prop	N-TOTAL
	20.40	22816405	1370860	24187265	17001351	509860	17511211	14573639	174280	14747919
	15.30			>100000000			>100000000			>100000000
	10.20			>100000000			>100000000			>100000000
	5.10			>100000000			>100000000			>100000000

TABLE 6. SINGLE PORE CONSTANT AMPLITUDE FATIGUE LIFE PREDICTIONS
THICKNESS = 1.0 INCH
ABS EH36

		Pore=0.1875 inch			Pore=0.250 inch			Pore=0.300 inch		
Stress Ratio=-1 Residual Stress=51 ksi	Stress Range (ksi)	N-Init	N-Prop	N-TOTAL	N-Init	N-Prop	N-TOTAL	N-Init	N-Prop	N-TOTAL
	81.60	2362	7323	9685	2251	4503	6754	2196	3051	5247
	61.20	7971	26722	34693	7554	16429	23983	7350	11131	18481
	40.80	68868	165677	234545	63821	101870	165691	61393	69020	130413
	20.40	25656872	3749100	29405972	22652879	2305130	24958009	21253360	1561690	22815050

		Pore=0.1875 inch			Pore=0.250 inch			Pore=0.300 inch		
Stress Ratio=0 Residual Stress=51 ksi	Stress Range (ksi)	N-Init	N-Prop	N-TOTAL	N-Init	N-Prop	N-TOTAL	N-Init	N-Prop	N-TOTAL
	40.80	22024	82841	104865	20317	50936	71253	19498	34511	54009
	30.60	201521	302333	503854	181869	185877	367746	172584	125938	298522
	20.40	10576766	1874400	12451166	9285158	1152510	10437668	8700163	780870	9481033
	10.20			>100000000			>100000000			>100000000

		Pore=0.1875 inch			Pore=0.250 inch			Pore=0.300 inch		
Stress Ratio=0.5 Residual Stress=51 ksi	Stress Range (ksi)	N-Init	N-Prop	N-TOTAL	N-Init	N-Prop	N-TOTAL	N-Init	N-Prop	N-TOTAL
	20.40	2585648	937230	3522878	2258772	576270	2835042	2107711	390450	2498161
	15.30	78718952	3420520	82139472	67927084	2103050	70030134	62977515	1424820	64402335
	10.20			>100000000			>100000000			>100000000
	5.10			>100000000			>100000000			>100000000

		Pore=0.1875 inch			Pore=0.250 inch			Pore=0.300 inch		
Stress Ratio=-1 Residual Stress=0 ksi	Stress Range (ksi)	N-Init	N-Prop	N-TOTAL	N-Init	N-Prop	N-TOTAL	N-Init	N-Prop	N-TOTAL
	81.60	8691	7323	16014	8175	4503	12678	7923	3051	10974
	61.20	42170	26722	68892	39270	16429	55699	37867	11131	48998
	40.80	772719	165677	938396	696953	101870	798823	661249	69020	730269
	20.40			>100000000			>100000000			>100000000

		Pore=0.1875 inch			Pore=0.250 inch			Pore=0.300 inch		
Stress Ratio=0 Residual Stress=0 ksi	Stress Range (ksi)	N-Init	N-Prop	N-TOTAL	N-Init	N-Prop	N-TOTAL	N-Init	N-Prop	N-TOTAL
	40.80	101635	82841	184476	92270	50936	143206	87833	34511	122344
	30.60	1469932	302333	1772265	1297597	185877	1483474	1217575	125938	1343513
	20.40			>100000000			>100000000			>100000000
	10.20			>100000000			>100000000			>100000000

		Pore=0.1875 inch			Pore=0.250 inch			Pore=0.300 inch		
Stress Ratio=0.5 Residual Stress=0 ksi	Stress Range (ksi)	N-Init	N-Prop	N-TOTAL	N-Init	N-Prop	N-TOTAL	N-Init	N-Prop	N-TOTAL
	20.40	17001351	937230	17938581	14573639	576270	15149909	13468239	390450	13858689
	15.30			>100000000			>100000000			>100000000
	10.20			>100000000			>100000000			>100000000
	5.10			>100000000			>100000000			>100000000

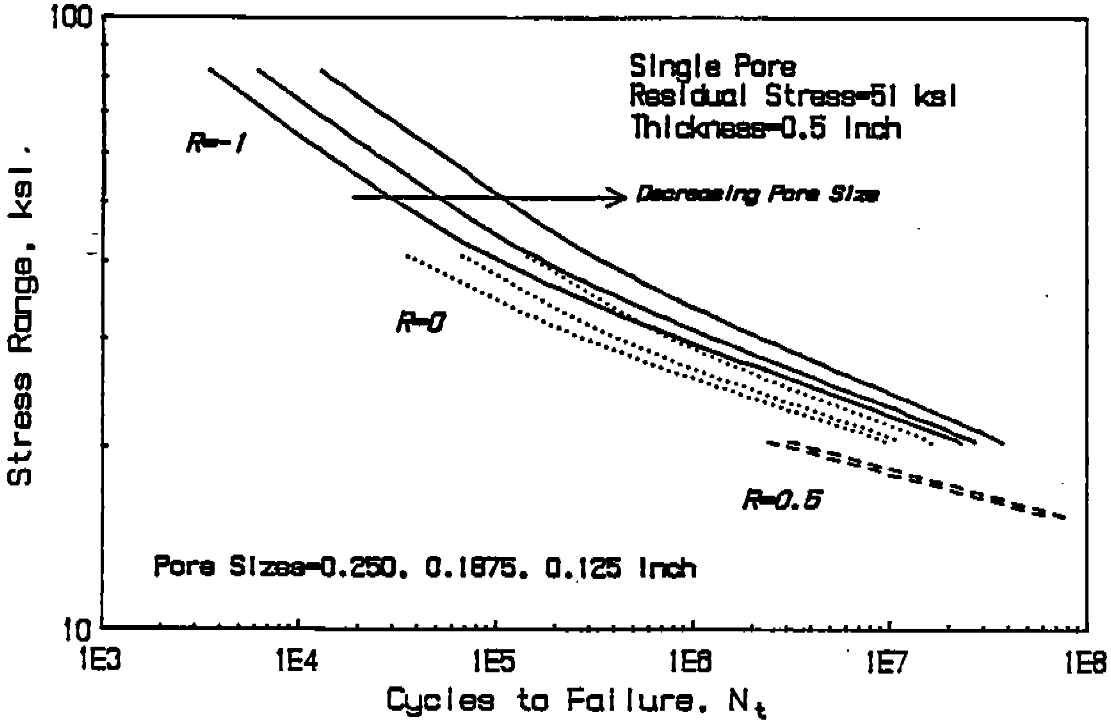

FIGURE 17. S-N CURVES FOR SINGLE PORE GEOMETRY IN 0.5-INCH THICK PLATE AND 51 KSI RESIDUAL STRESS

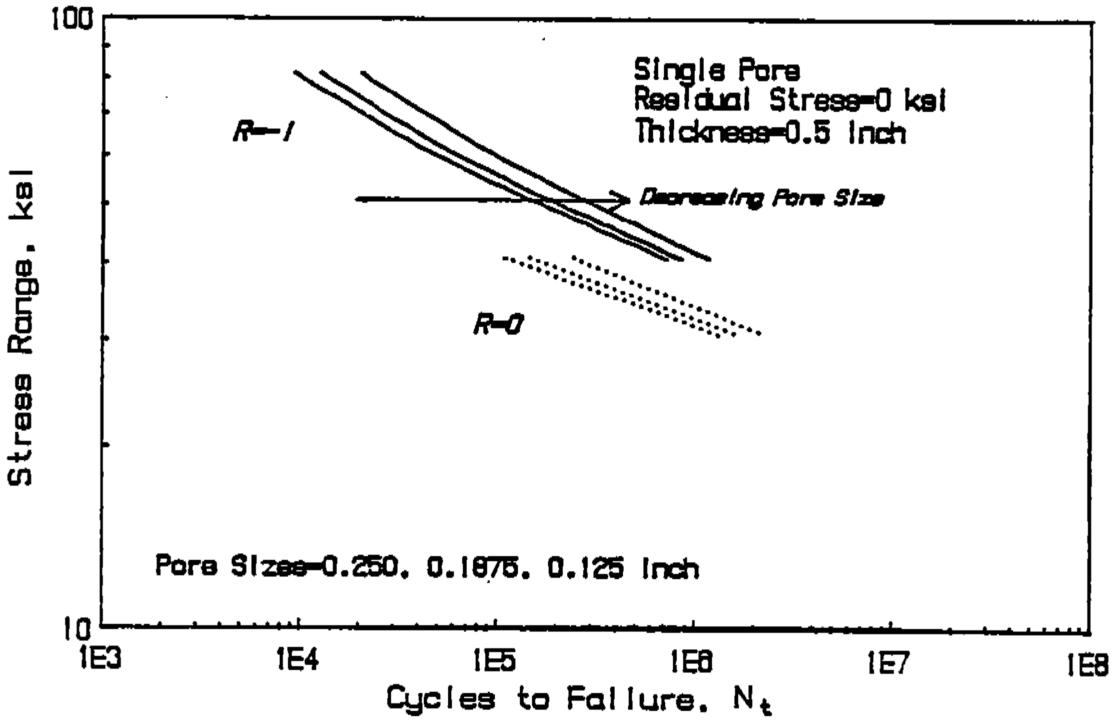

FIGURE 18. S-N CURVES FOR SINGLE PORE GEOMETRY IN 0.5-INCH THICK PLATE AND ZERO RESIDUAL STRESS

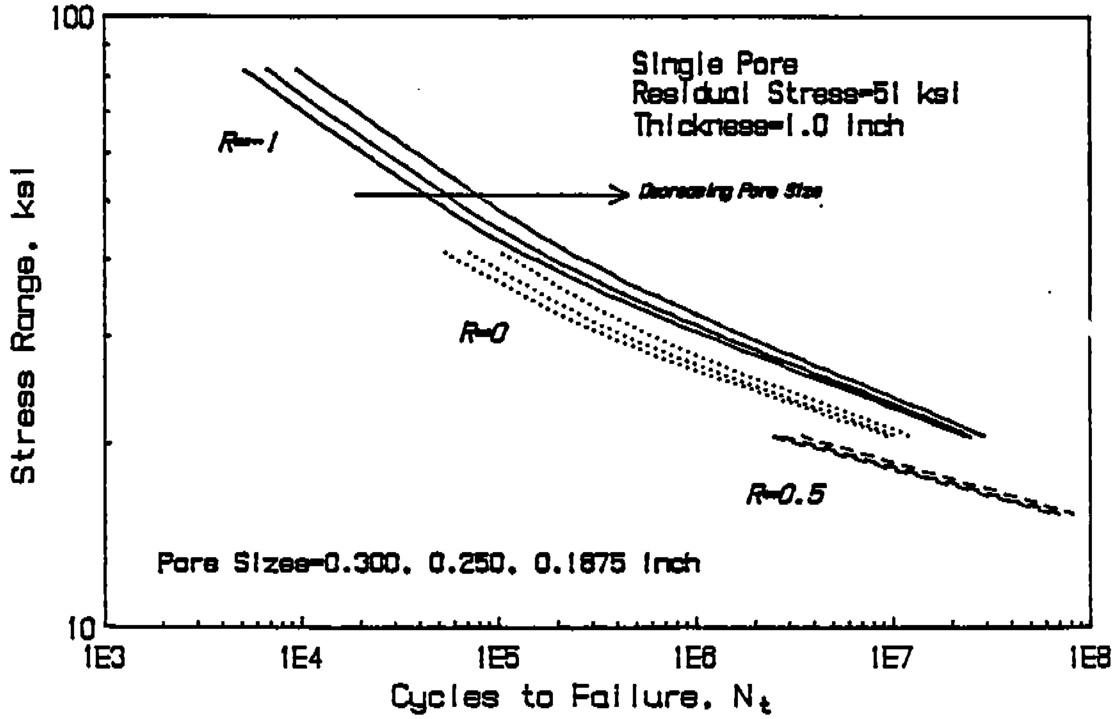

FIGURE 19. S-N CURVES FOR SINGLE PORE GEOMETRY IN 1.0-INCH THICK PLATE AND 51 KSI RESIDUAL STRESS

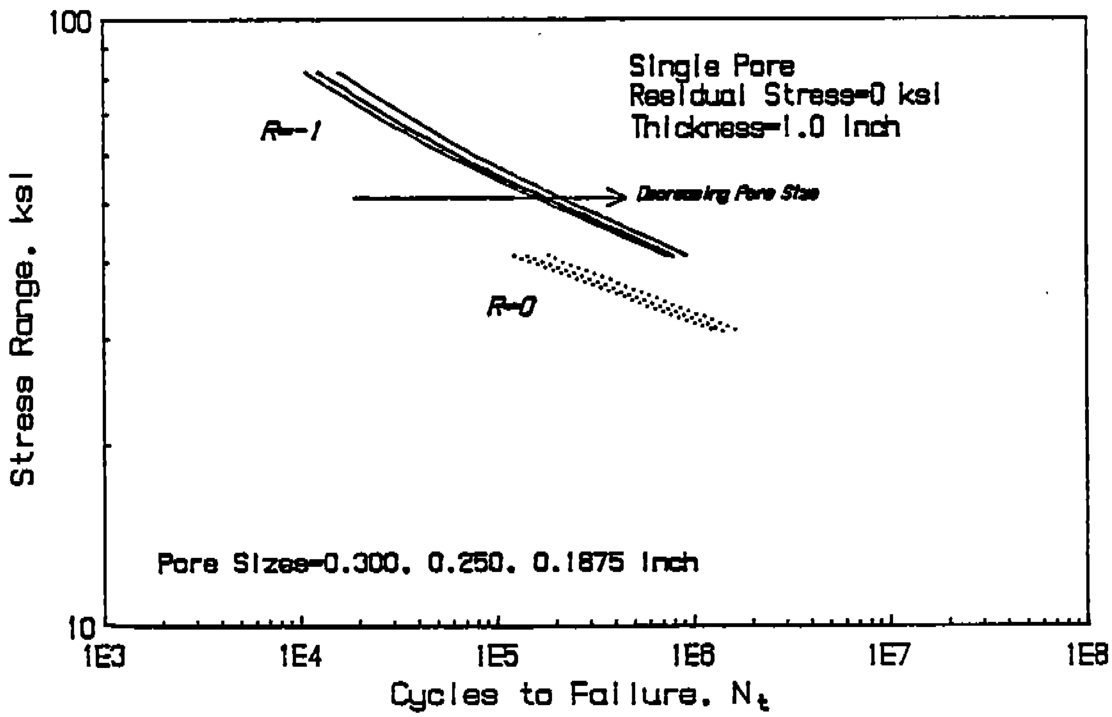

FIGURE 20. S-N CURVES FOR SINGLE PORE GEOMETRY IN 1.0-INCH THICK PLATE AND ZERO RESIDUAL STRESS

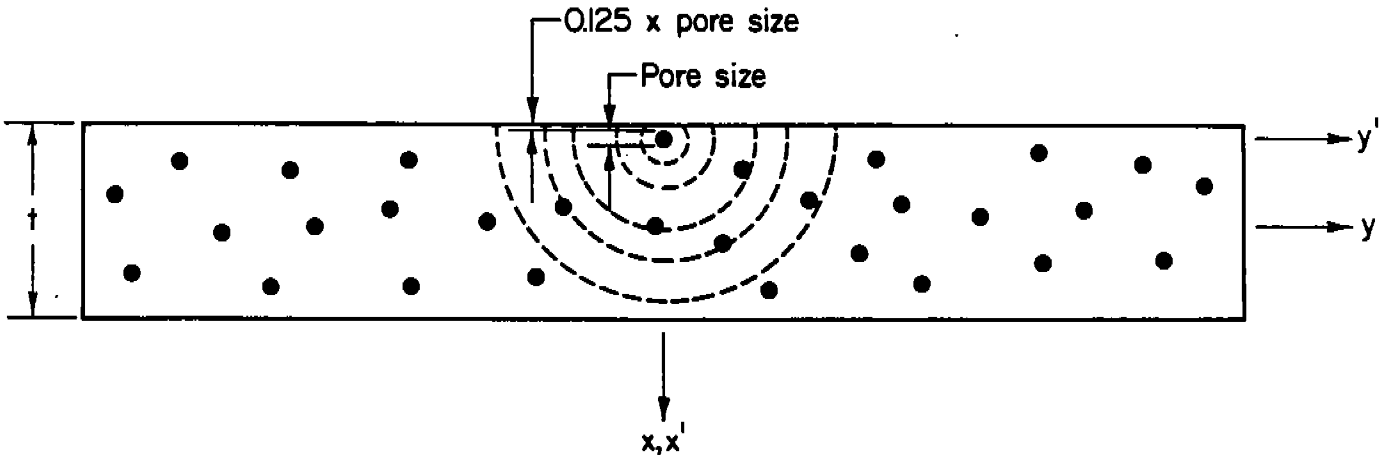

FIGURE 21. GEOMETRY AND ASSUMED CRACK GROWTH PATTERN (DASHED LINE) FOR UNIFORM POROSITY

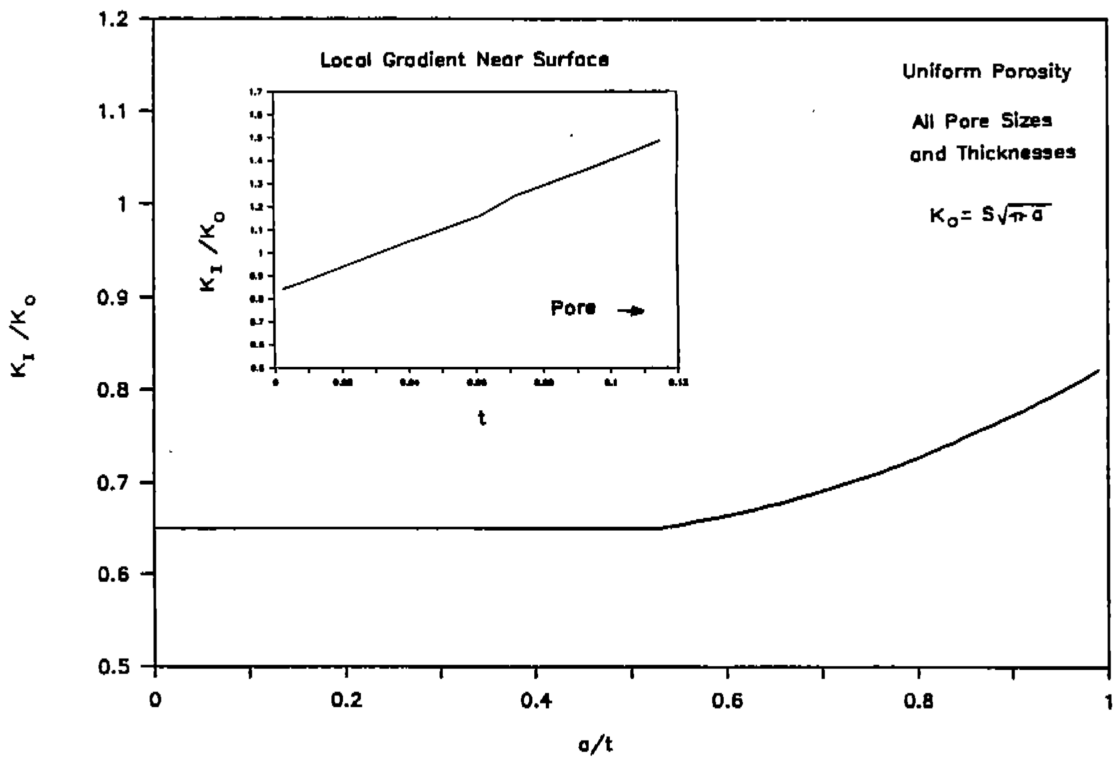

FIGURE 22. STRESS INTENSITY SOLUTION FOR UNIFORM POROSITY. INSET SHOWS THE DECAY OF THE STRESS INTENSITY AS THE CRACK GROWS AWAY FROM THE PORE STRESS GRADIENT TOWARD THE SURFACE

effect of raising the net section stress. (This assumption is not made for the other three geometries where the area reduction caused by the porosity is considered as negligible.)

The critical pore in this particular analysis is located in close proximity to the surface of the weldment. The elasticity result of Tsuchida and Nakahara[15] for a pore located 0.125 times the pore size (diameter) from the surface (a = 0.8 in Figure 4) is used to calculate the stress gradient to the surface. Since the pores relation to the surface causes an increase in the stress concentration, it is assumed that this pore will initiate a fatigue crack first. As this crack becomes the dominant singularity, no other cracks initiate. The stress intensity solution for the gradient near the surface is shown in the inset in Figure 22. The stress intensity steadily decreases until the crack breaks the surface. This near surface crack growth is assumed remain circular. When the crack intersects the near surface, the stress intensity solution is approximated as that of a semicircular crack in a slab. The stress intensity solution for this crack geometry is also found in[21] (page 298) and is represented by the expression

$$M_t = 0.70 - 0.34(a/t) + 0.47(a/t)^2 \quad (17)$$

where a is the crack radius and t is the plate thickness. The stress intensity solution for this geometry is shown in Figure 22.

The results of the fatigue life calculations are presented in Tables 7 and 8 and as S-N curves in Figures 23-26. Many of the cases which were analyzed proved to be non-propagating cracks, especially the small pores and high stress ratios.

7.3.5. Co-linear Porosity

The pore geometry and assumed crack growth pattern for the co-linear pores are shown in Figure 27. Lundin[17] indicates linear or aligned porosity is usually associated with a root or interpass and found in concert with lack of penetration or fusion. Caution should therefore be exercised when trying to ascertain the structural integrity of a weldment

TABLE 7. UNIFORM POROSITY CONSTANT AMPLITUDE FATIGUE LIFE F
THICKNESS = 0.5 INCH
ABS EH36

		Pore=0.015 inch			Pore=0.030 inch		
Stress Ratio=-1							
Residual Stress=51 ksi	Stress Range (ksi)	N-Init	N-Prop	N-TOTAL	N-Init	N-Prop	N-TOTAL
	81.6	2750	318171	320921	1397	143530	144927
	61.2			>100000000	4497	525029	529526
	40.8			>100000000			>100000000
	20.4			>100000000			>100000000
Stress Ratio=0							
Residual Stress=51 ksi	Stress Range (ksi)	N-Init	N-Prop	N-TOTAL	N-Init	N-Prop	N-TOTAL
	40.8	28519	3590119	3618638	9512	1626020	1635532
	30.6			>100000000	68592	5932650	6001242
	20.4			>100000000			>100000000
	10.2			>100000000			>100000000
Stress Ratio=0.5							
Residual Stress=51 ksi	Stress Range (ksi)	N-Init	N-Prop	N-TOTAL	N-Init	N-Prop	N-TOTAL
	20.4	3964242	40632010	44596252	609118	18395470	19004588
	15.3			>100000000	15936323	67131600	83067923
	10.2			>100000000			>100000000
	5.1			>100000000			>100000000
Stress Ratio=-1							
Residual Stress=0 ksi	Stress Range (ksi)	N-Init	N-Prop	N-TOTAL	N-Init	N-Prop	N-TOTAL
	81.6	10544	318171	328715	4500	143530	148030
	61.2			>100000000	19869	525029	544898
	40.8			>100000000			>100000000
	20.4			>100000000			>100000000
Stress Ratio=0							
Residual Stress=0 ksi	Stress Range (ksi)	N-Init	N-Prop	N-TOTAL	N-Init	N-Prop	N-TOTAL
	40.8	138567	3590119	3728686	37243	1626020	1663263
	30.6			>100000000	398443	5932650	6331093
	20.4			>100000000			>100000000
	10.2			>100000000			>100000000
Stress Ratio=0.5							
Residual Stress=0 ksi	Stress Range (ksi)	N-Init	N-Prop	N-TOTAL	N-Init	N-Prop	N-TOTAL
	20.4	27687956	40632010	68319966	3283635	18395470	21679105
	15.3			>100000000	136329370	67131600	203460970
	10.2			>100000000			>100000000
	5.1			>100000000			>100000000

TABLE 8. UNIFORM POROSITY CONSTANT AMPLITUDE FATIGUE LIFE PREDICTIONS
THICKNESS = 1.0 INCH
ABS EH36

Stress Ratio=-1		Pore=0.015 inch			Pore=0.045 inch			Pore=0.075 inch		
Residual Stress=51 ksi	Stress Range (ksi)	N-Init	N-Prop	N-TOTAL	N-Init	N-Prop	N-TOTAL	N-Init	N-Prop	N-TOTAL
	81.6	2750	301776	304526	1017	83852	84869	748	46906	47654
	61.2			>100000000	3217	305760	308977	2339	171234	173573
	40.8			>100000000			>100000000	13677	1061765	1075442
	20.4			>100000000			>100000000			>100000000

Stress Ratio=0		Pore=0.015 inch			Pore=0.045 inch			Pore=0.075 inch		
Residual Stress=51 ksi	Stress Range (ksi)	N-Init	N-Prop	N-TOTAL	N-Init	N-Prop	N-TOTAL	N-Init	N-Prop	N-TOTAL
	40.8	28519	3404936	3433455	5960	948497	954457	3890	530838	534728
	30.6			>100000000	37478	3458463	3495941	21668	1936353	1958021
	20.4			>100000000			>100000000	566259	12007410	12573669
	10.2			>100000000			>100000000			>100000000

Stress Ratio=0.5		Pore=0.015 inch			Pore=0.045 inch			Pore=0.075 inch		
Residual Stress=51 ksi	Stress Range (ksi)	N-Init	N-Prop	N-TOTAL	N-Init	N-Prop	N-TOTAL	N-Init	N-Prop	N-TOTAL
	20.4	3964242	38535230	42499472	263338	10725259	10988597	120732	6003703	6124435
	15.3			>100000000	6172568	39141260	45313828	2516148	21910630	24426778
	10.2			>100000000			>100000000			>100000000
	5.1			>100000000			>100000000			>100000000

Stress Ratio=-1		Pore=0.015 inch			Pore=0.045 inch			Pore=0.075 inch		
Residual Stress=0 ksi	Stress Range (ksi)	N-Init	N-Prop	N-TOTAL	N-Init	N-Prop	N-TOTAL	N-Init	N-Prop	N-TOTAL
	81.6	10544	301776	312320	3046	83852	86898	2098	46906	49004
	61.2			>100000000	12885	305760	318645	8584	171234	179818
	40.8			>100000000			>100000000	86719	1061765	1148484
	20.4			>100000000			>100000000			>100000000

Stress Ratio=0		Pore=0.015 inch			Pore=0.045 inch			Pore=0.075 inch		
Residual Stress=0 ksi	Stress Range (ksi)	N-Init	N-Prop	N-TOTAL	N-Init	N-Prop	N-TOTAL	N-Init	N-Prop	N-TOTAL
	40.8	138567	3404936	3543503	21349	948497	969846	12868	530838	543706
	30.6			>100000000	192393	3458463	3650856	99670	1936353	2036023
	20.4			>100000000			>100000000	5185915	12007410	17193325
	10.2			>100000000			>100000000			>100000000

Stress Ratio=0.5		Pore=0.015 inch			Pore=0.045 inch			Pore=0.075 inch		
Residual Stress=0 ksi	Stress Range (ksi)	N-Init	N-Prop	N-TOTAL	N-Init	N-Prop	N-TOTAL	N-Init	N-Prop	N-TOTAL
	20.4	27687956	38535230	66223186	1269566	10725259	11994825	525745	6003703	6529448
	15.3			>100000000	45936044	39141260	85077304	16481270	21910630	38391900
	10.2			>100000000			>100000000			>100000000
	5.1			>100000000			>100000000			>100000000

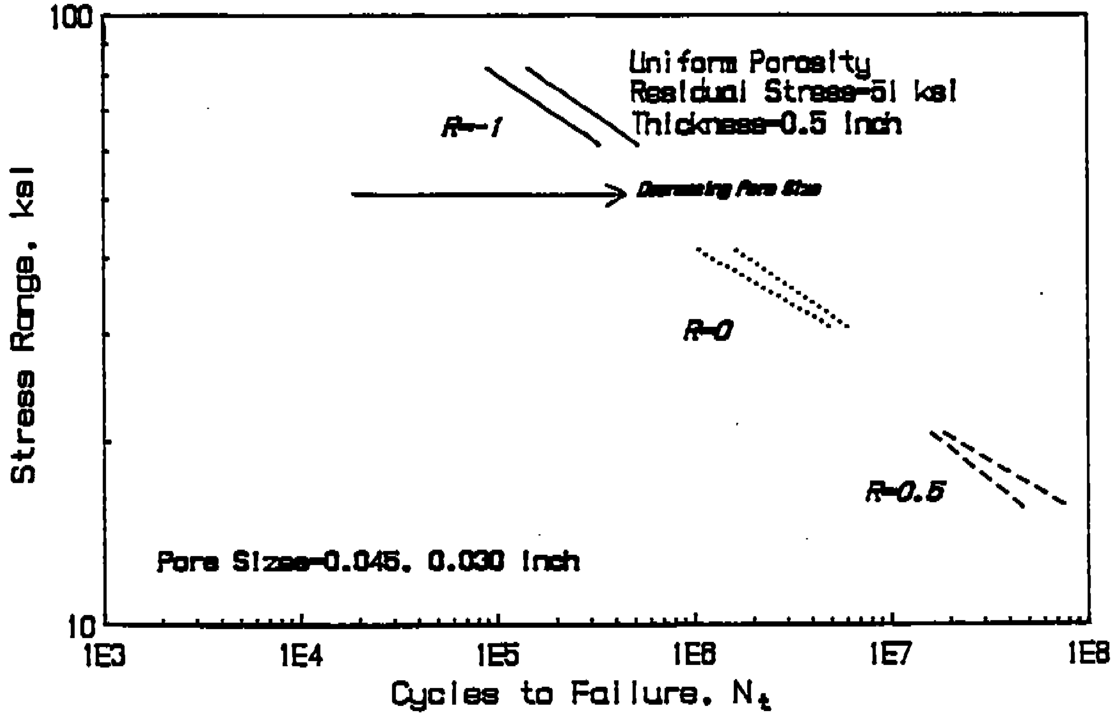

FIGURE 23. S-N CURVES FOR UNIFORM POROSITY GEOMETRY IN A 0.5-INCH THICK PLATE AND 51 KSI RESIDUAL STRESS

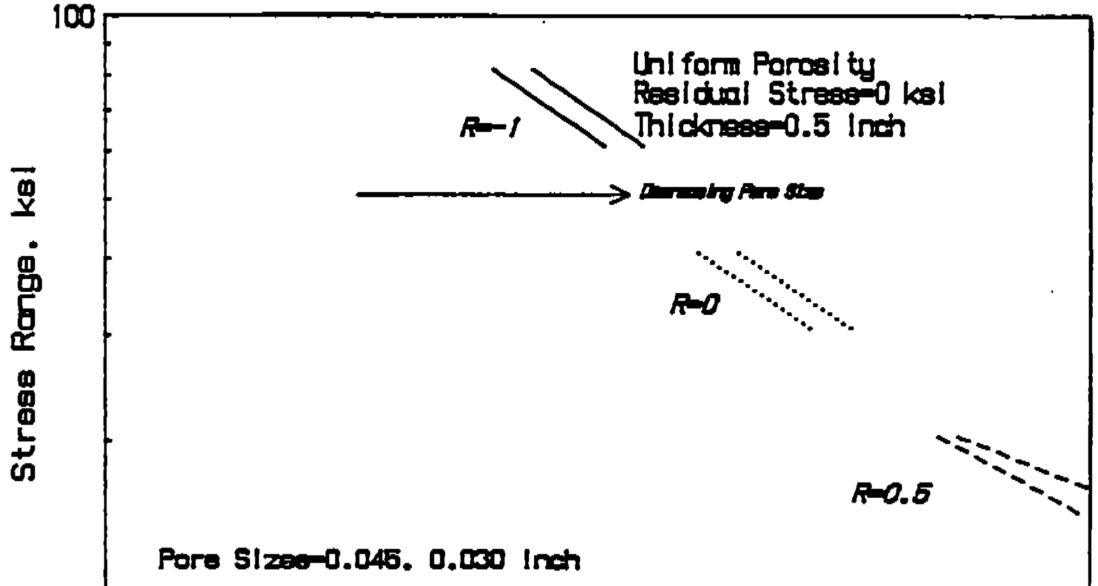

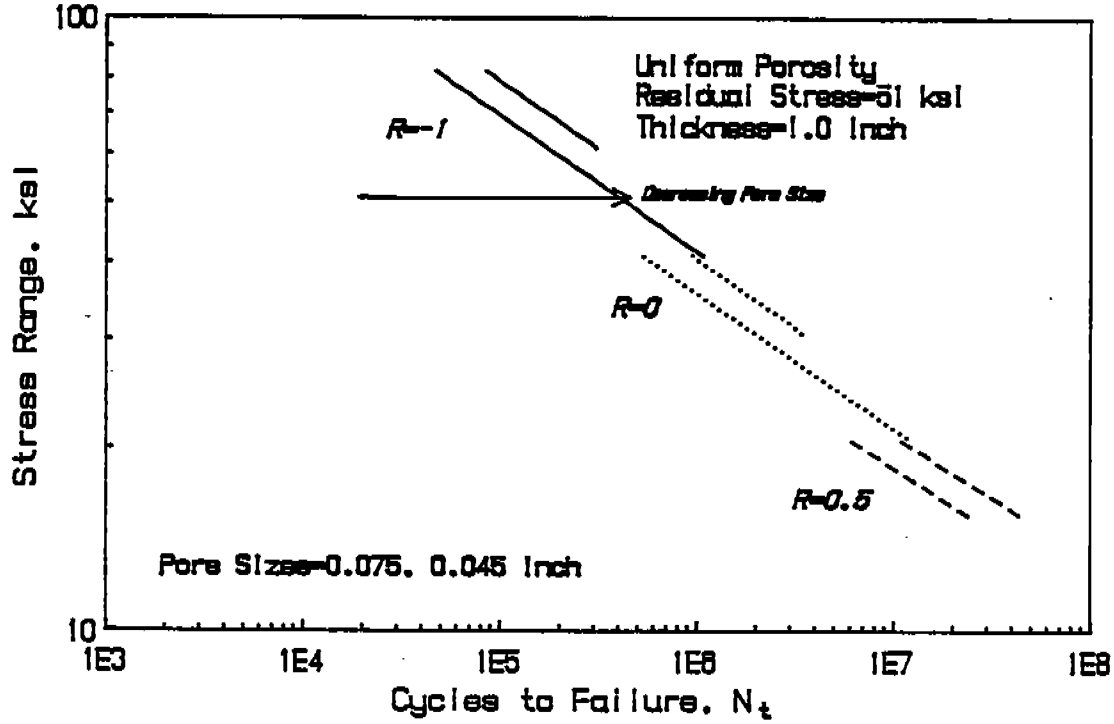

FIGURE 25. S-N CURVES FOR UNIFORM POROSITY GEOMETRY IN A 1.0-INCH THICK PLATE AND 51 KSI RESIDUAL STRESS

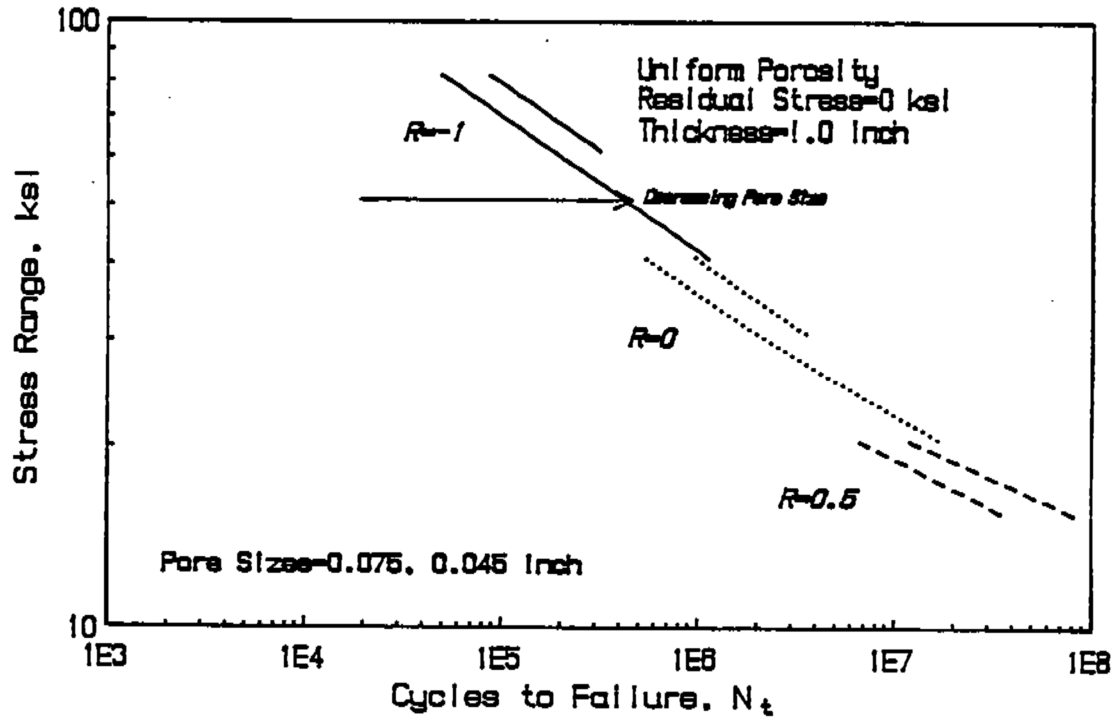

FIGURE 26. S-N CURVES FOR UNIFORM POROSITY GEOMETRY IN A 1.0-INCH THICK PLATE AND ZERO RESIDUAL STRESS

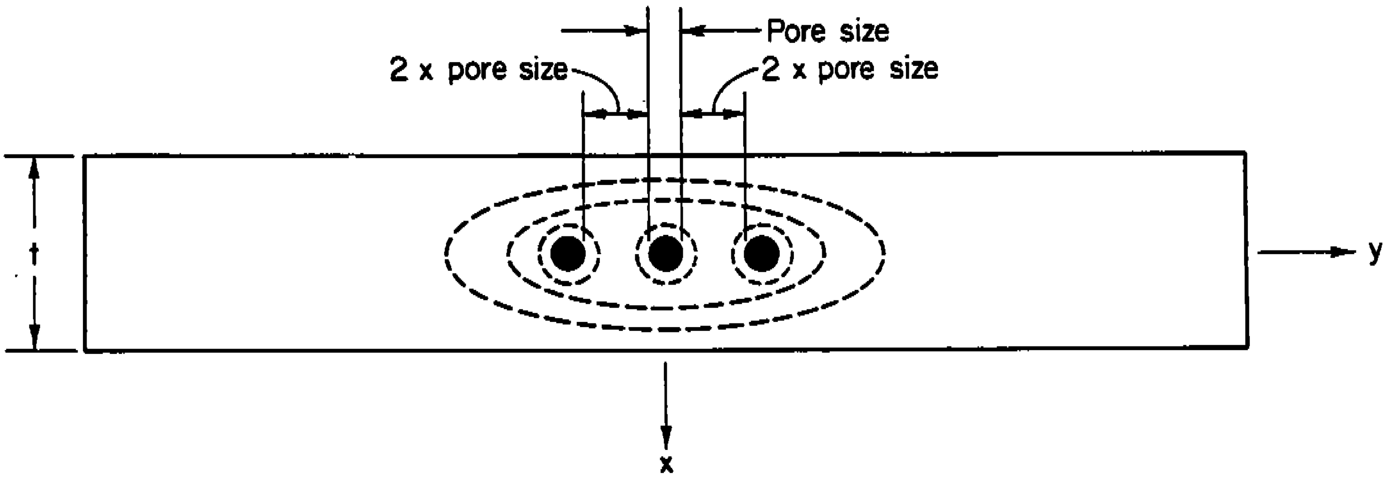

FIGURE 27. GEOMETRY AND ASSUMED CRACK GROWTH PATTERN (DASHED LINE) FOR CO-LINEAR PORES

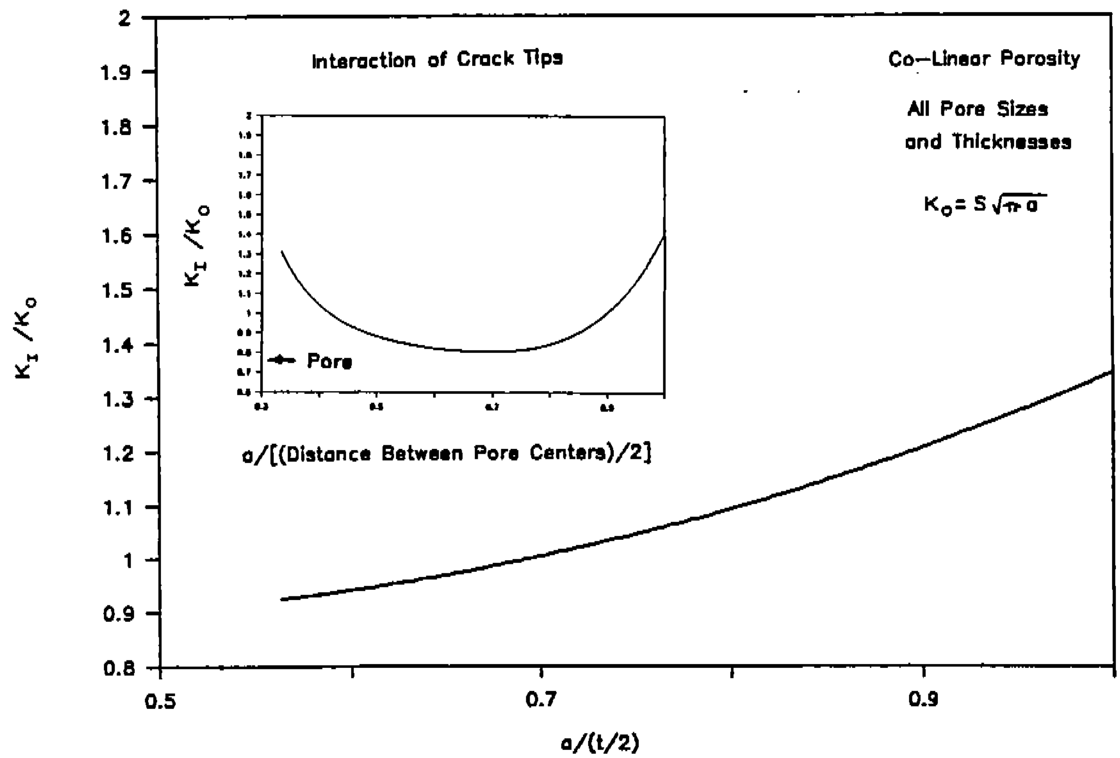

FIGURE 28. STRESS INTENSITY SOLUTION FOR CO-LINEAR POROSITY. INSET SHOWS THE RISE IN STRESS INTENSITY AS THE CRACK TIPS FROM INDIVIDUAL PORES APPROACH EACH OTHER

containing co-linear porosity based upon the pores alone. Assuming that the weld may have a significant crack initiation period may be highly unconservative if a planar defect such as lack of penetration is present. The analysis technique presented here does not account for any planar defects and should be considered in the light of the foregoing comments.

The pores are initially spaced two pore diameters apart so no stress gradient interaction is assumed. The cracks initiating from the pores are assumed to occur at nearly the same time and grow simultaneously. Before the individual circular cracks join, there will be interaction between the approaching crack tips resulting in an increased stress intensity factor and accelerated crack growth. No stress intensity solution was available for two co-planar cracks in a three dimensional medium so this interaction was approximated by the solution two dimensional sheet solution[21]. The solution is represented by the polynomial expression

$$M_{co} = 1 + 0.88(a/d) - 6.6(a/d)^2 + 23.3(a/d)^3 - 32.9(a/d)^4 + 16.6(a/d)^5 \qquad (18)$$

where a is the crack radius and d is the distance between pore centers. The stress intensity solution is shown in the inset in Figure 28. This assumption is conservative although somewhat tempered by the crack shape factor Φ_0 in Equation (13). For a circular crack, Φ_0 is 1.57 which reduces the stress intensity by about 0.6.

After the individual circular cracks join, the crack shape becomes elliptical (a/c equals approximately 0.4) and growth continues. As with the circular cracks, the elliptical crack is assumed to undergo self-similar growth. This assumption is less accurate since elliptical cracks actually tend to grow into the more energetically stable circular shape. The M_t correction factor for the elliptical crack is again found in[21] (pages 294-295) and is approximated by

$$M_t = 1.22 - 1.10(a/(t/2)) + 1.40(a/(t/2))^2 \quad . \qquad (19)$$

The stress intensity solution is plotted in Figure 28. The results of the fatigue predictions are given in Tables 9 and 10 and as S-N curves in Figures 29-32.

7.3.6. Cluster Porosity

The pore geometry and assumed crack growth pattern for the cluster porosity analysis is shown in Figure 33. The cluster porosity is the most difficult to model analytically because of the infinite variety of pore sizes and configurations which clusters can assume. This variety is apparent from the fracture surface photographs in Figure 8. The geometry for the analysis presented here was chosen to model the three dimensional nature of clusters (not all pores on the same plane) and the possibility of interaction between individual clusters. The individual pores are all equal size and are assumed to initiate a crack at the same time. They are spaced a distance of 0.25 times the individual pore size so the stress gradients will interact (see Figure 5). The interaction results in an increased stress concentration factor and, therefore, fatigue notch factor.

The initiation life for the clusters consists of two stages: individual pore cracking coalescence; and initiation of a crack around the periphery of the cluster. Because the stress concentration factor is higher for the material toward the center of the cluster due to interaction, that material is more severely damaged compared to the material on the periphery of the cluster. The cycles to coalescence is calculated using the higher, interaction-influenced, fatigue notch factor. Meanwhile the periphery material has accumulated a lesser amount of fatigue damage although not enough to have initiated cracking. Using the Palmgren-Miner linear damage rule,

$$\sum \frac{N_{(\text{at stress level } x)}}{N_{(\text{failure at stress level } x)}} = 1 \text{ at failure} \qquad (20)$$

TABLE 9. CO-LINEAR POROSITY CONSTANT AMPLITUDE FATIGUE LIFE PREDICTIONS
THICKNESS = 0.5 INCH
NUMBER OF PORES = 3
ABS EH36

Stress Ratio=-1 Residual Stress=51 ksi		Pore=0.125 inch			Pore=0.1875 inch			Pore=0.250 inch		
	Stress Range (ksi)	N-Init	N-Prop	N-TOTAL	N-Init	N-Prop	N-TOTAL	N-Init	N-Prop	N-TOTAL
	81.60	2590	5852	8442	2362	3307	5669	2251	1648	3899
	61.20	8835	21359	30194	7971	12070	20041	7554	6016	13570
	40.80	79753	132436	212189	68868	74820	143688	63821	37300	101121
	20.40	32537876	2996330	35534206	25656872	1693400	27350272	22652879	844100	23496979

Stress Ratio=0 Residual Stress=51 ksi		Pore=0.125 inch			Pore=0.1875 inch			Pore=0.250 inch		
	Stress Range (ksi)	N-Init	N-Prop	N-TOTAL	N-Init	N-Prop	N-TOTAL	N-Init	N-Prop	N-TOTAL
	40.80	25725	66199	91924	22024	37416	59440	20317	18650	38967
	30.60	245351	241645	486996	201521	136560	338081	181869	68070	249939
	20.40	13532427	1498360	15030787	10576766	846500	11423266	9285158	422000	9707158
	10.20			>100000000			>100000000			>100000000

Stress Ratio=0.5 Residual Stress=51 ksi		Pore=0.125 inch			Pore=0.1875 inch			Pore=0.250 inch		
	Stress Range (ksi)	N-Init	N-Prop	N-TOTAL	N-Init	N-Prop	N-TOTAL	N-Init	N-Prop	N-TOTAL
	20.40	3346237	748950	4095187	2585698	423310	3009008	2258772	211000	2469772
	15.30			>100000000	78718952	1545000	80263952	67927084	770100	68697184
	10.20			>100000000			>100000000			>100000000
	5.10			>100000000			>100000000			>100000000

Stress Ratio=-1 Residual Stress=0 ksi		Pore=0.125 inch			Pore=0.1875 inch			Pore=0.250 inch		
	Stress Range (ksi)	N-Init	N-Prop	N-TOTAL	N-Init	N-Prop	N-TOTAL	N-Init	N-Prop	N-TOTAL
	81.60	9766	5852	15618	8691	3307	11998	8175	1648	9823
	61.20	48345	21359	69704	42170	12070	54240	39270	6016	45286
	40.80	942751	132436	1075187	772719	74820	847539	696953	37300	734253
	20.40			>100000000			>100000000			>100000000

Stress Ratio=0 Residual Stress=0 ksi		Pore=0.125 inch			Pore=0.1875 inch			Pore=0.250 inch		
	Stress Range (ksi)	N-Init	N-Prop	N-TOTAL	N-Init	N-Prop	N-TOTAL	N-Init	N-Prop	N-TOTAL
	40.80	122443	66199	188642	101635	37416	139051	92270	18650	110920
	30.60	1867610	241645	2109255	1469932	136560	1606492	1297597	68070	1365667
	20.40			>100000000			>100000000			>100000000
	10.20			>100000000			>100000000			>100000000

Stress Ratio=0.5 Residual Stress=0 ksi		Pore=0.125 inch			Pore=0.1875 inch			Pore=0.250 inch		
	Stress Range (ksi)	N-Init	N-Prop	N-TOTAL	N-Init	N-Prop	N-TOTAL	N-Init	N-Prop	N-TOTAL
	20.40	22816405	748950	23565355	17001351	423310	17424661	14573639	211000	14784639
	15.30			>100000000			>100000000			>100000000
	10.20			>100000000			>100000000			>100000000
	5.10			>100000000			>100000000			>100000000

TABLE 10. CO-LINEAR POROSITY CONSTANT AMPLITUDE FATIGUE LIFE PREDICTIONS
THICKNESS = 1.0 INCH
NUMBER OF PORES = 3
ABS EH36

Stress Ratio=-1		Pore=0.1875 inch			Pore=0.250 inch			Pore=0.300 inch		
Residual Stress=51 ksi	Stress Range (ksi)	N-Init	N-Prop	N-TOTAL	N-Init	N-Prop	N-TOTAL	N-Init	N-Prop	N-TOTAL
	81.6	2362	3784	6146	2251	2462	4713	2196	1903	4099
	61.2	7971	13806	21777	7554	8978	16532	7350	6943	14293
	40.8	68868	85595	154463	63821	55665	119486	61393	43048	104441
	20.4	25656872	1937150	27594022	22652879	1259450	23912329	21253360	973990	22227350

Stress Ratio=0		Pore=0.1875 inch			Pore=0.250 inch			Pore=0.300 inch		
Residual Stress=51 ksi	Stress Range (ksi)	N-Init	N-Prop	N-TOTAL	N-Init	N-Prop	N-TOTAL	N-Init	N-Prop	N-TOTAL
	40.8	22024	42801	64825	20317	27834	48151	19498	21524	41022
	30.6	201521	156215	357736	181869	101566	283435	172584	78545	251129
	20.4	10576766	968396	11545162	9285158	629779	9914937	8700163	487030	9187193
	10.2			>100000000			>100000000			>100000000

Stress Ratio=0.5		Pore=0.1875 inch			Pore=0.250 inch			Pore=0.300 inch		
Residual Stress=51 ksi	Stress Range (ksi)	N-Init	N-Prop	N-TOTAL	N-Init	N-Prop	N-TOTAL	N-Init	N-Prop	N-TOTAL
	20.4	2585648	484219	3069867	2258772	314913	2573685	2107711	243524	2351235
	15.3	78718952	1767380	80486332	67927084	1149080	69076164	62977515	888630	63866145
	10.2			>100000000			>100000000			>100000000
	5.1			>100000000			>100000000			>100000000

Stress Ratio=-1		Pore=0.1875 inch			Pore=0.250 inch			Pore=0.300 inch		
Residual Stress=0 ksi	Stress Range (ksi)	N-Init	N-Prop	N-TOTAL	N-Init	N-Prop	N-TOTAL	N-Init	N-Prop	N-TOTAL
	81.6	8691	3784	12475	8175	2462	10637	7923	1903	9826
	61.2	42170	13806	55976	39270	8978	48248	37867	6943	44810
	40.8	772719	85595	858314	696953	55665	752618	661249	43048	704297
	20.4			>100000000			>100000000			>100000000

Stress Ratio=0		Pore=0.1875 inch			Pore=0.250 inch			Pore=0.300 inch		
Residual Stress=0 ksi	Stress Range (ksi)	N-Init	N-Prop	N-TOTAL	N-Init	N-Prop	N-TOTAL	N-Init	N-Prop	N-TOTAL
	40.8	101635	42801	144436	92270	27834	120104	87833	21524	109357
	30.6	1469932	156215	1626147	1297597	101566	1399163	1217575	78545	1296120
	20.4			>100000000			>100000000			>100000000
	10.2			>100000000			>100000000			>100000000

Stress Ratio=0.5		Pore=0.1875 inch			Pore=0.250 inch			Pore=0.300 inch		
Residual Stress=0 ksi	Stress Range (ksi)	N-Init	N-Prop	N-TOTAL	N-Init	N-Prop	N-TOTAL	N-Init	N-Prop	N-TOTAL
	20.4	17001351	484219	17485570	14573639	314913	14888552	13468239	243524	13711763
	15.3			>100000000			>100000000			>100000000
	10.2			>100000000			>100000000			>100000000
	5.1			>100000000			>100000000			>100000000

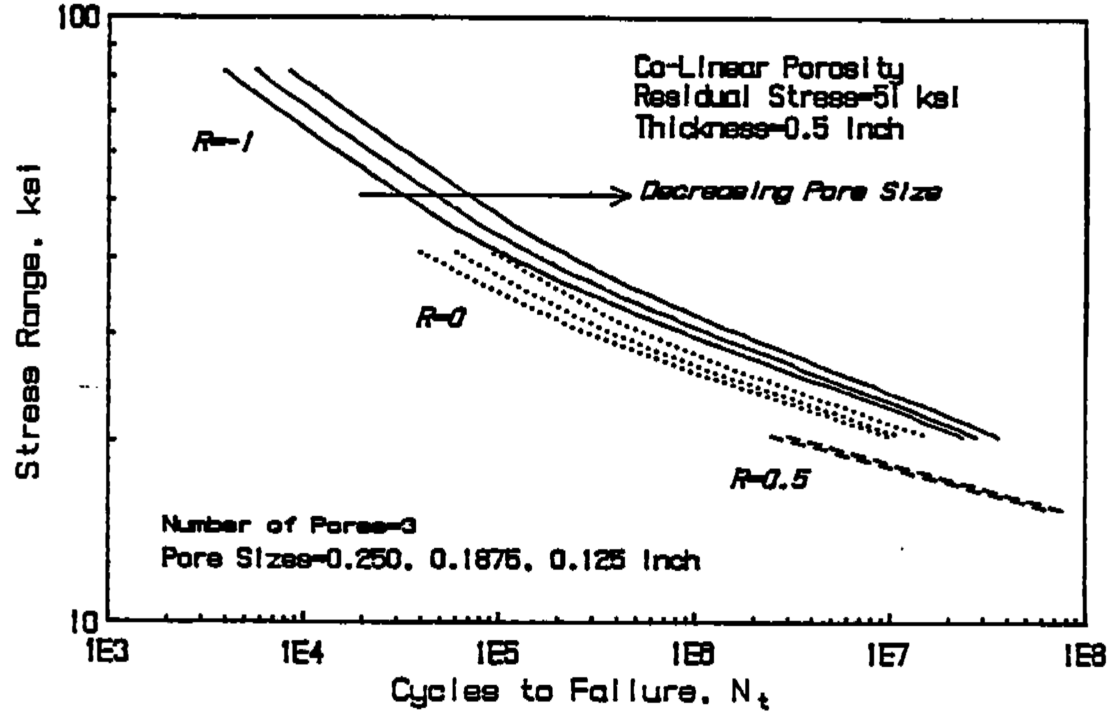

FIGURE 29. S-N CURVES FOR CO-LINEAR POROSITY GEOMETRY IN A 0.5-INCH THICK PLATE AND 51 KSI RESIDUAL STRESS

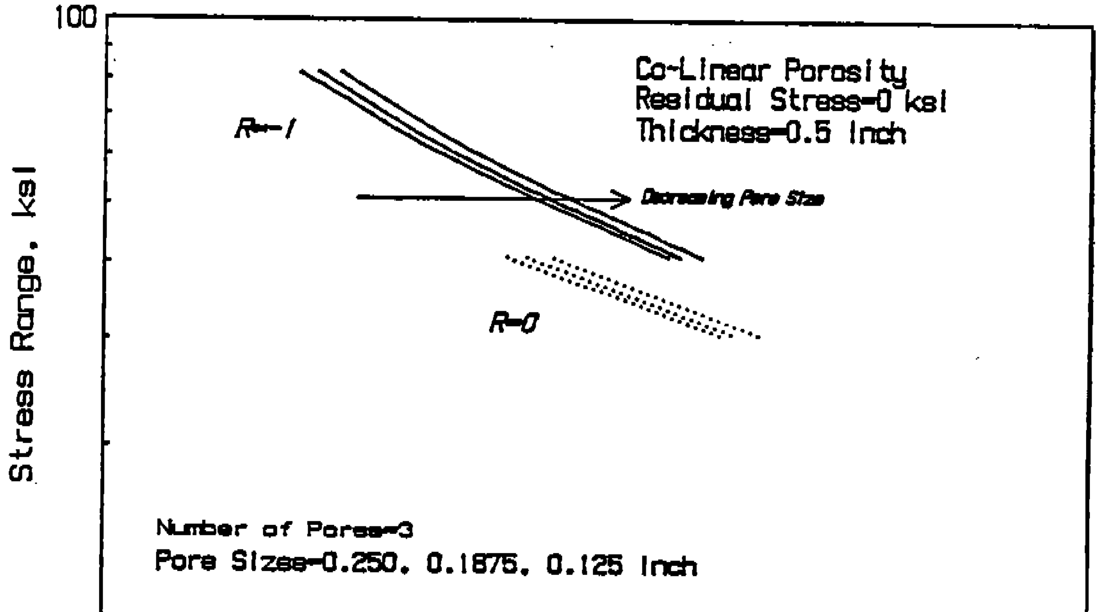

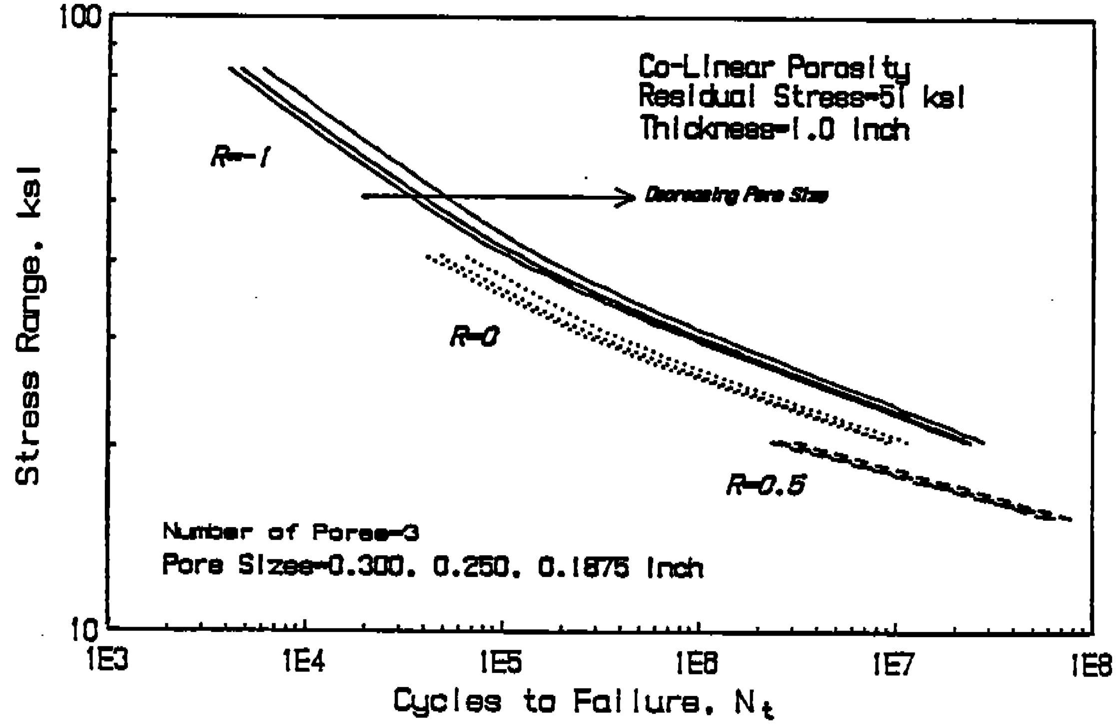

FIGURE 31. S-N CURVES FOR CO-LINEAR POROSITY GEOMETRY IN A 1.0-INCH THICK PLATE AND 51 KSI RESIDUAL STRESS

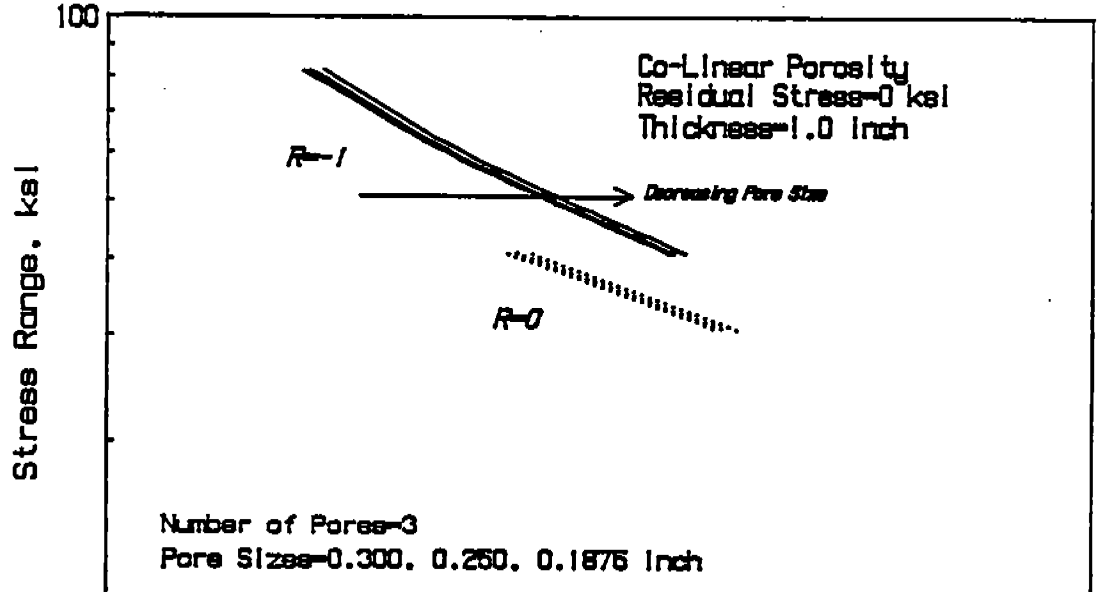

where N denotes cycles, the outer material has been damaged an amount

$$\frac{N_{(coalescence)}}{N_{(failure\ a\ periphery\ stress\ level)}} .$$

Before initiating a fatigue crack, the outer material must satisfy Miner's criteria (Equation 20). After the inner region of the pores coalesce, the load path around the cluster will change because load can no longer be carried between the pore ligaments. Although the stress field around the cluster will admittedly be very complex, it is assumed for our purposes to approximate the stress field around an ellipsoid of comparable dimensions. Observing Figure 33, the ellipsoid will be an oblate spheroid, half as high as it is wide. In reference to Figure 3, it would be of the shape a=b=1 and c=0.5. The remaining initiation life of the cluster (before a crack begins growing radially) at this new higher stress concentration level is calculated from Equation 20. The total initiation life is taken as the cycles to cause coalescence and the cycles remaining before the periphery initiates a crack. The crack growth stress intensity solution is shown in Figure 34. Note the high initial stress intensity factor. This is due to the high stresses resulting from the assumed ellipsoid shape of the coalesced cavity. The stress intensity factor decays rapidly and the solution becomes dominated by the M_t factor. This is the same as the single pore M_t solution, Equation 16, because both are circular cracks.

The fatigue life predictions for the cluster geometry are presented in Tables 11 and 12 and as S-N curves in Figures 35-38.

8. VARIABLE AMPLITUDE LOADING

8.1. SL-7 Containership Instrumentation Program

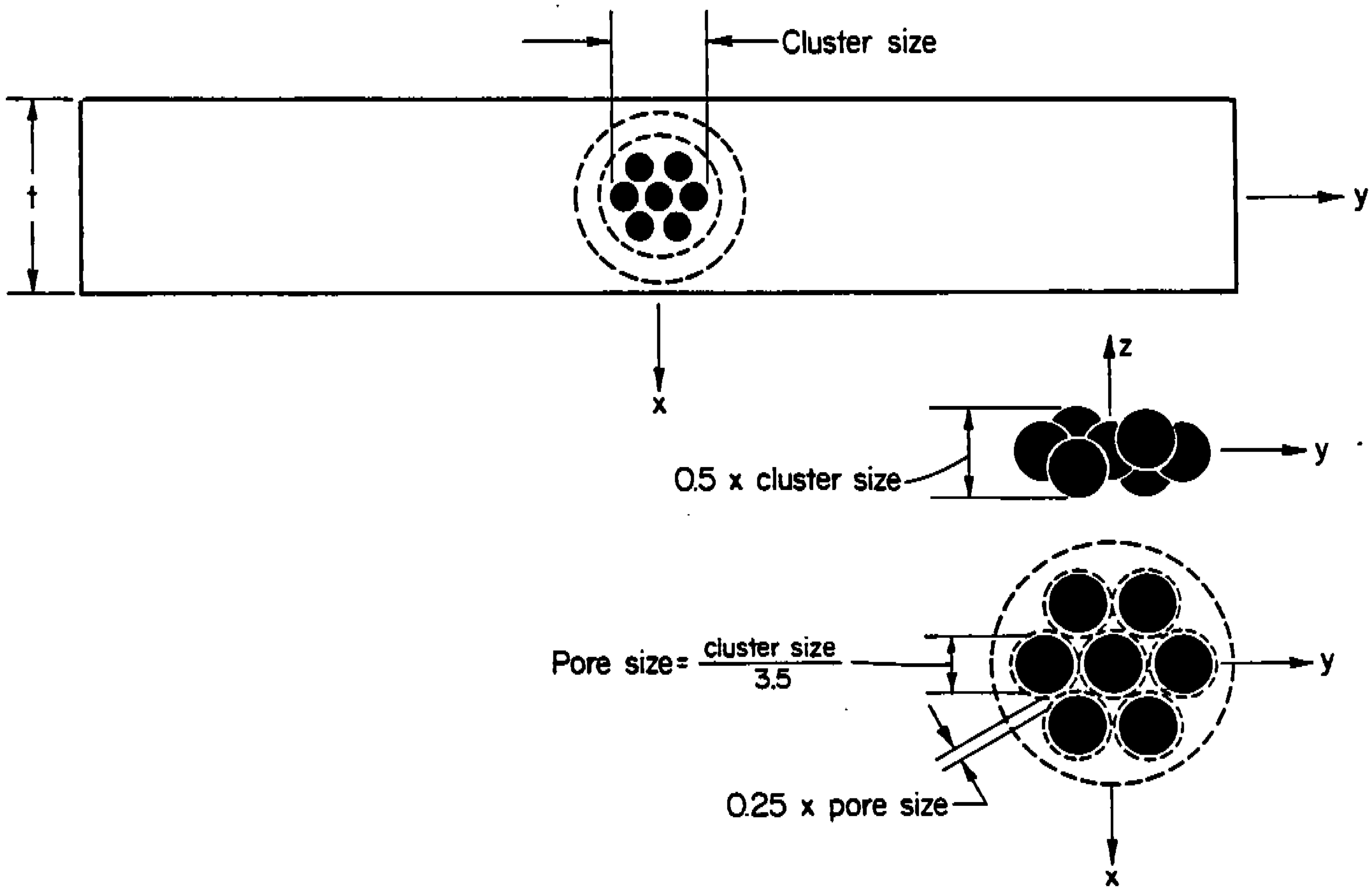

FIGURE 33. GEOMETRY AND ASSUMED CRACK GROWTH PATTERN (DASHED LINE) FOR CLUSTER POROSITY

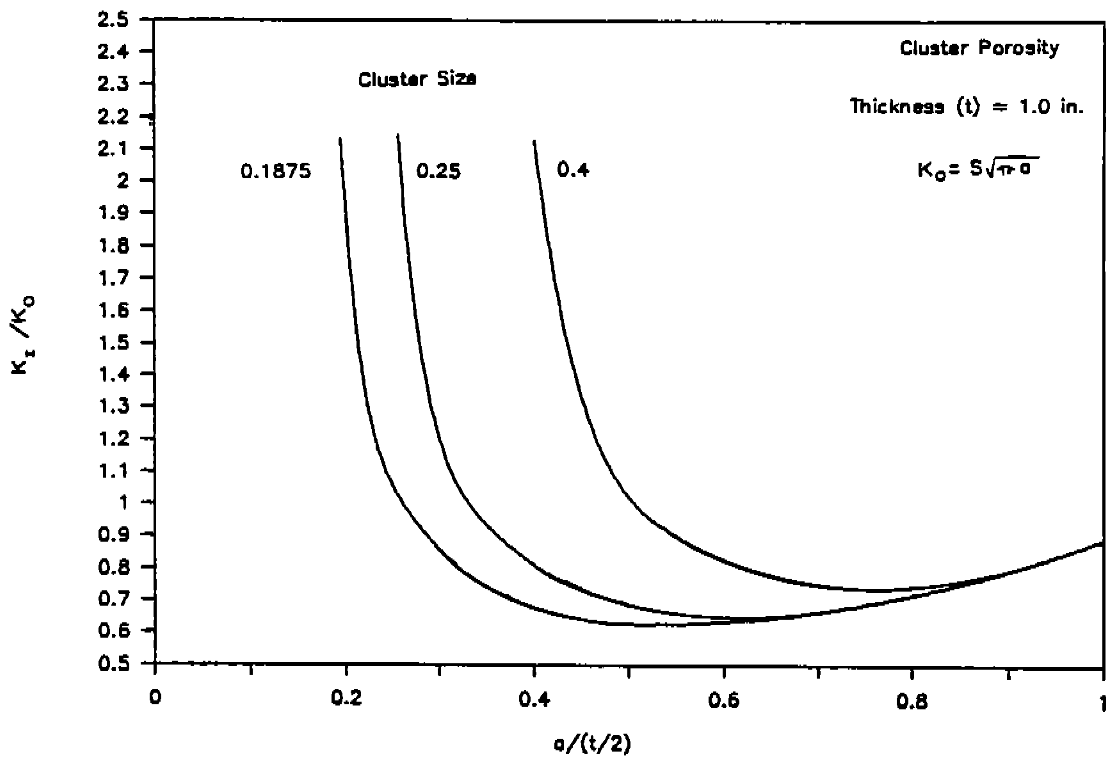

FIGURE 34. STRESS INTENSITY SOLUTION FOR CLUSTER POROSITY IN A 1.0-INCH THICK PLATE

TABLE 11. CLUSTER POROSITY CONSTANT AMPLITUDE FATIGUE LIFE PREDICTIONS
THICKNESS = 0.5 INCH
ABS EH36

Stress Ratio=-1		Pore=0.125 inch			Pore=0.1875 inch			Pore=0.300 inch		
Residual Stress=51 ksi	Stress Range (ksi)	N-Init	N-Prop	N-TOTAL	N-Init	N-Prop	N-TOTAL	N-Init	N-Prop	N-TOTAL
	81.60	3001	264	3265	2416	146	2562	1993	39	2032
	61.20	10339	26403	36742	8113	2455	10568	6567	140	6707
	40.80	94945	184396	279341	67455	66133	133588	50364	7379	57743
	20.40	39549543	4206900	43756443	22645488	1420820	24066308	13854792	171500	14026292

Stress Ratio=0		Pore=0.125 inch			Pore=0.1875 inch			Pore=0.300 inch		
Residual Stress=51 ksi	Stress Range (ksi)	N-Init	N-Prop	N-TOTAL	N-Init	N-Prop	N-TOTAL	N-Init	N-Prop	N-TOTAL
	40.80	30602	96121	126723	21297	32096	53393	15603	433	16036
	30.60	294409	306410	600819	185885	128011	313896	124795	12936	137731
	20.40	16524396	2011560	18535956	9265536	739750	10005286	5563810	85760	5649570
	10.20			>100000000			>100000000			>100000000

Stress Ratio=0.5		Pore=0.125 inch			Pore=0.1875 inch			Pore=0.300 inch		
Residual Stress=51 ksi	Stress Range (ksi)	N-Init	N-Prop	N-TOTAL	N-Init	N-Prop	N-TOTAL	N-Init	N-Prop	N-TOTAL
	20.40	4112120	1045220	5157340	2244159	365790	2609949	46141	1315703	1361844
	15.30			>100000000	66980861	1318920	68299781	153810	37222982	37376792
	10.20			>100000000			>100000000			>100000000
	5.10			>100000000			>100000000			>100000000

Stress Ratio=-1		Pore=0.125 inch			Pore=0.1875 inch			Pore=0.300 inch		
Residual Stress=0 ksi	Stress Range (ksi)	N-Init	N-Prop	N-TOTAL	N-Init	N-Prop	N-TOTAL	N-Init	N-Prop	N-TOTAL
	81.60	11398	264	11662	8664	146	8810	6804	39	6843
	61.20	56988	26403	83391	41356	2455	43811	31318	140	31458
	40.80	1136570	184396	1320966	714279	66133	780412	480025	7379	487404
	20.40			>100000000			>100000000			>100000000

Stress Ratio=0		Pore=0.125 inch			Pore=0.1875 inch			Pore=0.300 inch		
Residual Stress=0 ksi	Stress Range (ksi)	N-Init	N-Prop	N-TOTAL	N-Init	N-Prop	N-TOTAL	N-Init	N-Prop	N-TOTAL
	40.80	146864	96121	242985	95043	32096	127139	65459	433	65892
	30.60	2284339	306410	2590749	1303686	128011	1431697	802714	12936	815650
	20.40			>100000000			>100000000	85582813	85760	85668573
	10.20			>100000000			>100000000			>100000000

Stress Ratio=0.5		Pore=0.125 inch			Pore=0.1875 inch			Pore=0.300 inch		
Residual Stress=0 ksi	Stress Range (ksi)	N-Init	N-Prop	N-TOTAL	N-Init	N-Prop	N-TOTAL	N-Init	N-Prop	N-TOTAL
	20.40	28675574	1045220	29720794	14362233	365790	14728023	7814651	1315703	9130354
	15.30			>100000000			>100000000			>100000000
	10.20			>100000000			>100000000			>100000000
	5.10			>100000000			>100000000			>100000000

TABLE 12. CLUSTER PORE CONSTANT AMPLITUDE FATIGUE LIFE PREDICTIONS
THICKNESS = 1.0 INCH
ABS EH36

Stress Ratio=-1		Pore=0.1875 inch			Pore=0.250 inch			Pore=0.400 inch		
Residual Stress=51 ksi	Stress Range (ksi)	N-Init	N-Prop	N-TOTAL	N-Init	N-Prop	N-TOTAL	N-Init	N-Prop	N-TOTAL
	81.60	2416	151	2567	2132	112	2244	1823	55	1878
	61.20	8113	4762	12875	7068	404	7472	5958	196	6154
	40.80	67455	130813	198268	55727	82902	138629	44122	23137	67259
	20.40	22645488	2787320	25432808	16450388	1885270	18335658	11041311	557720	11599031

Stress Ratio=0		Pore=0.1875 inch			Pore=0.250 inch			Pore=0.400 inch		
Residual Stress=51 ksi	Stress Range (ksi)	N-Init	N-Prop	N-TOTAL	N-Init	N-Prop	N-TOTAL	N-Init	N-Prop	N-TOTAL
	40.80	21297	64368	85665	17380	38824	56204	13546	5640	19186
	30.60	185885	251111	436996	143330	151976	295306	104037	43862	147899
	20.40	9265536	1441270	10706806	6649569	925680	7575249	4395581	261050	4656631
	10.20			>100000000			>100000000			>100000000

Stress Ratio=0.5		Pore=0.1875 inch			Pore=0.250 inch			Pore=0.400 inch		
Residual Stress=51 ksi	Stress Range (ksi)	N-Init	N-Prop	N-TOTAL	N-Init	N-Prop	N-TOTAL	N-Init	N-Prop	N-TOTAL
	20.40	2244159	675320	2919479	1585675	442058	2027733	1027960	138664	1166624
	15.30	66980861	2791330	69772191	45742008	1734370	47476378	28309538	495850	28805388
	10.20			>100000000			>100000000			>100000000
	5.10			>100000000			>100000000			>100000000

Stress Ratio=-1		Pore=0.1875 inch			Pore=0.250 inch			Pore=0.400 inch		
Residual Stress=0 ksi	Stress Range (ksi)	N-Init	N-Prop	N-TOTAL	N-Init	N-Prop	N-TOTAL	N-Init	N-Prop	N-TOTAL
	81.60	8664	151	8815	7404	112	7516	6084	55	6139
	61.20	41356	4762	46118	34501	404	34905	27571	196	27767
	40.80	714279	130813	845092	550875	82902	633777	400954	23137	424091
	20.40			>100000000			>100000000			>100000000

Stress Ratio=0		Pore=0.1875 inch			Pore=0.250 inch			Pore=0.400 inch		
Residual Stress=0 ksi	Stress Range (ksi)	N-Init	N-Prop	N-TOTAL	N-Init	N-Prop	N-TOTAL	N-Init	N-Prop	N-TOTAL
	40.80	95043	64368	159411	74490	38824	113314	55270	5640	60910
	30.60	1303686	251111	1554797	950036	151976	1102012	643493	43862	687355
	20.40			>100000000			>100000000	63851693	261050	64112743
	10.20			>100000000			>100000000			>100000000

Stress Ratio=0.5		Pore=0.1875 inch			Pore=0.250 inch			Pore=0.400 inch		
Residual Stress=0 ksi	Stress Range (ksi)	N-Init	N-Prop	N-TOTAL	N-Init	N-Prop	N-TOTAL	N-Init	N-Prop	N-TOTAL
	20.40	28675574	675320	29350894	9666141	442058	10108199	5900281	138664	6038945
	15.30			>100000000			>100000000			>100000000
	10.20			>100000000			>100000000			>100000000
	5.10			>100000000			>100000000			>100000000

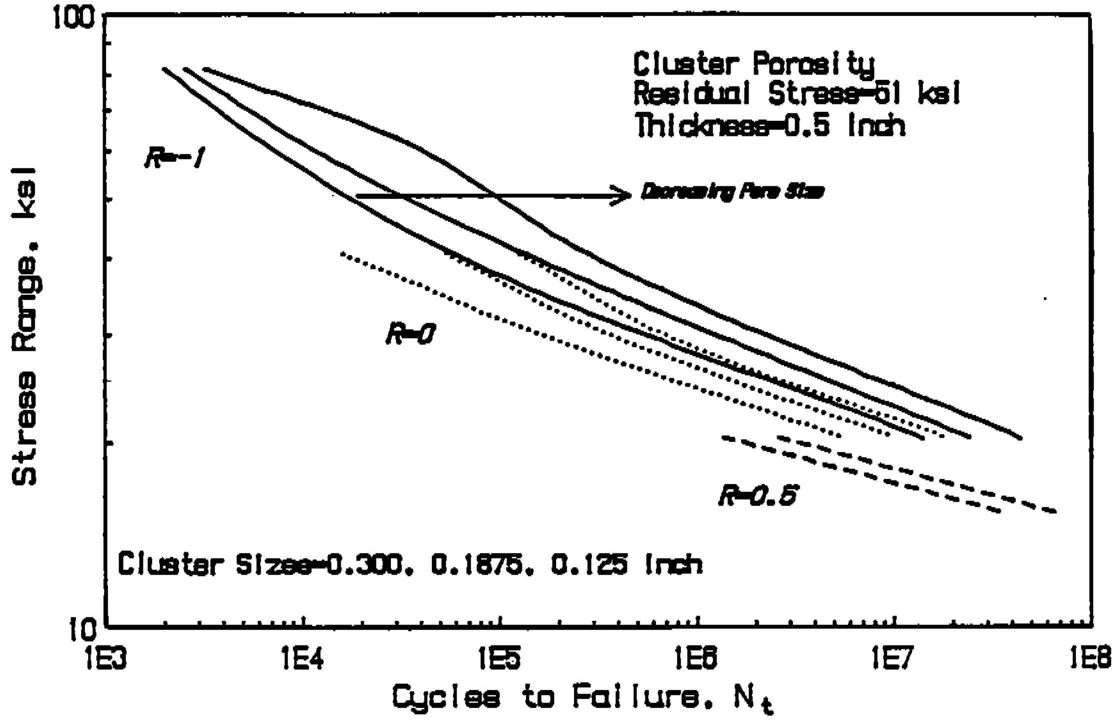

FIGURE 35. S-N CURVES FOR CLUSTER POROSITY IN A 0.5-INCH THICK PLATE AND 51 KSI RESIDUAL STRESS

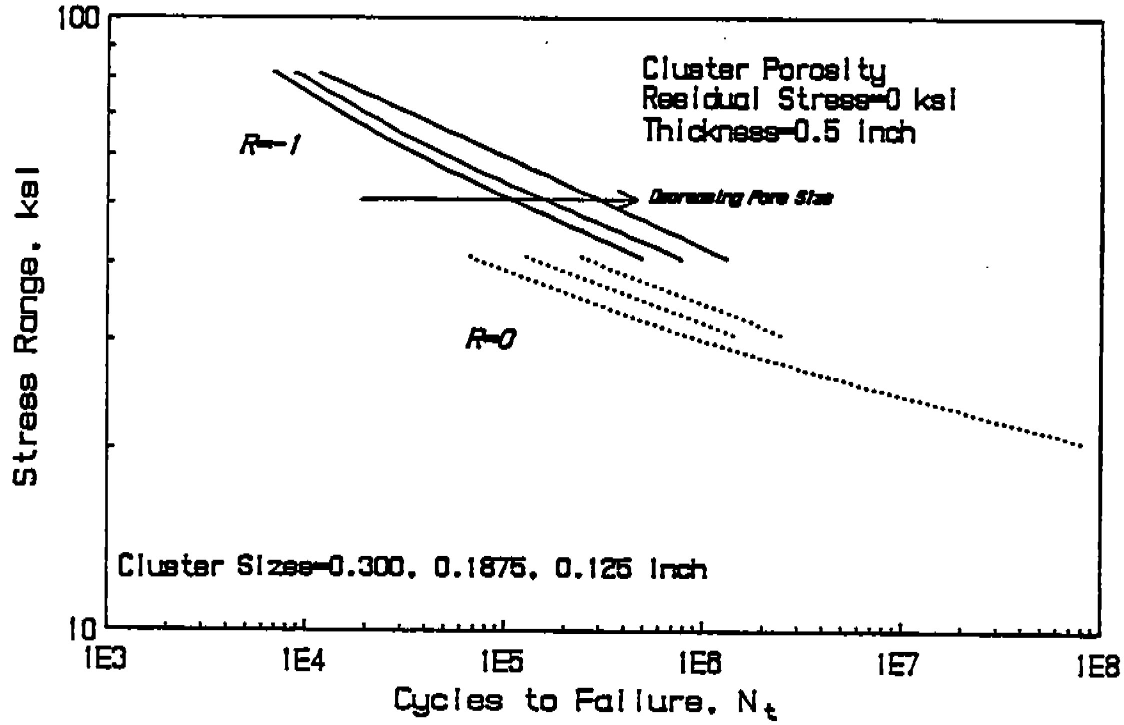

FIGURE 36. S-N CURVES FOR CLUSTER POROSITY IN A 0.5-INCH THICK PLATE AND ZERO RESIDUAL STRESS

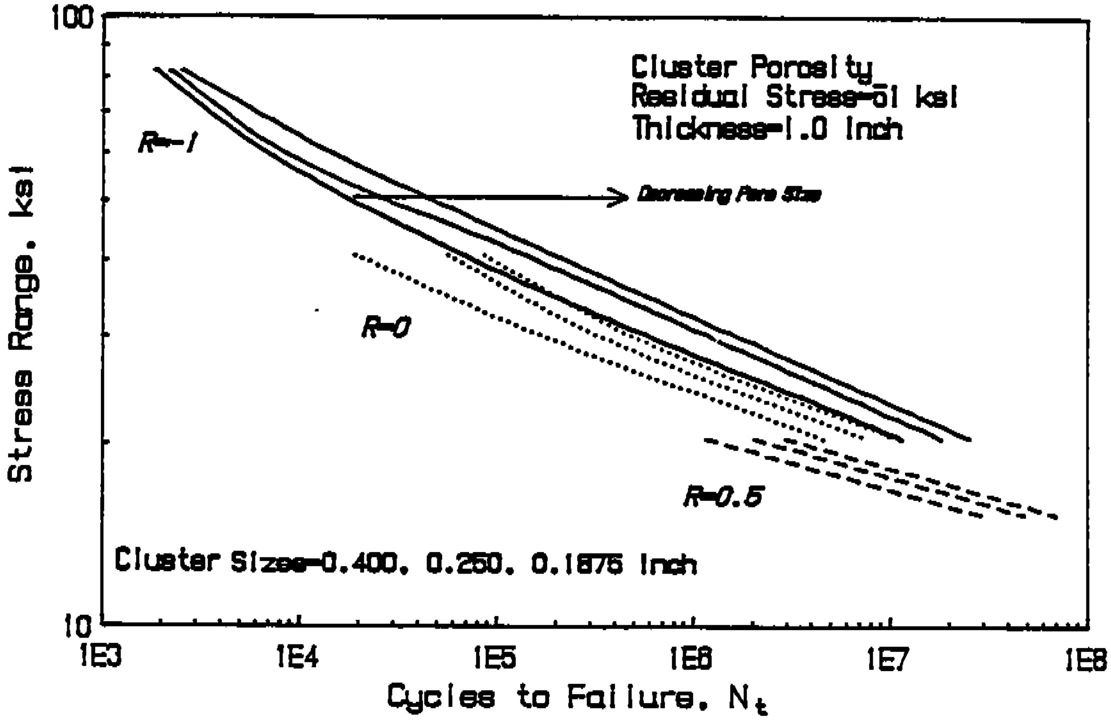

FIGURE 37. S-N CURVES FOR CLUSTER POROSITY IN A 1.0-INCH THICK PLATE AND 51 KSI RESIDUAL STRESS

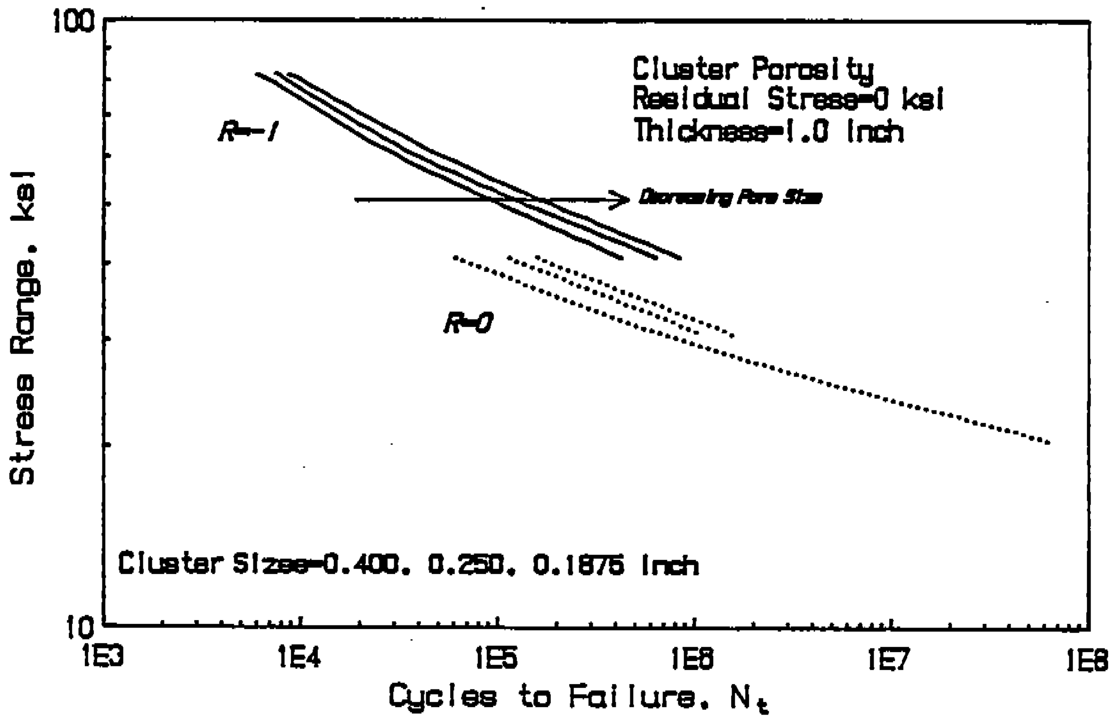

FIGURE 38. S-N CURVES FOR CLUSTER POROSITY IN A 1.0-INCH THICK PLATE AND ZERO RESIDUAL STRESS

transatlantic and transpacific routes. A sample of this data was used to generate a stress history to be used in the predictive model.

8.1.1. Data Characteristics

Stresses induced in a ship structural element have components from a number of sources. These include[12] local residual stress from fabrication or welding, initial still water bending stress, varying mean stress due to fuel burn off, the ships own wave system, diurnal thermal stresses, low frequency wave-induced stress, and high frequency wave induced stress. Of these only the wave induced stresses, both low and high frequency will be used in constructing a stress history for the model. The other sources will be considered as quasi-static, contributing to the instantaneous mean stress rather being than a source of cyclic loading.

High frequency wave induced stresses are caused by dynamic wave loading against the ship structure. These can consist of bottom slamming, shipping of water on deck, and flare impact. Dynamic loads produce whipping and springing elastic motions of the hull, typically at higher than the frequency of wave encounter. Low frequency wave-induced stresses occur at the same frequency as wave encounter. These are caused by the wave forces on the hull. The level of stress is directly related (although not directly proportional to) the significant wave height of the encountered seaway.

The stresses recorded during the SL-7 instrumentation program are the maximum peak stress and the maximum trough stress which occur during a four hour recording interval. These maximum stresses do not necessarily occur during the same cycle. In general, the maximum peak and trough stress recorded will be produced by a dynamic, high frequency load. Therefore, the majority of the reported data is high frequency data. A limited amount of low frequency data, however, has been reported[12]. A representative history can be constructed from the available low and high frequency data.

The low frequency are directly related to the significant wave height encountered by the ship. The significant wave height is the average height of the highest one third portion of the waves. Figure 39 illustrates the relation between the observed wave height and the root mean square (RMS) stress value. This data was collected on board the SL-7 SEA-LAND McLEAN during 1974; the first date year of the data collection program. The frequency of occurrence for each wave height is reported in[52] and presented in Table 13. From the loading summary sheets presented in Reference 12, the average number of wave cycles during a 20-minute interval is 176 cycles, or 385,440 cycles per month at sea. Using the cycle rate and the reported probability of occurrence for each wave group, a low frequency loading spectrum can be calculated based on RMS stresses.

The histogram[53] of maximum peak to trough stress recorded during date year one aboard the SL-7 SEA-LAND McLEAN (port) is shown Figure 40. Recall that each reported cycle is the maximum value, peak and trough, recorded during a 4-hour interval. The average rate of occurrence for high frequency or burst data is reported in Reference 12 as 18 bursts per 20-minute interval. This converts to 216 bursts for every one burst recorded. In constructing the high frequency portion of the loading spectrum, the conservative assumption will be made that 216 bursts occurred at the same value as the reported maximum. The number of cycles from the high and low frequency loadings are then combined on a per month basis as shown in Table 14. Any overlap of the high and low frequencies were assumed to be additive, i.e., an element of material will be damaged equally by a dynamic load and a low frequency load of equal magnitude.

8.2. Fatigue Predictions

Fatigue predictions were made using the same material properties and pore geometries as in the constant amplitude program. Reference 12 reported an average mean stress of 6.5 ksi. In service, the mean stress actually varies as fuel is spent and from ballast changes. Predictions were made at mean stress biases of 6.5 and 0. The stress history was scaled from 1 to 1.75 to provide a wide range of predicted service lives.

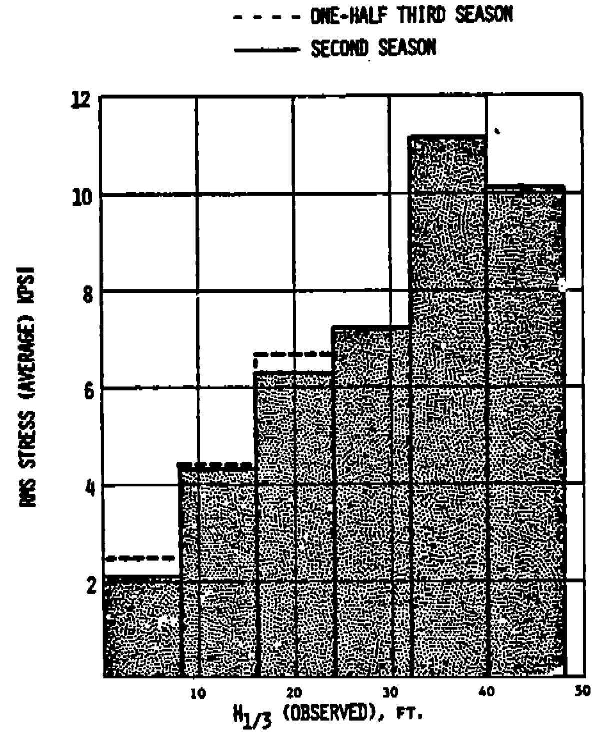

FIGURE 39. AVERAGE RMS STRESS VS. OBSERVED WAVE HEIGHT (AMIDSHIP BENDING STRESS). DASHED LINE REPRESENTS DATA FROM ONE-HALF OF THE THIRD SEASON. SOLID LINE REPRESENTS THE SECOND SEASON

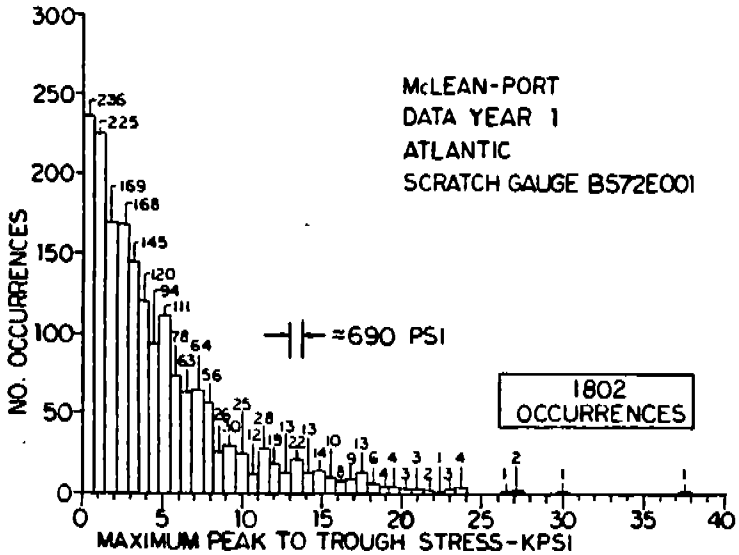

FIGURE 40. HISTOGRAM OF MAXIMUM PEAK TO THROUGH STRESS DURING DATA YEAR 1 ABOARD SL-7 MCLEAN (PORT)

TABLE 13. AVERAGE RMS STRESS BASED ON PROBABILITY OF OCCURRENCE FOR EACH WAVE GROUP

Wave Group	Probability of Occurrence of Wave Group	Average RMS Stress ksi
I	0.6294	2.037
II	0.3133	4.320
III	0.039	6.325
IV	0.0167	7.249
V	0.0012	11.093
VI	0.0004	10.694

TABLE 14. VARIABLE AMPLITUDE LOADING
SL-7 McLEAN
YEAR ONE DATA
ATLANTIC ROUTE

Stress Range (ksi)	Cycles/Month	Relative Frequency
2	261604	0.626
4.3	120758	0.289
6	23024	0.055
7.2	6437	0.015
10.2	3208	0.007
14	1296	0.003
18	864	0.002
22	432	0.001

The results are reported as blocks with each block representing 1 month of service at sea.

No attempt was made to employ a crack growth retardation model because the reported stress data consisted of either maximums recorded over a long time period (high frequency) or an averaged stress (low frequency). As such, no effect of the loading sequence can be accounted for.

8.2.1. Results

The results of the variable amplitude fatigue life predictions are presented in Tables 15-22 and Figures 41-46. In general, the results for the history without being scaled (scale = 1) represent lives many times longer than any design lives, some on the order of thousands of years. For the uniform porosity case where the smallest pores were considered, some cracks were predicted to arrest after growing outside of the pore stress field. As the scale was increased, lives on the order of tens or hundreds of years were predicted.

9. PARAMETRIC DISCUSSION

The model used to predict the fatigue life of weldments containing porosity has been formulated to account for parameters which have been demonstrated to affect fatigue life. Some aspects of the model have been included based upon findings in the literature search dealing specifically with porosity, such as the need for pore interaction in pore clusters. The majority of the model's features are based upon historical precedent of linear elastic fracture mechanics and life predictions in notched specimens. In this section, the model's dependence upon the various parameters is examined. Referring to Table 3, the following parameters were varied in this study: thickness, residual stress, stress ratio, pore size, and porosity type. The features of the model which are influenced by these parameters will be highlighted with examples.

TABLE 15. SINGLE PORE
VARIABLE AMPLITUDE FATIGUE LIFE PREDICTIONS
THICKNESS = 0.5 INCH
ABS EH36

Mean Stress Bias (ksi)	Scale (multiplied by base history)	Pore=0.125 inch N-Init	Pore=0.125 inch N-Prop	Pore=0.125 inch N-TOTAL	Pore=0.1875 inch N-Init	Pore=0.1875 inch N-Prop	Pore=0.1875 inch N-TOTAL	Pore=0.250 inch N-Init	Pore=0.250 inch N-Prop	Pore=0.250 inch N-TOTAL
6.5	1.75	87	124	211	70	46	116	61	15	76
	1.50	307	249	556	242	92	334	206	31	237
	1.25	1613	571	2184	1240	210	1450	1038	71	1109
	1.00	15443	1857	17300	11526	580	12106	9447	196	9643

Mean Stress Bias (ksi)	Scale (multiplied by base history)	Pore=0.125 inch N-Init	Pore=0.125 inch N-Prop	Pore=0.125 inch N-TOTAL	Pore=0.1875 inch N-Init	Pore=0.1875 inch N-Prop	Pore=0.1875 inch N-TOTAL	Pore=0.250 inch N-Init	Pore=0.250 inch N-Prop	Pore=0.250 inch N-TOTAL
0.0	1.75	180	322	502	146	111	257	128	37	165
	1.50	607	857	1464	483	237	720	414	76	490
	1.25	3032	1755	4787	2349	555	2904	1975	183	2158
	1.00	27331	7887	35218	20558	1809	22367	16936	520	17456

TABLE 16. SINGLE PORE
VARIABLE AMPLITUDE FATIGUE LIFE PREDICTIONS
THICKNESS = 1.0 INCH
ABS EH36

Mean Stress Bias (ksi)	Scale (multiplied by base history)	Pore=0.1875 inch N-Init	Pore=0.1875 inch N-Prop	Pore=0.1875 inch N-TOTAL	Pore=0.250 inch N-Init	Pore=0.250 inch N-Prop	Pore=0.250 inch N-TOTAL	Pore=0.300 inch N-Init	Pore=0.300 inch N-Prop	Pore=0.300 inch N-TOTAL
6.5	1.75	73	85	158	64	52	116	60	35	95
	1.50	252	170	422	221	104	325	204	71	275
	1.25	1295	387	1682	1119	237	1356	1022	161	1183
	1.00	12094	1066	13160	10279	649	10928	9289	439	9728

Mean Stress Bias (ksi)	Scale (multiplied by base history)	Pore=0.1875 inch N-Init	Pore=0.1875 inch N-Prop	Pore=0.1875 inch N-TOTAL	Pore=0.250 inch N-Init	Pore=0.250 inch N-Prop	Pore=0.250 inch N-TOTAL	Pore=0.300 inch N-Init	Pore=0.300 inch N-Prop	Pore=0.300 inch N-TOTAL
0.0	1.75	151	203	354	135	124	259	126	83	209
	1.50	501	427	928	442	250	692	409	169	578
	1.25	2449	1016	3465	2126	615	2741	1947	404	2351
	1.00	21544	3248	24792	18389	1844	20233	16661	1160	17821

TABLE 17. UNIFORM POROSITY
VARIABLE AMPLITUDE FATIGUE LIFE PREDICTIONS
THICKNESS = 0.5 INCH
ABS EH36

Mean Stress Bias (ksi)	Scale (multiplied by base history)	Pore=0.015 inch			Pore=0.030 inch			Pore=0.045 inch		
		N-Init	N-Prop	N-TOTAL	N-Init	N-Prop	N-TOTAL	N-Init	N-Prop	N-TOTAL
6.5	1.75		Non-propagating crack		28	2459	2487	16	1315	1331
	1.50		Non-propagating crack			Non-propagating crack		47	3040	3087
	1.25		Non-propagating crack			Non-propagating crack			Non-propagating crack	
	1.00		Non-propagating crack			Non-propagating crack			Non-propagating crack	

Mean Stress Bias (ksi)	Scale (multiplied by base history)	Pore=0.015 inch			Pore=0.030 inch			Pore=0.045 inch		
		N-Init	N-Prop	N-TOTAL	N-Init	N-Prop	N-TOTAL	N-Init	N-Prop	N-TOTAL
0.0	1.75		Non-propagating crack			Non-propagating crack			Non-propagating crack	
	1.50		Non-propagating crack			Non-propagating crack			Non-propagating crack	
	1.25		Non-propagating crack			Non-propagating crack			Non-propagating crack	
	1.00		Non-propagating crack			Non-propagating crack			Non-propagating crack	

TABLE 18. UNIFORM POROSITY
VARIABLE AMPLITUDE FATIGUE LIFE PREDICTIONS
THICKNESS = 1.0 INCH
ABS EH36

Mean Stress Bias (ksi)	Scale (multiplied by base history)	Pore=0.015 inch			Pore=0.045 inch			Pore=0.075 inch		
		N-Init	N-Prop	N-TOTAL	N-Init	N-Prop	N-TOTAL	N-Init	N-Prop	N-TOTAL
6.5	1.75		Non-propagating crack		16	1189	1205	10	575	585
	1.50		Non-propagating crack		47	2718	2765	27	1256	1283
	1.25		Non-propagating crack		197	8987	9184	104	3265	3369
	1.00		Non-propagating crack			Non-propagating crack		698	13426	14124

Mean Stress Bias (ksi)	Scale (multiplied by base history)	Pore=0.015 inch			Pore=0.045 inch			Pore=0.075 inch		
		N-Init	N-Prop	N-TOTAL	N-Init	N-Prop	N-TOTAL	N-Init	N-Prop	N-TOTAL
0.0	1.75		Non-propagating crack			Non-propagating crack		22	1872	1894
	1.50		Non-propagating crack			Non-propagating crack			Non-propagating crack	
	1.25		Non-propagating crack			Non-propagating crack			Non-propagating crack	
	1.00		Non-propagating crack			Non-propagating crack			Non-propagating crack	

TABLE 19. CO-LINEAR POROSITY
VARIABLE AMPLITUDE FATIGUE LIFE PREDICTIONS
NUMBER OF PORES = 3
THICKNESS = 1.0 INCH
ABS EH36

Mean Stress Bias (ksi)	Scale (multiplied by base history)	Pore=0.1875 inch N-Init	Pore=0.1875 inch N-Prop	Pore=0.1875 inch N-TOTAL	Pore=0.250 inch N-Init	Pore=0.250 inch N-Prop	Pore=0.250 inch N-TOTAL	Pore=0.300 inch N-Init	Pore=0.300 inch N-Prop	Pore=0.300 inch N-TOTAL
6.5	1.75	73	46	119	66	28	94	63	22	85
	1.50	253	94	347	228	58	286	217	44	261
	1.25	1300	215	1515	1161	131	1292	1096	100	1196
	1.00	12147	590	12737	10710	359	11069	10042	274	10316

Mean Stress Bias (ksi)	Scale (multiplied by base history)	Pore=0.1875 inch N-Init	Pore=0.1875 inch N-Prop	Pore=0.1875 inch N-TOTAL	Pore=0.250 inch N-Init	Pore=0.250 inch N-Prop	Pore=0.250 inch N-TOTAL	Pore=0.300 inch N-Init	Pore=0.300 inch N-Prop	Pore=0.300 inch N-TOTAL
0.0	1.75	152	111	263	139	68	207	133	51	184
	1.50	503	225	728	456	138	594	434	105	539
	1.25	2459	557	3016	2203	333	2536	2083	241	2324
	1.00	21637	1760	23397	19140	946	20086	17975	722	18697

TABLE 20. CO-LINEAR POROSITY
VARIABLE AMPLITUDE FATIGUE LIFE PREDICTIONS
NUMBER OF PORES = 3
THICKNESS = 0.5 INCH
ABS EH36

Mean Stress Bias (ksi)	Scale (multiplied by base history)	Pore=0.125 inch N-Init	Pore=0.125 inch N-Prop	Pore=0.125 inch N-TOTAL	Pore=0.1875 inch N-Init	Pore=0.1875 inch N-Prop	Pore=0.1875 inch N-TOTAL	Pore=0.250 inch N-Init	Pore=0.250 inch N-Prop	Pore=0.250 inch N-TOTAL
6.5	1.75	87	68	155	73	38	111	66	19	85
	1.50	307	138	445	253	77	330	228	38	266
	1.25	1613	313	1926	1300	174	1474	1161	87	1248
	1.00	15444	956	16400	12147	480	12627	10710	237	10947

Mean Stress Bias (ksi)	Scale (multiplied by base history)	Pore=0.125 inch N-Init	Pore=0.125 inch N-Prop	Pore=0.125 inch N-TOTAL	Pore=0.1875 inch N-Init	Pore=0.1875 inch N-Prop	Pore=0.1875 inch N-TOTAL	Pore=0.250 inch N-Init	Pore=0.250 inch N-Prop	Pore=0.250 inch N-TOTAL
0.0	1.75	180	174	354	152	92	244	139	45	184
	1.50	607	361	968	503	187	690	456	92	548
	1.25	3033	948	3981	2459	461	2920	2203	227	2430
	1.00	27334	3932	31266	21637	1486	23123	19140	631	19771

TABLE 21. CLUSTER POROSITY
VARIABLE AMPLITUDE FATIGUE LIFE PREDICTIONS
THICKNESS = 0.5 INCH
ABS EH36

Mean Stress Bias (ksi)	Scale (multiplied by base history)	Pore=0.125 inch			Pore=0.1875 inch			Pore=0.300 inch		
		N-Init	N-Prop	N-TOTAL	N-Init	N-Prop	N-TOTAL	N-Init	N-Prop	N-TOTAL
6.5	1.75	101	291	392	66	151	217	43	26	69
	1.50	360	604	964	223	303	526	141	70	211
	1.25	1901	1585	3486	1115	745	1860	666	159	825
	1.00	18327	5527	23854	10119	2485	12604	5668	461	6129

Mean Stress Bias (ksi)	Scale (multiplied by base history)	Pore=0.125 inch			Pore=0.1875 inch			Pore=0.300 inch		
		N-Init	N-Prop	N-TOTAL	N-Init	N-Prop	N-TOTAL	N-Init	N-Prop	N-TOTAL
0.0	1.75	210	958	1168	139	487	626	94	120	214
	1.50	711	2403	3114	448	1083	1531	288	246	534
	1.25	Non-propagating crack			2126	3658	5784	1289	639	1928
	1.00	Non-propagating crack			Non-propagating crack			10324	2625	12949

TABLE 22. CLUSTER POROSITY
VARIABLE AMPLITUDE FATIGUE LIFE PREDICTIONS
THICKNESS = 1.0 INCH
ABS EH36

Mean Stress Bias (ksi)	Scale (multiplied by base history)	Pore=0.1875 inch			Pore=0.250 inch			Pore=0.400 inch		
		N-Init	N-Prop	N-TOTAL	N-Init	N-Prop	N-TOTAL	N-Init	N-Prop	N-TOTAL
6.5	1.75	67	160	227	52	113	165	37	46	83
	1.50	228	338	566	173	229	402	119	91	210
	1.25	1143	770	1913	841	557	1398	551	251	802
	1.00	10402	2389	12791	7374	1639	9013	4580	688	5268

Mean Stress Bias (ksi)	Scale (multiplied by base history)	Pore=0.1875 inch			Pore=0.250 inch			Pore=0.400 inch		
		N-Init	N-Prop	N-TOTAL	N-Init	N-Prop	N-TOTAL	N-Init	N-Prop	N-TOTAL
0.0	1.75	142	470	612	112	342	454	81	157	238
	1.50	458	994	1452	352	709	1061	245	336	581
	1.25	2178	2527	4705	1617	1820	3437	1074	788	1862
	1.00	18643	10758	29401	13336	7267	20603	8390	2518	10908

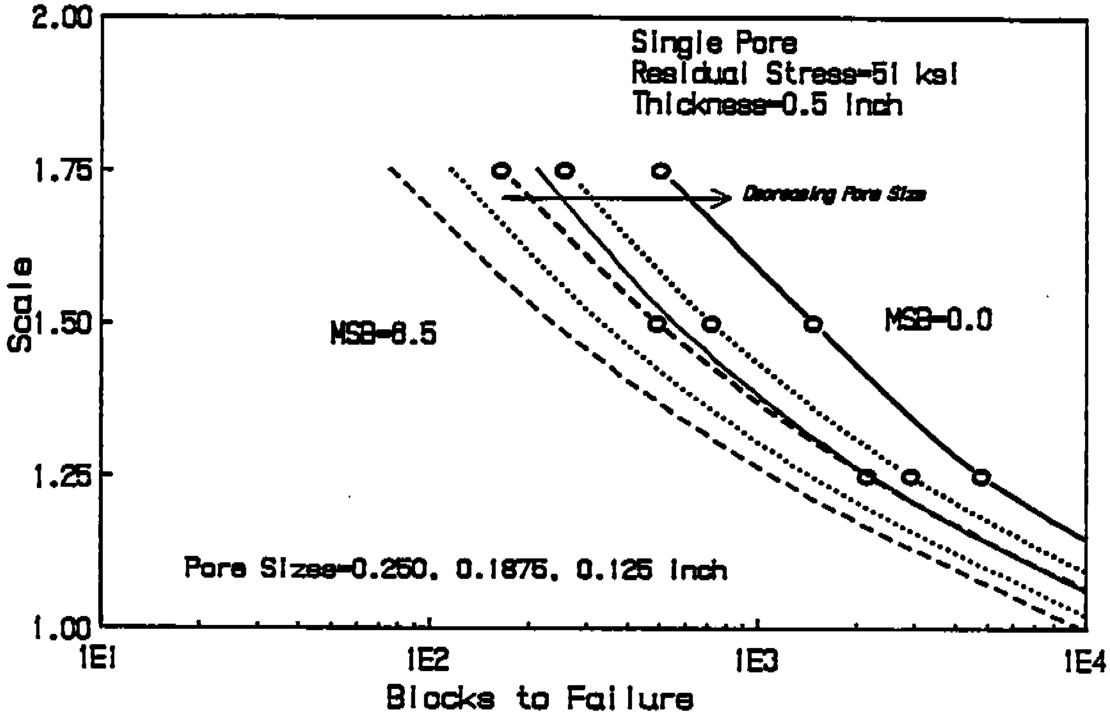

FIGURE 41. ENDURANCE CURVES FOR SINGLE PORES IN A 0.5-INCH THICK PLATE FOR SL-7 VARIABLE AMPLITUDE HISTORY CURVES CONNECTED BY CIRCLES REPRESENT A MEAN STRESS BIAS OF ZERO

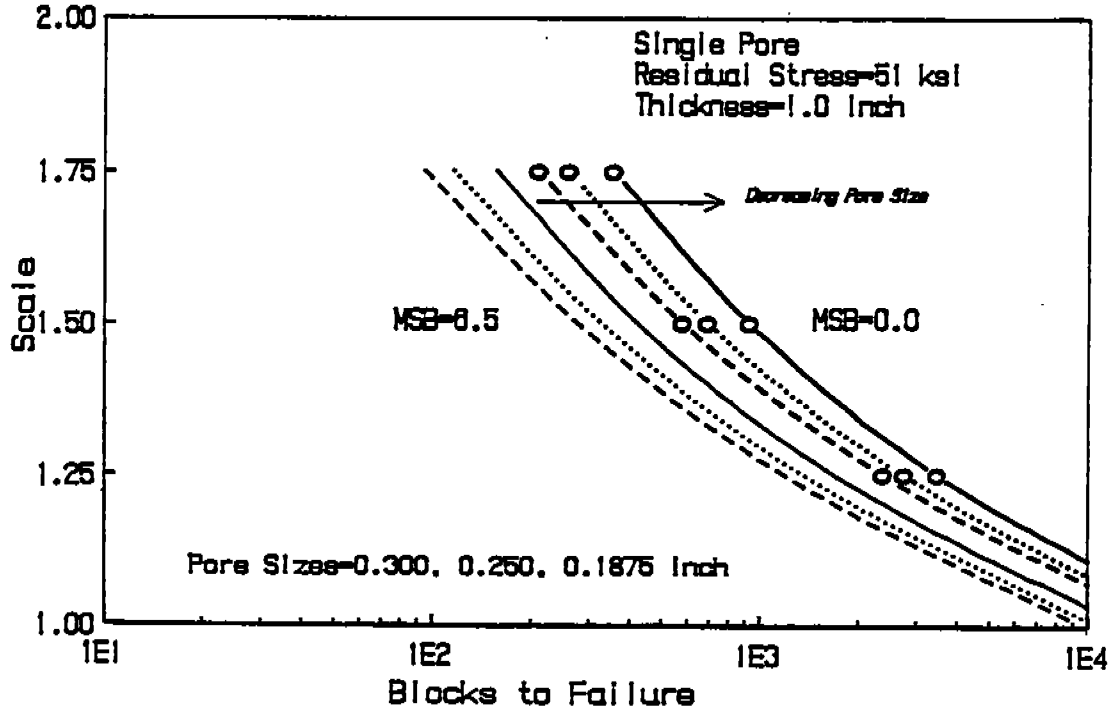

FIGURE 42. ENDURANCE CURVES FOR SINGLE PORES IN A 1.0 INCH THICK PLATE FOR SL-7 VARIABLE AMPLITUDE HISTORY. CURVES CONNECTED BY CIRCLES REPRESENT A MEAN STRESS BIAS OF ZERO

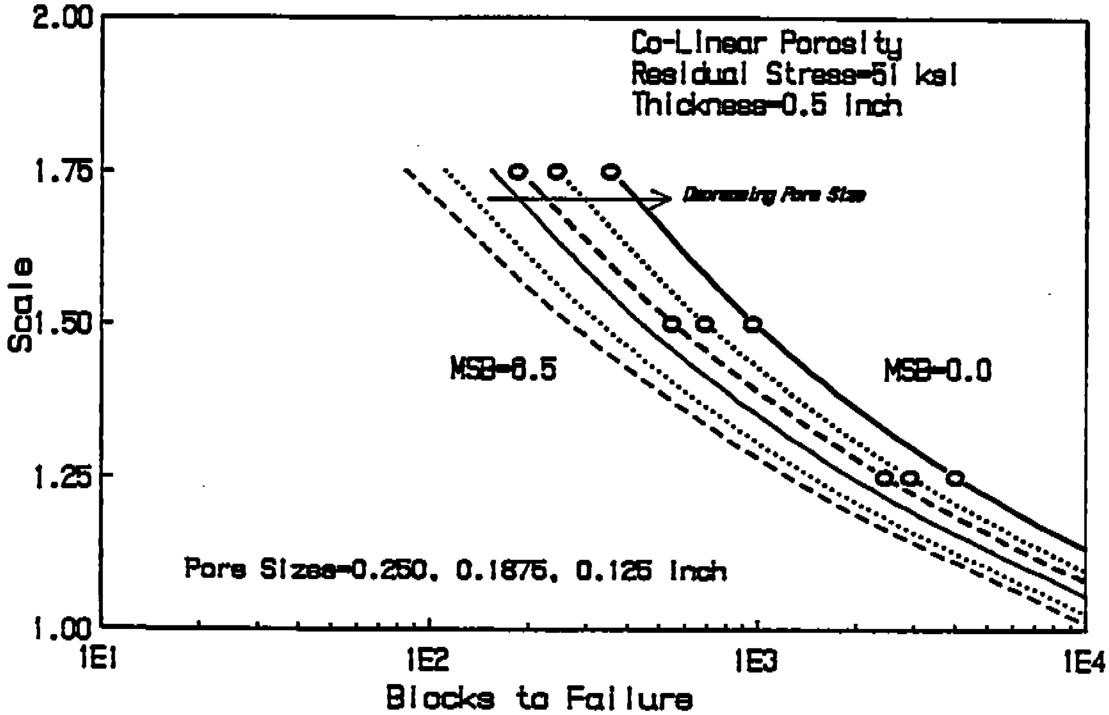

FIGURE 43. ENDURANCE CURVES FOR CO-LINEAR POROSITY IN A 0.5-INCH THICK PLATE FOR SL-7 VARIABLE AMPLITUDE HISTORY, CURVES CONNECTED BY CIRCLES REPRESENT A MEAN STRESS BIAS OF ZERO

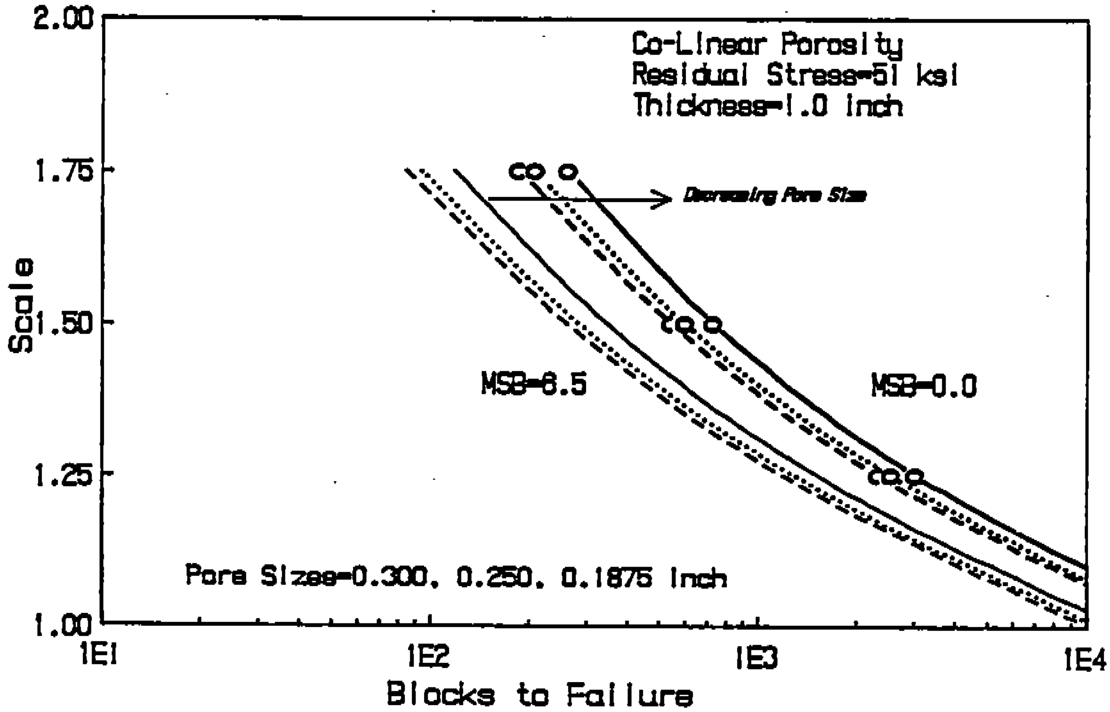

FIGURE 44. ENDURANCE CURVES FOR CO-LINEAR POROSITY IN A 1.0-INCH THICK PLATE FOR SL-7 VARIABLE AMPLITUDE HISTORY, CURVES CONNECTED BY CIRCLES REPRESENT A MEAN STRESS BIAS OF ZERO

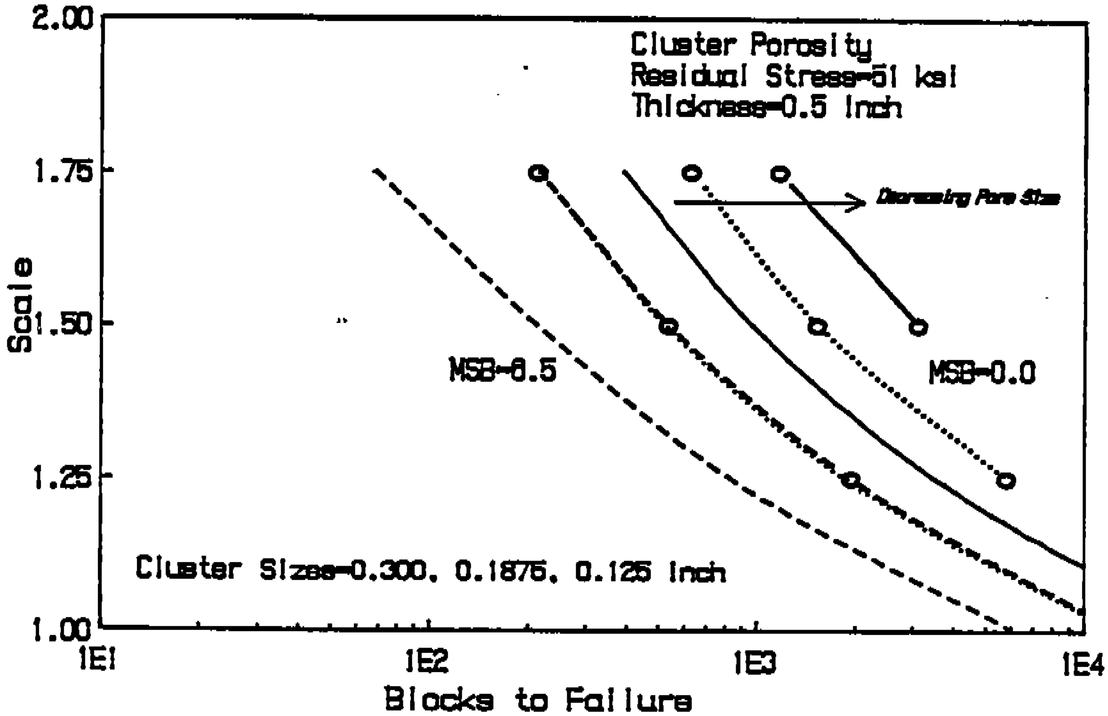

FIGURE 45. ENDURANCE CURVES FOR CLUSTER POROSITY IN A 0.5-INCH THICK PLATE FOR SL-7 VARIABLE AMPLITUDE HISTORY, CURVES CONNECTED BY CIRCLES REPRESENT A MEAN STRESS BIAS OF ZERO

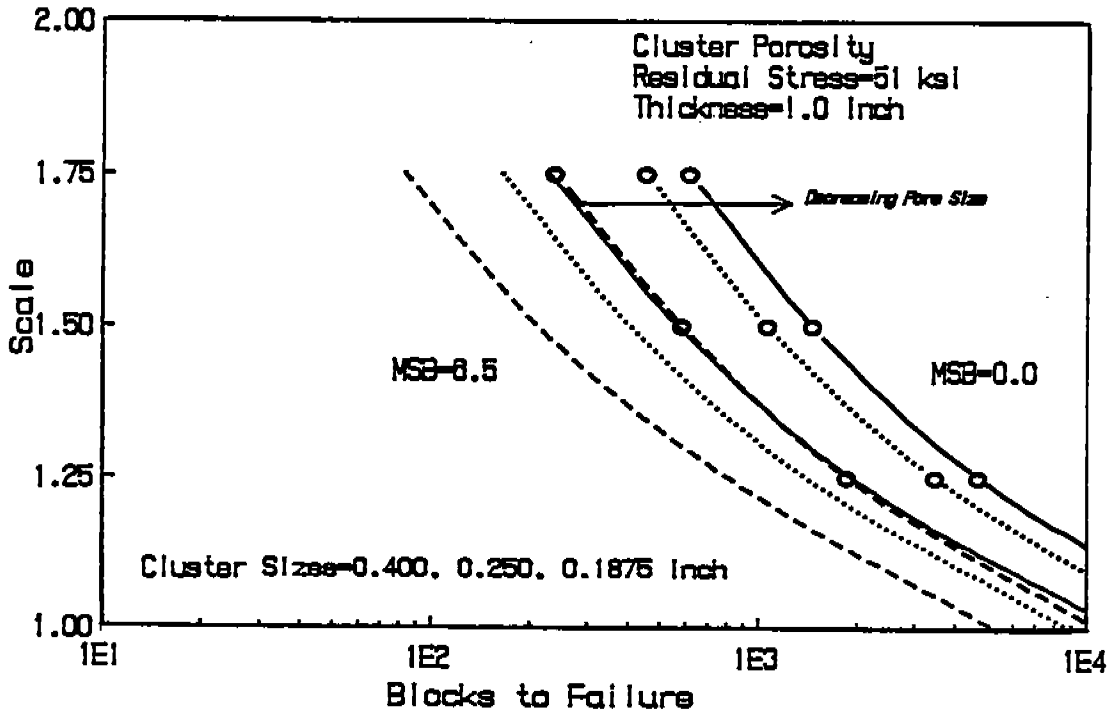

FIGURE 46. ENDURANCE CURVES FOR CLUSTER POROSITY IN A 1.0-INCH THICK PLATE FOR SL-7 VARIABLE AMPLITUDE HISTORY, CURVES CONNECTED BY CIRCLES REPRESENT A MEAN STRESS BIAS OF ZERO

9.1. Thickness

Two plate thicknesses were investigated in this study. It is important to note that since a specific width was not specified, the width of the plate is assumed to many times that of the plate thickness. The infinite width assumption means that the size of the porosity and subsequent crack are small in comparison to the plate and therefore the reduction in cross sectional area does not affect the nominal stress. The thickness of the plate, therefore, has no affect on the initiation life of the crack, all other parameters being equal. The difference in life between plate thicknesses is due to the propagation life. For equal pore sizes, it will simply take longer for a crack to grow toward the surface in a thicker plate. There is also a longer region where the stress intensity is not increased by the pore stress gradient or the back wall effect.

The fatigue life predictions proved to be relatively insensitive to the plate thickness. The larger thicknesses resulted in only slightly longer lives. This is due to the fact that life predictions are not greatly dependent upon the final crack length at failure (i.e., failure criterion and back surface effects). When the crack becomes large in size, the increased stress intensity drives the crack growth at an increasingly higher rate until failure occurs. Conversely, life predictions are very sensitive to initial crack lengths. See the initial crack length discussion in Section 7.1.

9.2. Residual Stress

As was noted in the literature survey, local residual stresses at the surface of pores is not reported. Masubuchi[22] indicated that tensile residual stresses as high as the yield strength of the base metal was measured near the centerline in butt welds. Two residual stress levels were used in the present study: the stress relieved condition (residual stress equals zero) and a residual stress equivalent to the yield stress in EH36 (51 ksi). The effect of residual stress is only accounted for in the initiation life calculations. Since the residual stress field is thought to vary throughout the weld, accounting for the changing stress field in crack growth calculations would prove to be very complex. Therefore, the residual stress is taken as zero for all the propagation calculations.

For the initiation life calculations, a residual stress dictates the starting point for the loading. Figure 17 from Reference 10 illustrates the effect of the residual stress upon the stress-strain response of the material near the notch root of a weldment with reinforcement. An analogy can be drawn between the notch root material and the material near the surface of a pore since both act as geometrical stress concentrations or notches. The plot shows the stress-strain response for three materials; one strong, one tough, and one ductile; and the effect the residual stress, σ_r, has on the set-up cycle. The result is a higher local mean stress than would be realized in the stress-free condition. The increase in mean stress is detrimental to fatigue life (see Section 9.3 Stress Ratio). Figure 48 shows the influence of residual stress on the fatigue life for a single pore as predicted by the model. Note the increase in life as residual stress is decreased.

9.3. Stress Ratio

The stress ratio, defined as

$$R = S_{min} / S_{max} \quad ,$$

is incorporated into the model for both the initiation and propagation calculations. The stress ratio is directly related to the mean stress, S_{mean}, by

$$S_{mean} = \frac{S_{max}}{2} (1 + R) \quad . \tag{20}$$

As the stress ratio increases, the tensile mean stress also increases. A tensile mean stress is generally observed to be detrimental for fatigue

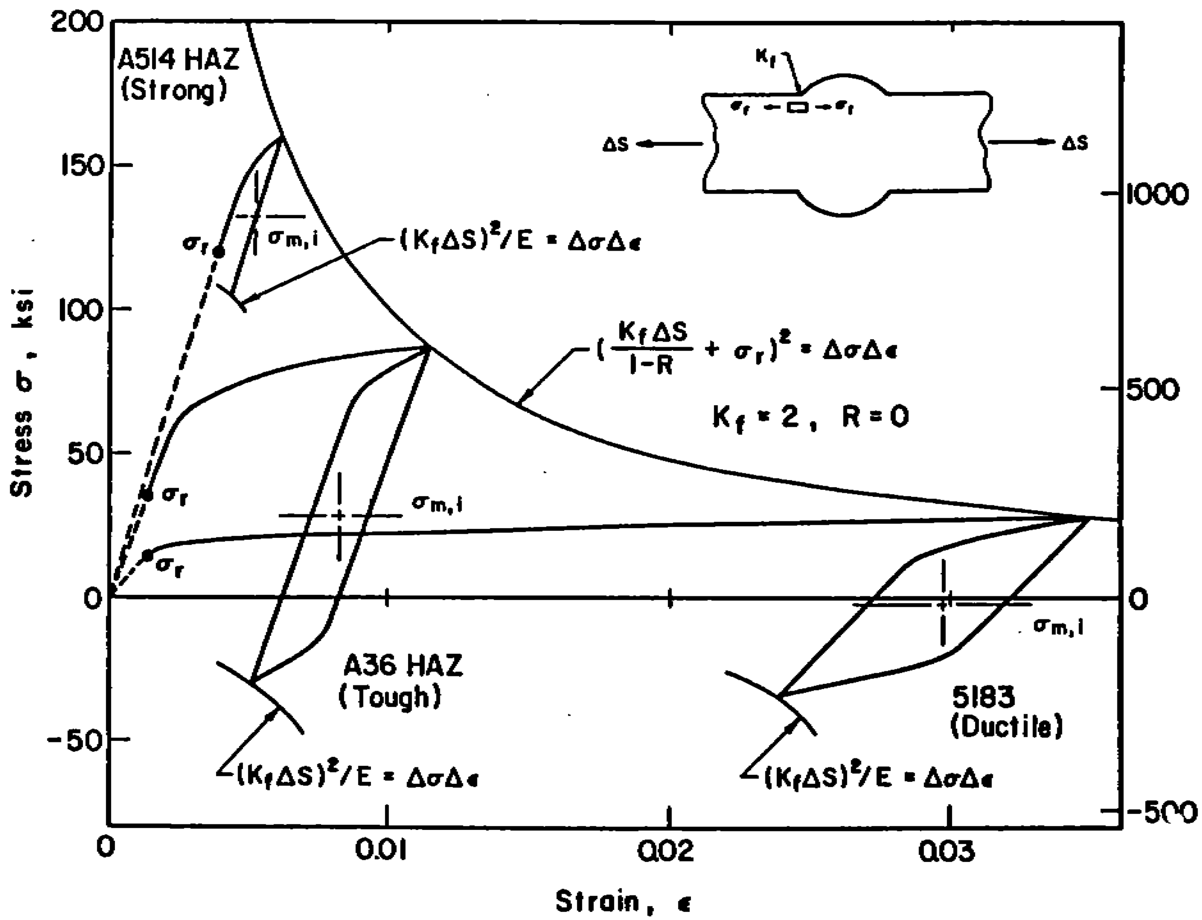

FIGURE 47. SET UP CYCLE FOR ASTM 514 HAZ (STRONG), A36 HAZ (TOUGH) STEELS, AND ALUMINUM ALLOY 5183 WM (DUCTILE) MATERIALS. THE SET UP CYCLE RESULTS IN A TENSILE MEAN STRESS FOR THE STRONG AND TOUGH MATERIALS

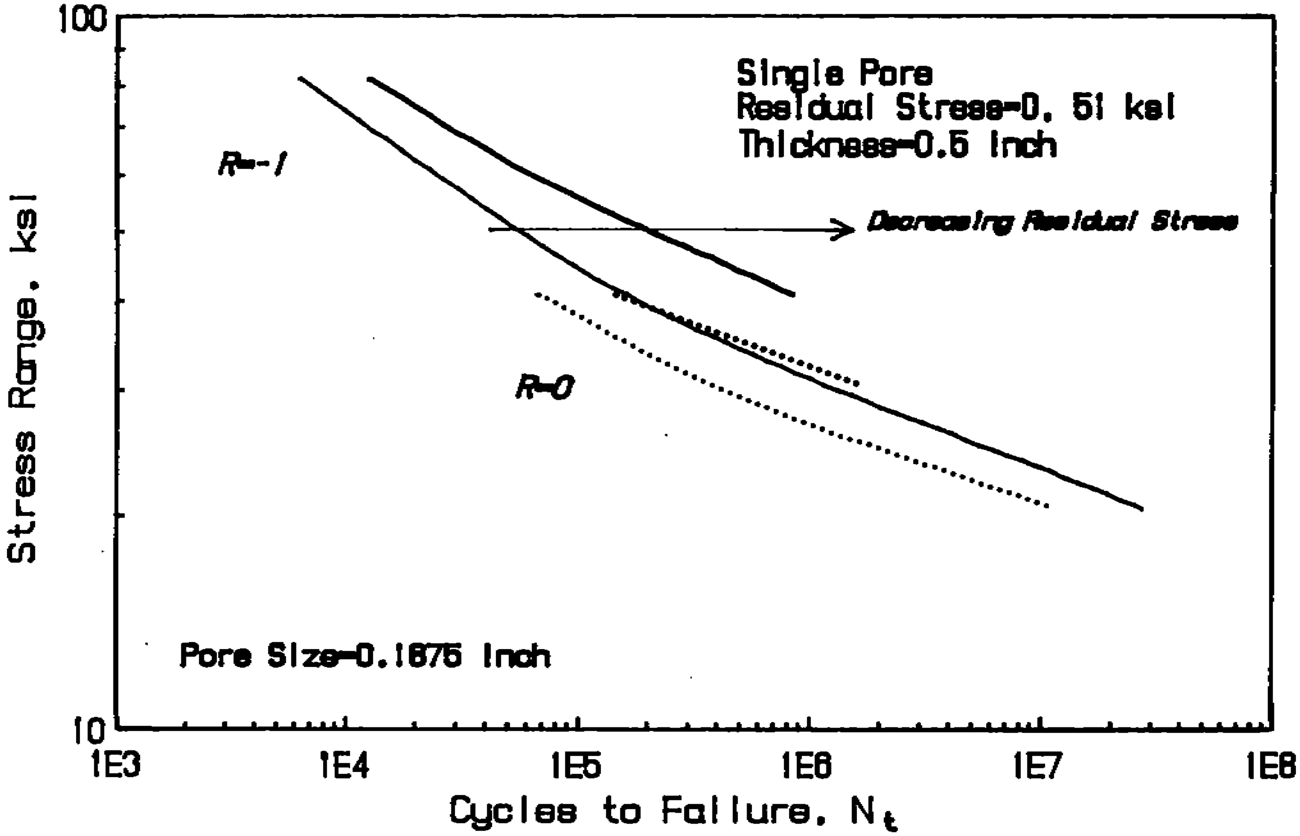

FIGURE 48. S-N PLOT SHOWING THE TREND OF INCREASING FATIGUE RESISTANCE
WITH DECREASING TENSILE RESIDUAL STRESS

life, provided that the strains are not great enough to cause complete mean stress relaxation. It can be seen from Equation 9,

$$\frac{\Delta\epsilon}{2} = \epsilon_f'(2N_f)^c + \left(\frac{\sigma_f' - \sigma_m}{E}\right)(2N_f)^b$$

that a tensile mean stress decreases the effective fatigue strength coefficient which is a measure of high cycle fatigue resistance. The strain-life equation is used to predict the initiation life at the pore surface, so a tensile mean stress will predict lesser initiation lives than zero or compressive mean stresses.

A high tensile mean stress is also found to increase crack growth rates. The crack growth rate relation,

$$\frac{da}{dN} = \frac{A\ \Delta K^m}{(1-R)}$$

was developed to account for the higher observed crack growth rates at higher stress ratios (and therefore higher mean stresses). Because both Equations 9 and 10 are used in the predictions, the trend on all of the S-N plots show a decreasing fatigue resistance with increased stress ratio.

The S-N plots show that none of the R = 0.5 predictions result in low lives ($< 10^5$). This seems to contradict the assertion that the high stress ratio loading is the most damaging. Actually this is the result of the method of choosing the stress levels for the predictions. Since the maximum stress for the predictions are chosen as 0.8, 0.6, 0.4, and 0.2 times the yield stress of the material, the stress ranges for the R = 0.5 are smaller than the other stress ratios. Stress range is the most influential parameter in the life prediction model. The small stress ranges in the R = 0.5 predictions therefore result in long lives.

9.4. Pore Size

The influence of pore size affects both the crack initiation and propagation estimates. The fatigue notch factor, K_f, was developed to account for the observation that smaller notches were found to be less detrimental in fatigue than larger notches of similar geometry. The relation used in the model to account for this phenomenon (Equation 7),

$$K_f = 1 + \frac{K_t - 1}{1 + a/r} \quad ,$$

was introduced by Peterson. It models the tendency of larger pores to have lesser initiation lives.

The propagation lives are also affected by the pore size. The effective flaw size, once the crack initiates or sharpens, is defined as the sum of the pore radius and the emerging crack. The larger the pore size, therefore, the larger the initial crack size and shorter growth period required to reach the surface. The effect of decreasing pore size on fatigue life is noted on all of the S-N plots.

9.5. Porosity Type

The effect of the type of porosity on fatigue life as predicted by the model can be inferred somewhat from Figure 49. The plot shows the stress ranges at total fatigue lives, N_t of 10,000 for the four porosity types. This plot illustrates that the geometry or porosity type influences fatigue. In view of the assumptions made for each of the pore geometries, the uniform porosity geometry would be expected to have the greatest fatigue resistance, and the cluster geometry the least for equal pore sizes. For the larger pore sizes, the single pores would be expected to have only slightly more fatigue resistance than a co-linear arrangement of non-interacting pores of equal size. The infinite width assumption, where area percent porosity is not accounted for, is important to consider when making comparisons between the porosity types. For instance, the reduction in cross sectional area for the co-linear pores would result in

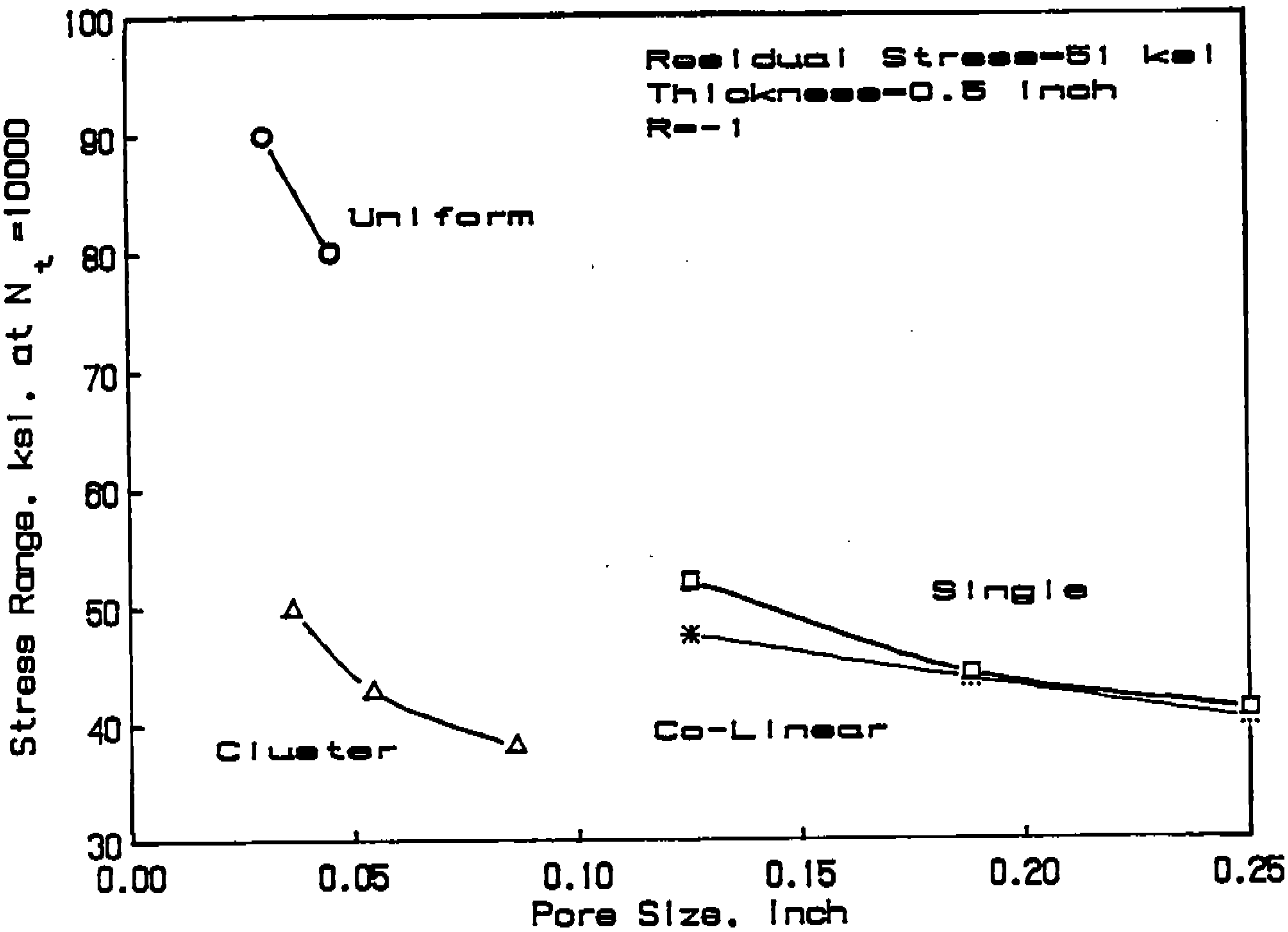

FIGURE 49. PLOT OF STRESS RANGE VS. PORE SIZE FOR THE FOUR TYPES OF POROSITY CONSIDERED IN THIS STUDY AT N_T = 10,000

a higher nominal stress, and the single and co-linear curves would be spread farther apart. If trends observed in this figure were extrapolated over the range of pore sizes, it is reasonable to assume that the single pore would show the greatest fatigue resistance, followed by the co-linear porosity, the uniform porosity, and the cluster porosity.

9.6. Relation to the Rules for Nondestructive Inspection of Hull Welds

The pore sizes chosen for the parametric study were based upon the Rules for Nondestructive Inspection of Hull Welds, 1986, prepared by the American Bureau of Shipping[54]. For uniform porosity, called "fine porosity" in the code, pore sizes less than 0.015 inch in diameter are not considered to be detrimental. This 0.015 inch pore was the smallest size examined in this study. For all the uniform porosity cases, the maximum allowed area percent porosity, 1.5 percent, was assumed. This pore size was generally found to have lives greater than 10^8 except at the highest stresses. The lowest predicted life for this pore size was 320,921 for fully reversed loading at a stress range of 81.6 ksi. Larger pore sizes were predicted to have decreasing fatigue resistance as seen in the S-N plots. These predictions indicate that the 0.015 inch pore size is a conservative value from a fatigue standpoint, for the minimum pore to be considered in design.

The largest isolated or single pore allowed in the code is 0.25 times the thickness of the plate, or 0.1875 inch, whichever is less. For the 0.5 inch-thick plate, the largest allowed pore is 0.125 inch. For the 1.0 inch-thick plate, the largest allowed pore is 0.1875 inch. Both of these maximum allowed pore sizes were predicted to have fatigue lives of about 10^5 for fully reversed loading at a stress range of 81.6 ksi, the worst case considered. Larger pores are predicted to have correspondingly lesser lives. The predictions indicate that these minimum values are again somewhat conservative and would not prove to be fatigue critical, at least for the material being considered.

The code also indicates that the concentration of porosity is not to exceed that shown in the charts in Figures 11 and 12. The fatigue life predictions for clusters do indicate decreased fatigue life with increased pore concentration because of interaction. However, as discussed in Section 6.3, pores separated by a distance of two pore diameters do not affect the others stress field. The charts shown in Figures 11 and 12 would disallow pore separated by any less than five pore diameters. Again, this aspect of the code is conservative.

The assertion that the ABS code is conservative in its porosity allowables from a fatigue standpoint is not to be construed as an endorsement for its abandonment of even amendment. The presence of porosity, especially cluster porosity, in weld metal suggests improper welding practice and often masks other irregularities such as material degradation.

10. SUMMARY

The aim of this study was to examine the effect of porosity upon the structural integrity of marine weldments. The parameters which influence the fatigue life of weldments with porosity were found from literature related specifically to porosity as well as traditional linear elastic fracture mechanics and low cycle fatigue concepts. Using this data, a model was developed to predict the fatigue lives of weldments with porosity and with reinforcement removed. Specific analysis routines were developed for life prediction of single pores, uniform porosity, co-linear porosity, and cluster porosity. The model was used to predict the lives of a limited number of actual fatigue tests of welds containing severe clusters of porosity. The predictions agreed with the test results nearly within a factor of two. The model was used to examine the dependence of fatigue life on a number of parameters found to be influential. A variable amplitude loading history was developed using SL-7 stress history data. This history was used to generate variable amplitude life predictions for the four types of porosity being considered.

11. CONCLUSIONS

(1) Porosity is not fatigue critical in butt weldments which have reinforcement intact. The stress concentration at the toe of the reinforcement is much more severe than internal porosity so fatigue cracks will initiate at the toe rather than a pore.

(2) For butt welds with reinforcement removed, the following parameters have been found to influence fatigue life: material, thickness, residual stress, stress ratio, stress range, pore size and type of porosity.

(3) In view of the assumptions made regarding pore geometry, for equal pore sizes, the single pore would be least detrimental in fatigue followed by co-linear porosity, and uniform porosity. Cluster porosity is predicted to be most detrimental.

(4) For the SL-7 variable amplitude stress history, all pore geometries were predicted to last indefinitely. For members subjected to stresses 1.75 times that of the base history, lives on the order of tens of years were predicted.

(5) In relation to the findings of this study, the Nondestructive Inspection of Hull Welds, 1986, prepared by the American Bureau of Shipping, was found to be conservative from a fatigue standpoint. However, since the presence of porosity suggests improper welding procedure, other problems may with the weld may be present. The finding that the code is conservative from a fatigue standpoint is not sufficient reason for amendment of the porosity allowables.

12. RECOMMENDATIONS FOR FUTURE WORK

To further substantiate the methodology presentated in this report, there is a need for more fatigue test data of weldment porosity. The authors were able to uncover only eight fatigue tests with sufficient documentation to which to apply the model. This sample is far from being statistically significant. It is recommended that a laboratory program be initiated investigate the models sensitivity to its various parameters.

A test program including a number of different ship steels and weld metals would prove insightful.

A method for predicting the three dimensional pore geomerty would greatly improve the usefulness of the proposed methodology. These life estimates were made with fracture surfaces showing the positional relationship of the pores. It would presently be difficult to determine the geometry from radiographs to predict fatigue lives of components prior to failure.

The problem of cavity interaction is not covered in any great depth in the literature. Interaction is a complex stress analysis problem perhaps best approached using photoelastic techniques. The availability of solutions to this problem would enhance the physical soundness of the methodology.

13. REFERENCES

[1] J. D. Harrison, "Basis for a Proposed Acceptance-Standard for Weld Defects. Part 1: Porosity", Met. Constr. Br. Weld. J. Vol. 4, pp. 99-107.

[2] A. Matting and M. Neitzel, "The Evaluation of Weld Defects in Fatigue Testing", Weld. Res. Abroad, Vol. 12, pp. 34-60, August-September, 1966.

[3] M. B. Kasen, "Significance of Blunt Flaws in Pipeline Girth Welds", Welding J., pp. 117-s-122-s, May, 1983.

[4] F. V. Lawrence, Jr., W. H. Munse, and J. D. Burk, "Effects of Porosity on the Fatigue Properties of 5083 Aluminum Alloy Weldments", Report to Naval Ship Systems Command, U.S. Navy, (Contract N00024-73-C-5344), October, 1974.

[5] F. M. Burdekin, J. D. Harrison, and J. G. Young, "The Effect of Weld Defects with Special Reference to BWRA Research", Weld. Res. Abroad, Vol. 14, pp. 58-67, August-September 1968.

[6] B. N. Leis, D. P. Goetz, and P. M. Scott, "The Influence of Defects on the Fatigue Resistance of Butt and Girth Welds in A106B Steel", NASA Contractor Report 178114, July, 1986.

[7] Y. Ishii and K. Iida, "Low and Intermediate Cycle Fatigue Strength of Butt Welds Containing Defects", J. of the Soc. of Non-destructive Testing, (Japan), Vol. 18, No. 10 (1969).

[8] M. D. Bowman and W. H. Munse, "The Effects of Discontinuities on the Fatigue Behavior of Transverse Butt Welds in Steel", Report UILU-ENG-812006, The Civil Engineering Dept., University of Illinois, April, 1981.

[9] V. I. Trufyakov, "Welded Joints and Residual Stresses", Weld. Res. Abroad, Vol. 5, No. 3, pp. 11-18, March, 1959.

[10] J. D. Burk and F. V. Lawrence, Jr., "The Effect of Residual Stresses on Weld Fatigue Life", Fracture Control Program Report No. 29, College of Engineering, University of Illinois, January, 1978.

[11] F. V. Lawrence, Jr., N. J. Ho, and P. K. Mazumdar, "Predicting the Fatigue Resistance of Welds", Fracture Control Program Report No. 36, College of Engineering, University of Illinois, October, 1980.

[12] W. G., Dobson, R. F. Brodrick, J. W. Wheaton, J. Giannotti, and K. A. Stambaugh, "Fatigue Considerations in View of Measured Load Spectra", Ship Structure Committee Report SSC-315, 1982.

[13] E. Sternberg, "Three-dimensional Stress Concentration in the Theory of Elasticity," Applied Mechanics Review, Vol. 11, No. 1, pp. 1-4, 1958.

[14] G. N. Savin, "Stress Concentration Around Holes," Pergamon Press, New York, 1964.

[15] E. Tsuchida, and I. Nakahara, "Three-Dimensional Stress Concentration Around a Spherical Cavity in a Semi-Infinite Elastic Body," Bulletin of the JSME, Vol. 13, No. 58, 1970.

[16] I. I. Makarov, et al., "Stress Concentration in the Vicinity of Spherical Cylindrical Pores in Butt Welded Joints," Svar. Proiz, No. 5, pp. 25-26, 1975.

[17] C. D. Lundin, "Fundamentals of Weld Discontinuities and Their Significance," Welding Research Council Bulletin 295, 1984.

[18] K. Masubuchi, "Integration of NASA-Sponsored Studies on Aluminum Welding," NASA Contractor Report 2064, 1972.

[19] V. D. Krstic, "Fracture of Brittle Solids in the Presence of a Spherical Cavity," Acta Metall., Vol. 33. No. 3, pp. 521-526, 1985.

[20] H. Tada, P. C. Paris, and G. R. Irwin, "The Stress Analysis of Cracks Handbook," Del Research Corporation, 1973.

[21] D. P. Rooke and D. J. Cartwright, "Compendium of Stress Intensity Factors," The Hillingdon Press, 1976.

[22] K. Masubuchi, "Analysis of Welded Structures," Pergamon Press, 1980.

[23] A. V. Babaev, "The Effects of Pores on the Fatigue Strengths of Welded Joints," Avt. Svarka, No. 10, pp. 6-10, 1980.

[24] J. M. Barsom, "Fatigue Considerations for Steel Bridges," Fatigue Crack Growth Measurement and Data Analysis, ASTM STP 738, pp. 300-318, 1981.

[25] K. Masubuchi, "Materials for Ocean Engineering," The M.I.T. Press, 1970.

[26] C. M. Hudson and S. K. Seward, "A Compendium of Sources of Fracture Toughness and Fatigue-Crack Growth Data for Metallic Alloys," International Journal of Fracture, Vol. 14, pp. R151-R184, 1978.

[27] C. M. Hudson and W. K. Seward, "A Compendium of Sources of Fracture Toughness and Fatigue-Crack Growth Data for Metallic Alloys," International Journal of Fracture, Vol. 20, pp. R57-R117, 1978.

[28] S. J. Maddox, "Fatigue Crack Propagation Data Obtained from Parent Metal, Weld Metal and HAZ in Structural Steels," Welding Research International, Vol. 4, No. 1, 1974.

[29] S. T. Rofle and J. M. Barsom, "Fracture and Fatigue Control in Structures, Application of Fracture Mechanics," Prentice-Hall, 1977.

[30] P. M. Sesuner, K. Ortiz, J. M. Thomas, and S. O. Adams, "Fracture Control for Fixed Offshore Structures," Ship Structure Committee Report No. 328, 1985.

[31] K. Masubuchi, R. E. Monroe, and D. C. Martin, "Interpretive Report on Weld-Metal Toughness," Welding Research Council Bulletin, No. 111, 1966.

[32] J. R. Hawthorne and F. J. Loss, "Fracture Toughness Characterization of Shipbuilding Steels," Ship Structure Committee Report 248, 1975.

[33] P. H. Francis, T. S. Cook and A. Nagy, "Fracture Behavior Characterization of Ship Steels and Weldments," Ship Structure Committee Report 276, 1978.

[34] J. McCarthy, H. Lamba, and F. V. Lawrence, "Effects of Porosity on the Fracture Toughness of 5083, 5456, and 6061 Aluminum Alloy Weldments," Welding Research Council Bulletin 261, 1980.

[35] American Society for Metals, "Properties and Selection: Iron and Steels, Vol. 1," Metal Handbook, 9th edition, 1978.

[36] Y. Higashida, J. D. Burk, and F. V. Lawrence, "Strain-Controlled Fatigue Behavior of ASTM A36 and A514 Grade F Steels and 5083-0 Aluminum Weld Materials," Welding Journal, Vol. 57, pp. 334-344S, 1978.

[37] British Standards Institute, "Guidance on Some Methods of the Derivation of Acceptance Levels for Defects in Fusion Welded Joints," PD6493, 1980.

[38] M. A. Hirt and J. W. Fisher, "Fatigue Crack Growth in Welded Beams," Engineering Fracture Mechanics, Vol. 5, No. 2, 1973.

[39] N.-J. Ho and F. V. Lawrence, " Constant Amplitude and Variable Load History Fatigue Test Results and Predictions for Cruciform and Lap Welds," Theoretical and Applied Fracture Mechanics, Vol. 1, pp. 3-21, 1981.

[40] H. S. Reemsnyder, "Evaluating the Effect of Residual Stresses on Notched Fatigue Resistance," Materials, Experimentation, and Design in Fatigue, Proceedings of Fatigue '81, Westbury Press, England, pp. 273-295, 1981.

[41] B. N. Leis, "Microcrack Initiation and Growth in a Pearlitic Steel - Experiments and Analysis," Fracture Mechanics, Fifteenth Symposium, ASTM 833, American Society for Testing and Materials, Philadelphia, pp. 449-480, 1981.

[42] H. Neuber, "Theory of Stress Concentration for Shear Strained Pragmatical Bodies With Arbitrary Nonlinear Stress-Strain Law", Trans. ASME, J. of Applied Mechanics, pp. 544-550, December, 1961.

[43] R. E. Peterson, "Notch Sensitivity", Chapter 13, Metal Fatigue, Sines and Waisman (ed.), McGraw-Hill, New York, NY, 1959.

[44] J. C. McMahon and F. V. Lawrence, "Predicting Fatigue Properties Through Hardness Measurements", Fracture Control Program Report No. 105, University of Illinois, February, 1984.

[45] P. C. Paris and F. Erdogan, J. Basic Eng. Trans., ASME, Series D, 85(4), p. 528, 1963.

[46] R. C. Shah, A. S. Kobayashi, "Stress Intensity Factors for an Elliptical Crack Approaching the Surface of a Semi-Infinite Solid", Intl. J. Fracture Mechanics, 1972.

[47] P. Albrecht and K. Yamada, "Rapid Calculation of Stress Intensity Factors", J. Str. Div. of ASCE, Vol. 2, pp. 377-389, 1977.

[48] M. A. Sadowsky and E. Sternberg, "Stress Concentration Around a Triaxial Ellipsoidal Cavity", J. Appl. Mech., Vol. 16, No. 2, pp. 149-157, 1949.

[49] R. E. Peterson, "The Interaction Effect of Neighboring Holes or Cavities, with Particular Reference to Pressure Vessels and Rocket Cases", J. of Basic Eng., Vol. 87, No. 4, pp. 879, 886, 1965.

[50] R. A. Smith and K. J. Miller, International J. of Mechanical Sci., Vol. 19, pp. 11-22, 1977.

[51] D. H. Ekstrom and W. H. Munse, "The Effect of Internal Weld Defects on the Fatigue Behavior of Welded Connections", University of Illinois Department of Civil Engineering Experiment Station, December, 1971.

[52] S. G., Stiason and H. H. Chen, "Application of Probabilistic Design Methods to Wave Load Predictions for Ship Structure Analysis", American Bureau of Shipping, November, 1979.

[53] E. T. Booth, "SL-7 Extreme Data Collection and Reduction", Ship Structure Committee Report SCC-304, 1981.

[54] American Bureau of Shipping, "Rules for Nondestructive Inspection of Hull Welds", 1986.

APPENDIX

STEP-BY-STEP EXAMPLE OF THE PREDICTIVE MODEL

APPENDIX

Step-by-Step Example of the Predictive Model

Single Pore

Parameters:

Stress range:	61.2 ksi
Stress ratio:	-1
Residual stress:	51 ksi
Pore diameter:	0.1875 inch
Pore K_t:	2.054
Weld thickness:	1.0 inch

Step 1. Notch analysis

The notch analysis determines the strains expected at the material adjacent to the pore surface. As discussed in Section 5.1.2, the fatigue notch factor is often used in place of the stress concentration factor when analysing fatigue loading. Solving for the material constant 'a' in Equation (8),

$$a = \left(\frac{300}{S_u}\right)^{1.8} \times 10^{-3} \text{ in.} \qquad (8)$$

using the ultimate strength of the ABS EH36 steel in Table 4 as 75 ksi, a = 0.01 inch. Using Equation (7),

$$K_f = 1 + \left(\frac{K_t - 1}{1 + a/r}\right) , \qquad (7)$$

and the values above, the fatigue notch factor, K_f, is 1.95.

To determine the maximum and minimum strains at the pore surface due to cyclic loading, Nueber's rule is used. Because the loading is cyclic, the cyclic strength coefficient, K', and the cyclic strain hardening exponent, n', can be used in the final form of Equation (3),

$$\frac{\Delta S^2}{E} \quad K_t^2 = \Delta\sigma \left(\frac{\Delta\sigma}{E} + \left(\frac{\Delta\sigma}{K} \right)^{1/n} \right) \quad .$$

The residual stress of 51 ksi is added to the left hand term giving,

$$\frac{(\Delta S K_t + \sigma_r)^2}{E} \quad K_t = \Delta\sigma \left(\frac{\Delta\sigma}{E} + \left(\frac{\Delta\sigma}{K} \right)^{1/n} \right) \quad .$$

Solving for $\Delta\sigma$, the result is $\Delta\sigma$ = 56.51 ksi and $\Delta\epsilon$ = 0.00716. The reversal switches the coordinate axes of stress and strain, and the equation is solved again, this time without the added residual stress. This and all subsequent reversals use a value of the cyclic strength coefficient, K'_{rev}, equal to $2^{(1-n')}*K'$. This is necessary because K' is used to define the cyclic stress-strain curve which is constructed of the tensile hysteresis loop tips. The actual material stress-strain response during revesals follows a larger path when going into compression. The results for the reversal local stress range and strain range are 89.08 ksi and 0.00534. The minimum local stress is therefore -32.56 ksi and the minimum local strain is 0.0018. The local mean stress, σ_m, is 11.97 ksi. Figure A1 shows the hysteresis loop for the material at the pore surface for this loading case. Note that the residual stress state initially includes a large plastic strain value. In reality, the residual stress is generally below yield because at this stage the material stress-strain response follows the monotonic stress-strain curve. The fatigue life prediction model makes the assumption that the notch material assumes cyclic behavior relatively early in the loading history, so it is used throughout the analysis. The presence of the initial plastic strain does not affect the numerical computations in estimating the crack initiation life.

Step 2. Estimate cycles to initiation using low-cycle fatigue properties.

Equation (9), the Coffin-Manson equation with Morrow's mean stress correction,

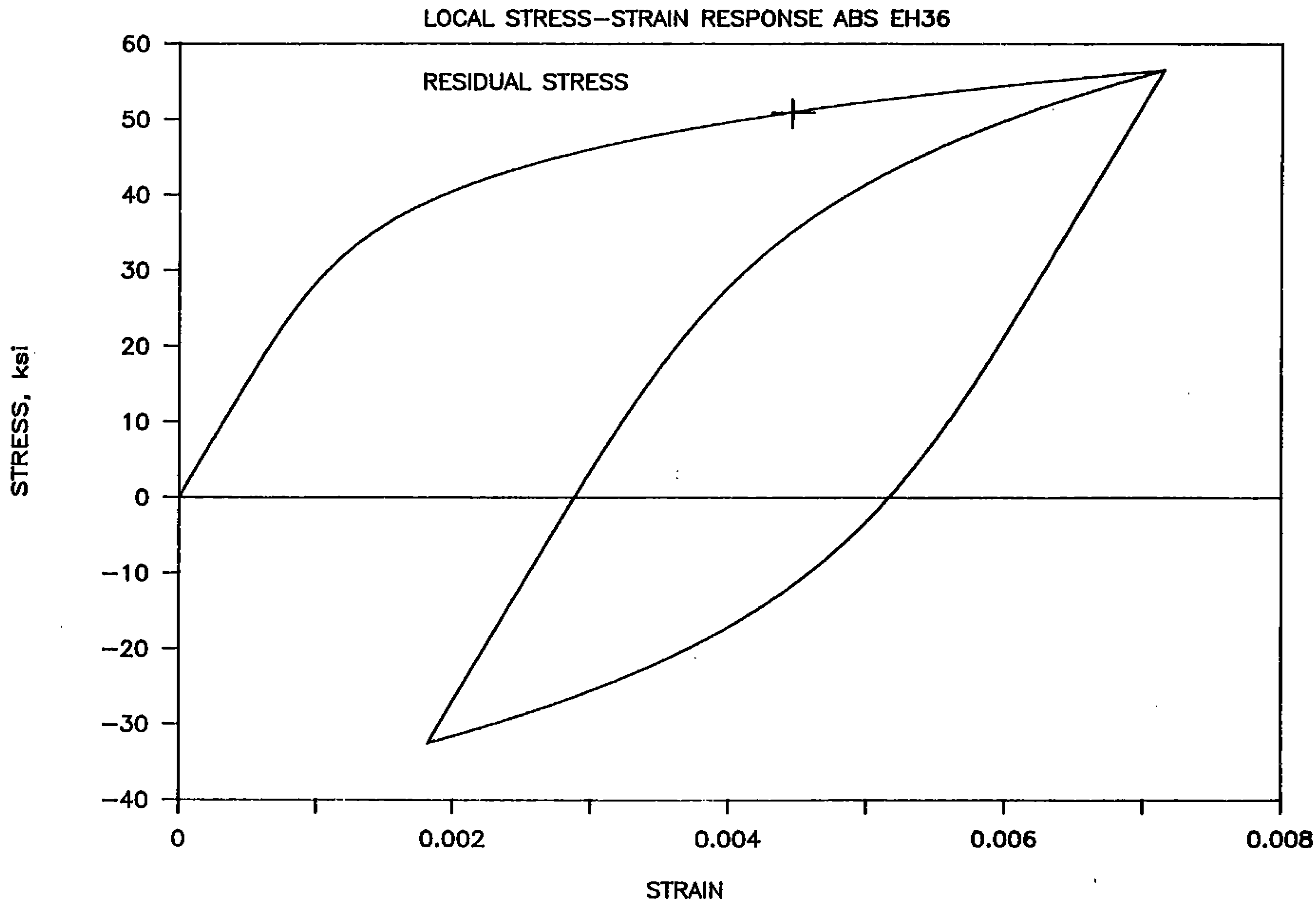

FIGURE A1. STRESS-STRAIN RESPONSE AT PORE SURFACE FOR EXAMPLE LIFE PREDICTION

$$\frac{\Delta\epsilon}{2} = \epsilon_f'(2N_f)^c + \left(\frac{\sigma_f - \sigma_m}{E}\right)(2N_f)^b \quad (9)$$

is used to solve for the estimated cycles to failure, N_f. This again is an iterative procedure. For this example, the cycles to crack initation is 7971 cycles. The resulting N_f is actually the number of cycles required to initiate a fatigue crack at the pore surface since the calculated strains are local to this region. The remaining weldment is still intact at this cycle count. The rest of the analysis estimates the number of cycles to failure by crack propagation through the weldment.

Step 3. Estimate cycles required to propagate crack to failure.

The crack propagation model is outlined in section 5.2. The initial crack size assumption used throughout this study was 0.05 times the pore diameter. The initial crack size for this case is 0.0094 inch. To determine the stress intensity range for a given crack size and loading, the geometry correction factor from Equation (13)

$$Y = \frac{M_s\ M_t\ M_k}{\Phi_0} \quad (13)$$

is calculated. When the crack is in the region of the stress concentration due to the pore, the stress intensity range solution is dominated by the stress gradient term, M_k. Calculating the M_k term requires a numerical procedure[47] taking into account the stress gradient away from the pore. The M_k term is calculated by superposition of the notch stress gradient upon the crack. The expression is

$$M_k = \frac{2}{\pi} \sum_{i=1}^{n} \sigma_{bi} \left(\arcsin \frac{b_{i+1}}{a} - \arcsin \frac{b_i}{a}\right)$$

where b_i is the position b along the crack, σ_{bi} is the stress at position b_i due to the notch (assuming no crack), and a is the crack length. In this example, at the initial crack length of 0.0094 inch, the value of M_k is 2.11. The finite thickness correction factor, M_t is negligible (equal to one) at this small crack length. Also, the front surface term, M_s, is equal to unity for an internal crack. The crack shape factor, Φ_o, for a circular crack is 1.57. The geometry correction factor, Y, is therefore 1.34 at the initial crack length. This value decreases rapidly with increasing crack length as shown in Figure 16. As the crack grows near to the surface, the value of Y begins to increase. For comparison, apply Equation 16 at a = t/2, the position of the crack front just before breaking the surface. M_t is 1.4, and M_k becomes near unity. The final value of Y is therefore 0.89.

Estimating the number of cycles to failure by crack propagation is accomplished by calculating the stress intensity factor range, ΔK, at every cycle and incrementing the crack length according to the material crack growth rate. The estimated propagation cycles to failure for this example is 26722 cycles. The total estimated fatigue life is therefore 34693 cycles.

COMMITTEE ON MARINE STRUCTURES
Commission on Engineering and Technical Systems
National Academy of Sciences - National Research Council

The COMMITTEE ON MARINE STRUCTURES has technical cognizance of the interagency Ship Structure Committee's research program.

Mr. Stanley G. Stiansen, Chairman, Riverhead, NY
Prof. C. Allin Cornell, Stanford Univesity, Stanford, CA
Mr. Peter A. Gale, Webb Institute of Naval Architecture, Glen Cove, NY
Mr. Griff C. Lee, Griff C. Lee, Inc., New Orleans, LA
Prof. David L. Olson, Colorado School of Mines, Goldon, CO
Mr. Paul H. Wirsching, University of Arizona, Tucson, AZ
Mr. Alexander B. Stavovy, Staff Officer, National Research Council, Washington, DC
CDR Michael K. Parmelee, Secretary, Ship Structure Committee, Washington, DC

LOADS WORK GROUP

Mr. Paul H. Wirsching, Chairman, University of Arizona, Tucson, AZ
Prof. Keith D. Hjelmstad, University of Illinois, Urbana, IL
Dr. Hsien Yun Jan, President of Martech Inc., Neshanic Station, NJ
Prof. Jack Y. K. Lou ,Texas A & M University, College Station, TX
Mr. Edward K. Moll, Bath Iron Works Corp., Bath, MA
Mr. Naresh Maniar, M. Rosenblatt & Son, Inc., New York , NY
Prof. Anastassios N. Perakis, The University of Michigan, Ann Arbor, MI

MATERIALS WORK GROUP

Prof. David L. Olson, Chairman, Colorado School of Mines, Golden,CO
Prof. William H. Hartt, Vice Chairman, Florida Atlantic University, Boca Raton, FL
Dr. Santiago Ibarra Jr., Amoco Corporation, Naperville, IL
Mr. Paul A. Lagace, Massachusetts Institute of Tech., Cambridge, MA
Mr. Mamdouh M. Salama, Conoco Inc., Ponca City, OK
Mr. James M. Sawhill, Jr., Newport News Shipbuilding, Newport News, VA
Mr. Thomas A. Siewert, National Bureau of Standards, Boulder, CO

SHIP STRUCTURE COMMITTEE PUBLICATIONS

SSC-322 Analysis and Assessment of Major Uncertainties Associated With Ship Hull Ultimate Failure by P. Kaplan, M. Benatar, J. Bentson and T. A. Achtarides, 1984

SSC-323 Updating of Fillet Weld Strength Parameters for Commercial Shipbuilding by R. P. Krumpen, Jr., and C. R. Jordan, 1984

SSC-324 Analytical Techniques for Predicting Grounded Ship Response by J. D. Porricelli and J. H. Boyd, 1984

SSC-325 Correlation of Theoretical and Measured Hydrodynamic Pressures for the SL-7 Containership and the Great Lakes Bulk Carrier S. J. Cort by H. H. Chen, Y. S. Shin & I. S. Aulakh, 1984

SSC-326 Long-Term Corrosion Fatigue of Welded Marine Steels by O. H. Burnside, S. J. Hudak, E. Oelkers, K. B. Chan, and R. J. Dexter, 1984

SSC-327 Investigation of Steels for Improved Weldability in Ship Construction by L. J. Cuddy, J. S. Lally and L. F. Porter 1985

SSC-328 Fracture Control for Fixed Offshore Structures by P. M. Besuner, K. Ortiz, J. M. Thomas and S. D. Adams 1985

SSC-329 Ice Loads and Ship Response to Ice by J. W. St. John, C. Daley, and H. Blount, 1985

SSC-330 Practical Guide for Shipboard Vibration Control by E. F. Noonan, G. P. Antonides and W. A. Woods, 1985

SSC-331 Design Guide for Ship Structural Details by C. R. Jordan and R. P. Krumpen, Jr., 1985

SSC-332 Guide for Ship Structural Inspections by Nedret S. Basar & Victor W. Jovino, 1985

SSC-333 Advance Methods for Ship Motion and Wave Load Prediction by William J. Walsh, Brian N. Leis, and J. Y. Yung, 1989

SSC-334 Influence of Weld Porosity on the Integrity of Marine Structures by William J. Walsh , Brian N. Leis, and J. Y. Yung, 1989

None Ship Structure Committee Publications - A Special Bibliography, AD-A140339